

- I. A STUDY OF THE EFFECTS OF DISLOCATIONS IN SILVER ON THE
RATE OF OXIDATION OF CARBON MONOXIDE
- II. A MECHANISM FOR THE FORMATION OF DISLOCATIONS DURING
THE OXIDATION OF ZINC

Thesis by
John Wayne Miller

In Partial Fulfillment of the Requirements
For the Degree of
Doctor of Philosophy

California Institute of Technology

Pasadena, California

1976

(Submitted September 19, 1975)

ACKNOWLEDGMENTS

I wish to express my sincere appreciation to Dr. William H. Corcoran and Dr. Thad Vreeland, Jr. for their encouragement, valuable guidance, and patience throughout the course of the work. I would also like to thank other members of the faculty who helped to advance my education.

The efforts of George Griffith in the Chemical Engineering Shop, and of Erich Siegel and Sig Jenner in the Chemistry Glass Shop were most helpful toward the completion of the research program and are gratefully acknowledged.

Financial support was received from the Department of Health, Education, and Welfare, the Donald Baxter Foundation, and the Institute, and it was deeply appreciated.

The efforts of Mrs. Elaine Tustin, Mrs. Ruth Stratton, Mr. Alvin Illig, and Mr. Gregory Hamill saved me many hours in the preparation of the thesis, for which I am thankful.

Finally, a special thanks to my wife, Wendy, the most important person in my life.

PREFACE

It was felt that an introduction might help to clarify the objective of the thesis, and to indicate the continuity between the first topic on silver and the second topic on zinc. The intent of the project was to transcend the traditional barriers between Chemical Engineering and Materials Science and to look for answers to questions which were in the other's domain. For example, the first project on heterogeneous catalysis is a conventional topic in Chemical Engineering, but usually the catalyst is thought of as a solid with immovable surface atoms. Thus, little interest is developed on changes to the physical properties of the solid because of the interaction with a gaseous phase. Similarly, only a few studies have attempted to measure the effect on reaction kinetics when the surface atoms are moved from their normal crystallographic positions. These questions are examples of the type of information that was sought in this project.

Surface chemistry is the common thread which connects both the work of silver and that of zinc. Both studies investigate changes to the solid and gaseous phases. A simplified statement of the problems would be: The first study asks the effects of dislocations on the surface catalysis, and the second study inquires as to how dislocations can be generated by a surface reaction.

Although many problems were solved in the work, some questions remained unanswered because of the diversity of information in both fields. It did become apparent, however, that more communication will be needed between chemical engineers and material scientists in order to solve the

technologically difficult problems in the areas of catalyst design, corrosion prevention, and chemical effects on the deformation of materials.

ABSTRACT

I. Effect of Dislocations in Silver on the Rate of Oxidation of Carbon Monoxide

An investigation was made to determine the effects of the number of dislocations in a silver catalyst on the rate of oxidation of carbon monoxide. The reaction was catalyzed by the (111) face of several silver crystals which had a dislocation density of either 10^4 cm^{-2} or 10^8 cm^{-2} . Activation of the catalyst was accomplished by alternate treatments of hydrogen and oxygen at 800°F .

The reaction was carried out in a pyrex recirculation reactor with a reactant mixture of 75% carbon monoxide and 25% oxygen. Gas chromatography was utilized to analyze the reactor gases, and about 1% carbon dioxide was produced at 170°F during the time of reaction. Reactor composition data were fitted as a function of time to an expression which was developed from a proposed model of the surface kinetics. The model used the assumptions that there existed adsorption equilibrium and that the rate of formation of carbon dioxide was proportional to the number of carbon monoxide-oxygen sites on the surface.

Results of the study indicated that the greatest change to the rate of reaction was caused by impurities which adsorbed on the catalyst surface. During the study the chemical-etch-pit count of silver was increased after pretreatment with oxygen. However, other measurements showed the dislocation density had remained the same, so comparison of the reaction rates was made for crystals with different initial dislocation densities. This comparison indicated that dislocations did not alter the rate of reaction, thus dislocations were not considered to be the most important catalytic sites under the conditions of this study.

II. A Mechanism for the Formation of Dislocations during the Oxidation of Zinc

A study was made of the changes which occurred to an oxidized zinc crystal. It was determined that the normal oxide film was thin and epitaxial but this film would form many micro-cracks when exposed to an aqueous environment. The rate of subsequent oxidation of the crystal was increased because the cracks formed low energy paths for the zinc to get to the surface. The increased oxidation rate also increased the number of the vacancies in the solid and the vacancies in excess of the thermodynamic value formed dislocations. The dislocations were in the shape of loops and spirals, and were presumed to result from the coalescence of the excess vacancies. Berg-Barrett topography was utilized to view the dislocations and to investigate the Burgers Vector. The information from both the experimental data and the calculations of the configuration with the lowest energy suggested that the Burgers Vector was a full \bar{c} .

As an addendum to the work on zinc, a discussion is included of a chemical etching solution that was developed to reveal dislocations which intersected the basal plane. The chemical solution worked well for surfaces whose orientation was within 0.5° of the basal plane. Evidence was presented which suggested a one-to-one correspondence between dislocations and etch pits.

TABLE OF CONTENTS

I. Effect of Dislocations in Silver on the Rate of Oxidation of Carbon Monoxide	
Introduction	1
Experimental Apparatus	12
Experimental Procedure	17
Results and Interpretation	21
Comparison with Studies in the Literature	36
Summary	39
Recommendations for Further Study	43
References	44
Nomenclature	48
Tables	49
Figures	52
Appendix A. Reactor Design	65
Appendix B. Purification and Analysis of Reactor Gases	75
Appendix C. Pump Design for Recirculation of Gases	81
Appendix D. Specimen Preparation	89
Appendix E. Experimental Data	103

II. A Mechanism for the Formation of Dislocations during the Oxidation of Zinc	
Introduction	158
Experimental Method	161
Experimental Results	163
Discussion	165
Summary	174
References	175
Figures	177
Appendix A	182

LIST OF TABLES

<u>Table</u>		<u>Page</u>
1	Summary of Reaction Rate Constants at 175°F for the Different Single Crystal of Silver	49
2	Effect of the Concentration of Oxygen on the Rate of Oxidation of Carbon Monoxide	50
3	Comparison of Kinetic and Adsorption Constants	51

LIST OF FIGURES

I. Effect of Dislocations in Silver on the Rate of Oxidation of Carbon Monoxide

<u>Figure</u>		<u>Page</u>
1	Schematic of experimental apparatus	52
2	Schematic of reaction zone	53
3	Rate of reaction as a function of the number of oxidation-reduction cycles used to pretreat the silver catalyst	54
4	Photomicrographs of a (111) surface of a silver crystal showing changes in morphology (a) as polished, (b) after use in reactor	55
5	Photomicrographs of etch pits as a function of depth on a (111) surface of a silver crystal heated in oxygen	56
6	Transmission electron micrograph of a foil made from a silver crystal which was heated in oxygen	57
7	Transmission electron micrograph of a foil made from a silver crystal which was heated in oxygen	58
8	Comparison of the calculated concentration profile of oxygen diffusing into silver with the measured etch pit profile	59
9	Photomicrographs of (111) surface as etched to reveal dislocations. (a) low density crystal, (b) high density after 5% strain	60
10	X-ray diffraction topograph with CoK_{α} radiation of a (111) silver crystal which was strained 5%	61
11	Graphical plot of experimental and calculated curves	62
12	Temperature dependence of rate constant, k , from Langmuir model	63
13	Temperature dependence of adsorption constant, K , for carbon dioxide on a silver surface with pre-adsorbed oxygen	64

II. A Mechanism for the Formation of Dislocations during the Oxidation of Zinc

<u>Figure</u>		<u>Page</u>
1	Berg-Barrett topograph of a zinc crystal showing an area with a high density of loop and spiral dislocations	177
2	Three Berg-Barrett topographs of the same area which were taken by rotating the crystal in 120° intervals with respect to the incident beam	178
3	Berg-Barrett topographs with a spiral dislocation near a large loop (a) and a grain boundary (b)	179
4	Berg-Barrett topographs showing loop dislocations near a cleavage step (a) and the outline of a water droplet which was placed on the crystal before the second anneal (b)	180
5	Dislocations in zinc	181

I. A STUDY OF THE EFFECTS OF DISLOCATIONS IN SILVER ON THE
RATE OF OXIDATION OF CARBON MONOXIDE

INTRODUCTION

The economic value of catalysts to the chemical industry makes their study valuable, and catalyst selection can improve with a systematic approach in deciding which parameters define the performance of a catalyst. It is still difficult either to choose a catalyst for a given reaction or to measure the stability and performance of a catalyst in use. The intuitive appreciation of the role of the catalyst surface has given way to a more orderly characterization. The use of modern instruments has led to properly defined catalysts and to a better understanding of the role of defects and impurities on the surface. Experimental measurements by different researchers have not always agreed, and further work is needed to characterize catalysts, to allow a common basis for comparison of experimental data. This thesis attempts to improve the understanding of the role of dislocations in single crystals of silver on the rate of the catalytic oxidation of carbon monoxide and to give further insight into the parameters of the catalyst that must be understood for comparative purposes.

Silver Catalysts

Silver was the catalyst selected for this work because previous studies indicated that the rate of reaction on silver was related to the dislocation density. Silver catalysts also have commercial importance in the manufacture of ethylene oxide. The mechanism of producing ethylene oxide from a gaseous mixture of ethylene and oxygen is still not understood, although many attempts (1-8) have been made. It was generally assumed that silver was a good oxidation catalyst because of

the formation of a unique and reactive oxygen-silver complex on the catalyst surface. A goal of the study was to improve the understanding of the oxygen-silver interactions. The ethylene-oxygen reaction, although attractive, was not selected because of its apparent complications, and instead, the oxidation of carbon monoxide was studied. Justification for this choice is discussed after a consideration of other silver-oxygen interactions.

Silver-Oxygen Interactions

Interactions between silver and oxygen have been observed over a wide temperature range. For example, the surface tension of molten silver was three times lower in air than in vacuo. Below the melting temperature, a flat silver surface became etched either on exposure to oxygen (9,10) or when used as a cathode in a discharge with oxygen (11). The morphological changes suggested that silver was chemically sensitive to oxygen molecules and, in fact, stable silver oxide compounds (12,13) can be formulated. Ag_2O and AgO exist below 200°C at one atmosphere oxygen pressure (12,13) and presumably can be formed by the diffusion of oxygen into the silver lattice.

The recent experimental measurements for the diffusion coefficient and solubility of oxygen in silver give about the same values. Verfurth (14) established from his studies that diffusion was rapid and that the activation energy was 11.0 kcal. The low value suggested that diffusion of oxygen took place over interstitial sites. He measured the solubility to be 2 ppm by volume at 400°C and 50 ppm by volume at 800°C . By comparison with hydrogen (65) at 800°C , diffusion was as rapid but the

solubility of hydrogen was an order of magnitude lower. Other changes in the physical properties of the silver were also related to oxygen diffusion into the silver lattice.

In 1974, Ehrlich (15) reported that the residual resistivity ratio in silver increased by three orders of magnitude after a low oxygen pressure (10^{-6} torr) anneal. His explanation relied upon the precipitation of impurity oxides and the increase in the mean free path of electrons. He also found the hardness of the silver to increase during the treatment, but he gave no reason for the change.

In summary, silver does have an affinity for oxygen, and the diffusion of oxygen into the silver lattice resulted in chemical and physical changes to the silver. The diffusion of oxygen into silver was preceded by the adsorption of oxygen on the surface.

Adsorption of Oxygen on Silver

Adsorption of oxygen on silver has generated much interest because it is recognized as the important precursory step in the formation of a reactive silver-oxygen complex. The process of adsorption is complicated and experiments that were carried out forty years ago are being repeated today with more sophisticated equipment. Benton and Drake (16) made an early study of the interaction between oxygen and silver powder over a range of temperatures. They concluded that both physical adsorption and chemisorption took place. A similar conclusion for the high temperature region was reached by Smeltzer (17).

The silver powder used in the earliest oxygen adsorption measurements was replaced by single crystals as more fundamental criteria

were sought. Kummer (18) measured the work function of silver crystals and noticed a change when the silver was exposed to oxygen. He stated that about 5% of the silver surface was covered with O_2^- . Degeilh (19) also found a change in the work function of silver upon exposure to oxygen and he further remarked that oxygen would not adsorb unless the surface was clean. The exchange of oxygen isotopes was also used to study the adsorption process.

Sandler and Durigon (20-22) found the isotope exchange reaction was very slow below $150^\circ C$ but above that temperature it was reversible. They noticed residual oxygen was retained by the silver and that the rate of exchange was faster than the rate of desorption. They were unable to detect a paramagnetic species of oxygen on the surface and thus concluded that its existence would be one of short lifetime and low concentration. Other studies (23,24) utilized the isotope exchange reaction and the investigators found similar results.

Over a period of ten years, Czanderna (25-31) published his measurements with a micro-balance of the interactions between silver powder and oxygen. He also investigated the effects of hydrogen, ethylene, carbon dioxide, and carbon monoxide on a reproducible oxygen-silver surface. He made reproducible surfaces for adsorption studies by cyclically oxidizing and reducing the silver. From the studies, he suggested that there existed five levels of strength of the silver-oxygen bonds, from physically adsorbed to very tightly chemisorbed. He noted that the activation energy was a function of the coverage and that the problem of oxygen adsorption on silver was complicated. The question of the level of impurities on the surface during the adsorption was

attacked in the 1960's by the use of equipment capable of detecting changes in the surface properties of a specimen under an ultrahigh vacuum.

Steiger et al. (32) studied single crystals of silver in an ultrahigh vacuum with low-energy-electron diffraction (LEED) and ellipsometry. They encountered problems with etching of the silver surface when the oxygen was introduced. A question was later raised (33) as to whether impurities in the system reached the silver surface and interfered with the measurements. Wood (64) also used an ultrahigh vacuum apparatus for his measurements of the change in flux of oxygen atoms through a chamber with and without a silver film. He found the silver was quite efficient at adsorbing or occluding the oxygen atoms on its surface.

Clarkson and Cirrillo (34,35) attempted to identify the chemical state of the adsorbed oxygen with electron paramagnetic resonance and found a resonance in the field strength where O_2^- is expected. Their signal increased with exposure to oxygen and was partially removed by reduction with carbon monoxide. Schmidt (36) and Jansen (37) used a field ion microscope which was another instrument that contained the specimen in ultrahigh vacuum while the surface was monitored. Schmidt was not able to detect any silver-oxygen compounds coming from the surface. Jansen studied the interactions of silver and nitrous oxide and concluded that two forms of oxygen were adsorbed on the surface. Even containment in ultrahigh vacuum did not assure that the surface was not contaminated, and so the availability of Auger equipment in the 1970's gave the impetus for new studies.

Rovida et al. (38) employed low-energy-electron diffraction, Auger spectroscopy, and work function measurements during the adsorption of oxygen on silver single crystals. They observed the surface to facet with exposure to oxygen, and upon flash desorption peaks were noted in the pressure of oxygen in a mass spectrometer for specimen temperature of 280 C and 500 C. The later peak was associated with diffusion of oxygen from the bulk. Bradshaw et al. (39) used similar equipment and concluded that adsorption of oxygen was activated. They correlated a change in the work function of silver to a change in the low-energy-electron diffraction pattern. Oxygen diffusion into the bulk was not ruled out and, in fact, in their work they considered the change in work function might be explained by oxygen passing through to bulk or to immediate sub-surface regions. They proposed a dissociative chemisorption mechanism for the oxygen. In a later note (40) the authors demonstrated that even as careful as they were with their initial observations, interference from residual carbon monoxide in the apparatus could have caused the measurement of work function to be in error. Dweyari (41) found a similar change in the work function while studying a different crystallographic plane of silver.

In summary, the mechanism of the oxygen adsorption on silver is not well understood, and it is apparent from the large number of studies that the problem is complicated. As more data were taken, the awareness of other problems surfaced, and even with systems equipped with the best modern instruments, not all of the difficulties were removed. In general, the investigators concluded that the mechanism of adsorption went from physically adsorbed at low temperatures to dissociative

activated adsorption at higher temperatures. Neither the existence of the paramagnetic species, O_2^- , nor the interaction of the adsorbed oxygen with the bulk was ruled out. Only with a meticulous program of experiments will the global picture of oxygen adsorption on silver be understood. That knowledge might still be different from a complete understanding of how the silver-oxygen complex reacts in the presence of a reducing gas such as ethylene oxide or carbon monoxide.

Oxidation of Carbon Monoxide over a Silver Catalyst

The oxidation of carbon monoxide allows one to study the silver-oxygen interactions under reaction conditions which are not as complex as in the case of ethylene oxide formation. Benton and Bell (42) found the rate expression to be first order in carbon monoxide and zero order for carbon dioxide and oxygen. Yamada (43) found the state of reduction of the silver surface was important. Recently, Keulks and Chang (24) investigated the kinetics under the same conditions of temperature and pressure as Benton and Bell, but found the rate was directly proportional to the concentration of the carbon monoxide and inversely proportional to the concentration of carbon dioxide.

Studies of the adsorption of carbon monoxide or carbon dioxide on silver determined that the silver surface must be covered with oxygen for adsorption to occur. The reaction of carbon monoxide on silver covered with oxygen had a resonant peak in the infrared spectrum (44-46). It was learned that the observed resonance was due to the C-O stretching frequency of the carbon monoxide molecule and not to a stretching frequency involving the oxygen attached to silver. Another

study (24) with isotopes of carbon dioxide measured the interaction between a surface covered with $^{18}\text{O}_2$ and C^{16}O_2 and found no exchange. However, homonuclear exchange occurred over oxygenated silver surfaces between C^{16}O_2 and C^{18}O_2 suggesting the formation of a C_2O_4 complex. Results on silver agreed with the earlier work of Smith (47) on copper.

Dislocations as Active Sites

The existence of active sites has been an important concept since first hypothesized by H. S. Taylor. Numerous examples of active sites have been proposed and one of them is the intersection of dislocations at the surface. The intersection of a dislocation with a surface can usually be revealed with chemical etching (48) because of the difference in the chemical activity of the atoms at the core of the dislocation and that of the remaining surface. The difference in chemical potential of a dislocation and the range in the number of dislocations that can intersect a surface (10^2 - $10^{12}/\text{cm}^2$) suggested that their effect on the catalytic activity of a surface be investigated.

Eckell (49) used polycrystalline nickel as a catalyst for the hydrogenation of ethylene and found the rate increased by two to three orders of magnitude when the metal was plastically deformed by cold working. Cratty and Granato (50) later attributed the increased catalytic activity to dislocations. Uhara and associates (51-54) studied several cold-worked metals as catalysts and reached the conclusion that the active sites were the surface terminations of dislocations. The result became evident to them when the reaction rate decreased at the annealing temperature. Criado (55) obtained a similar result with the

measurement of rate of ortho-para-hydrogen conversion over a nickel-chromium-iron alloy. Methods other than rolling were employed to change the dislocation density.

Sosnovsky (56) investigated the catalytic activity of silver crystals after bombardment with positive ions and decided that the reactions occurred at sites where dislocation lines intersected the surface. It was later related by Thomas (57), however, that it was no longer legitimate to explain the results entirely in terms of dislocations, for there was some doubt as to whether the energies of the ions were sufficient to introduce dislocations. Bragg et al. (58) and Jaeger (59) investigated the influence of defects in silver on the catalytic decomposition of formic acid, but found none and concluded that dislocations did not function as active sites. Perkins (60) obtained the same conclusion with bulk crystals of silver and the same reaction system.

Robertson (61) presented the results of a series of experiments where the catalytic decomposition of formic acid was measured over nickel. Early results gave indications of a superactivity due to trapped vacancies which were introduced by quenching. However, later experiments did not substantiate that conclusion, and demonstrated the effect of impurities could easily mask any effect from the vacancies. Impurities were also found to mask the effects of dislocations introduced by twisting the wire in a very high vacuum apparatus. Some studies directly measured the dislocation density, but the different investigators did not reach the same conclusion as to the effect of dislocations.

Hall and Rase (62) found a considerable increase in the rate of the dehydrogenation of ethanol with an increased dislocation density in single crystals of lithium fluoride. They measured the dislocation density by the chemical-etch-pit technique. Woodward et al. (63) also used the chemical-etch-pit method, but found the opposite effect of dislocations in silver crystals on the partial oxidation of ethylene. They attributed the result to a stronger silver-oxygen bond. Recently Grenga (67) studied nickel foils in a transmission electron microscope and found that nucleation sites from the catalytic decomposition of carbon monoxide did not preferentially correspond to dislocations, stacking faults or surface imperfections.

There is good reason to suspect that dislocations may have an effect on surface reaction because of a change in geometric and electronic factors in the metal. The data collected to date must be scrutinized to decide whether the results obtained were from contaminated dislocations. Contamination effects may produce great complications when experiments are carried out to investigate active sites, but in many papers they were not considered, and hence any effects found were ascribed to the various treatments.

Summary

A review of the literature indicated that further information was needed about the role of dislocations in a catalytic reaction, and about interactions between silver and oxygen. The reported differences in the chemical rate data and the various oxidation mechanisms for carbon

monoxide also invited further study. Based on the foregoing, it was determined that a study should be undertaken with emphasis in the following areas:

1. Obtain chemical rate data for the oxidation of carbon monoxide on the (111) surface of a single crystal of silver. The reactor design should minimize both the effects of heat and mass transfer and catalyst poisons on the rate data.
2. Observe the physical and chemical interactions of oxygen with the silver surface.
3. Find the effect on the chemical rate when the density of dislocations intersecting the surface is increased by several orders of magnitude.

EXPERIMENTAL APPARATUS

In assembling the apparatus for this project, special attention was given to the choice of reactor and to the preparation of the catalyst. This section discusses only the final equipment which was utilized in the measurement of the reaction data. Details about earlier designs and the particulars for the final equipment can be found in the appendices. Figure 1 is a schematic of the experimental apparatus.

Reactor

The choice of reactor was considered a key element in the project and some preparatory efforts were expended before making the selection. Preliminary reaction studies indicated the significance of the effects of transport limitations and catalyst poisons on the reaction rate. The problem with catalyst poisons was resolved in the final design by choosing only either metal or glass for materials of construction. Interconnections between metal tubes were done with soldering, and Kovar was used to link the glass to the metal. Admittedly, there was difficulty in fabricating some parts, but the efforts were rewarded with a more reproducible rate constant. The effects of transport limitations were minimized by the choice of a "gradientless" reactor (66).

The recirculation reactor system used total internal recycle and was representative of a well-mixed batch reactor. It was constructed solely of glass and consisted of a pump and a heated reaction zone. The pump operated at room temperature and was especially designed for the reactor (Appendix C). It had an adjustable flow rate and was

usually operated near the maximum output of 8ℓ/min. The design of the heated reaction zone was another issue.

The reactor was preceded by a spiral preheater for the reaction gases, and both were enclosed by a pyrex jacket as shown in Figure 2. The catalyst, a disk-shaped crystal of silver, was suspended in the reactor just above the exit of the preheater. The reactor segment which contained the catalyst was built with a thin rectangular cross-section in order to increase the Reynolds Number in the vicinity of the catalyst. Unfortunately, the catalyst could only be removed by cutting the glass. The pyrex jacket and reactor-preheater were warmed by positioning them in a vertical tube furnace.

Heated air with a high mass flow was circulated inside the pyrex jacket to make the reaction zone isothermal. The temperature was regulated with a proportional controller which was backed up by an "on-off" controller. The second controller was adopted as a safety measure to prevent possible explosions from a temperature runaway. The temperature in the jacket and near the catalyst surface was monitored with calibrated thermocouples of chromel-alumel. An indent was placed in the glass reactor to get the thermocouple near the catalyst surface. This couple activated the temperature controller and its output was continuously recorded on a strip recorder with a full-scale deflection of 1.0 millivolt.

Reactor Gases and Vacuum Systems

The as-supplied cylinders of hydrogen, oxygen and carbon monoxide were further purified to remove catalyst poisons before going to the reactor (Appendix B). The gas went from the cylinder to the manifold.

Installed in the manifold were a mercury manometer and a thermal conductivity gauge to measure pressure at either atmospheric or near vacuum. The mercury in the manometer was isolated from the manifold by a valve and a cold trap. Several vacuum pumps were also incorporated into the equipment.

A mechanical roughing pump was connected directly to the manifold and to the reactor after opening a second valve. The pump could reduce the pressure in either the reactor or manifold to below 10^{-2} torr. The pressure of the reactor was lowered further to 10^{-6} - 10^{-7} torr with an oil diffusion pump. High vacuum valves were necessary to isolate the reactor under vacuo from the manifold and gas sampling section. A cold trap was situated between each of the vacuum pumps and the reactor to reduce the backstreaming of pump oil.

Analytical Equipment

Gas chromatography was chosen as the method to measure the change in concentration of the reactant and product gases. Two areas of concern arose when interfacing the equipment with the planned experiments. The first centered on getting an accurate measurement of the gas composition, and the second was obtaining representative samples from the reactor. It was decided to base the chemical analysis on carbon dioxide, since it had the greatest percentage change in concentration. Several chromatographic columns were tested for sensitivity to carbon dioxide and Porapak T appeared to be the best (Appendix B). The measurement of the low concentrations of carbon dioxide after reactor start-up was difficult and so the electrical output of the thermal conductivity detector was amplified before being recorded. The use of the

amplifier plus the installation of a low noise power supply for the detector circuit were responsible for an increased sensitivity and stability in the purchased chromatograph. Placing a representative sample from the reactor into the gas chromatograph was another topic.

A gas-sampling valve was used to remove a sample from the gas stream and inject it into the chromatograph. The valve is commonly placed in-line for flow systems, but that scheme was not used in this project because the materials used to make the valve seals could poison the catalyst. Instead, the gas sample loop was evacuated and opened to the reactor when acquiring a sample. In order to obtain a representative sample of the reactor, the dead space in the sample line was minimized by extending the sample line from the valve at the reactor to the main gas stream. The reactor sample was fed from the sample loop into the chromatograph and analyzed. Calibration curves were prepared from known concentrations of carbon dioxide and the curves are presented in Appendix B.

Catalyst Preparation

The preparation and characterization of the catalyst was as important as assembling the equipment for the reactor. The plan was to use a single crystal of silver with a controlled dislocation density as the catalyst. The crystals could not be purchased with a low dislocation density, and so were grown from high-purity silver (99.999%) in cylindrical graphite molds. The as-grown single crystals were sawed and polished into thin disks with special equipment that maintained the low dislocation density. Before beginning to machine, the crystal was aligned with a back-reflected Laue so the faces of the discs were within $\pm .25^\circ$ of the (111) plane. After the disk was flat, a hole was

spark-cut into one end so it could be suspended in the reactor. The disk was then ready for the reactor, but first some physical characteristics were measured.

The dislocation density and the geometric area were two values that would later be needed when correlating the chemical rate data. The number of dislocations intersecting the face of the disk was found by chemically etching the silver and counting the number of etch pits under an optical microscope. The Berg-Barrett X-ray diffraction method was used for studying isolated dislocations and the surface topography. The geometric surface area was obtained by taking a low magnification photograph and mechanically integrating the circumference. Optical microscopes and metallographs were routinely employed between magnifications of 10X and 1000X to study the surface of the catalyst. Equipment that was sparingly used included the microhardness tester, an electron microprobe, scanning electron microscope, and transmission electron microscope. Details about the preparation procedures for the catalyst are found in Appendix D.

EXPERIMENTAL PROCEDURE

The experimental design called for comparing the rate of oxidation of carbon monoxide over the (111) face of silver with various dislocation densities. In the final experiments only two densities were studied, 10^4 dislocations cm^{-2} and greater than 10^8 dislocations cm^{-2} . The latter high density was obtained by cold-rolling the specimen until it was strained by 5%. The experiments began by shaping the single crystal into a disk as described in the section on apparatus and by measuring its area and dislocation density. The catalyst was then ready for reaction studies.

Activation of the Catalyst

The prepared catalyst was connected with a silver "S" hook to a quartz rod and suspended in the reactor. It was necessary to cut the pyrex reactor to hang the crystal, and while open, the reactor was rinsed with a cleaning solution. The reactor was cleaned each time a catalyst was changed to prevent impurities from accumulating on the glass. After the catalyst was in the reactor the break in the pyrex pieces was heated and fused together. The temperature of the furnace was raised to 300°F in preparation for the activation of the catalyst.

The equipment was evacuated with the diffusion pump until the pressure fell below 10^{-6} torr, and it took overnight if the reactor was opened to the atmosphere. Once the pressure was reached, the system was assumed to be outgassed and the reactor was isolated from the diffusion pump. Presumably, the outgassing took a long time because of the multiple layers of water and hydrocarbons that adsorbed on the glass when it was

opened to the atmosphere.

The temperature of the furnace was set at 800°F and oxygen at one atmosphere pressure was recirculated through the system for one hour. The temperature was lowered below 400°F and the oxygen was removed from the reactor and replaced with hydrogen. As before, the hydrogen was recirculated for one hour with the catalyst at 800°F. After several cycles of oxygen-hydrogen treatments the silver was tested for its catalytic activity.

Chemical Reactor Studies

After the last hydrogen treatment, the flow of preheated air was increased to 18 l/min in the glass jacket of the reaction zone, and the temperature was lowered from 800°F to the reaction temperature. It was estimated that a reaction temperature of 170°F represented a good balance between the effects of transport limitations with a high reaction rate and the analytical difficulties with a low reaction rate. However, the selected temperature was too low for the proportional controller to function properly. To overcome that difficulty, the thermocouple output was displayed on a chart with a full scale reading of 1.0 millivolt, and the temperature was manually controlled. Temperature fluctuations during the experiment were regulated to $\pm 2^\circ\text{F}$, or about 5% of the full scale reading on the chart. After the temperature was stabilized and the reactor was evacuated to a pressure of 10^{-6} torr, the reactants were admitted.

Carbon monoxide was added to the reactor until the pressure reached 570 torr. It was then evacuated from the manifold and replaced

by oxygen. The oxygen was forced into the reactor to raise the pressure to atmospheric and the pump was initiated to recirculate the gases through the reactor at 8 l/min. A clock which displayed the extent of reaction time was also started and read each time a sample was withdrawn from the reactor for analysis. The samples were periodically pulled from the reactor and analyzed with a gas chromatograph for the concentration of carbon dioxide. Each analysis took less than three minutes.

After a reaction time of about one hour, the reactor was evacuated and prepared for another run. If the reactor was not opened to the atmosphere before the second experiment, then only one oxygen-hydrogen cycle was sufficient to prepare the catalyst. After several determinations of the chemical rate data under similar experimental conditions, the silver catalyst was removed from the reactor by cutting the pyrex and withdrawing the quartz rod.

Inspection of the Used Catalyst

The surface of the catalyst was examined with an optical microscope and photographs were taken with a metallograph of any changes to the morphology from the reaction. Berg-Barrett X-ray diffraction topographs were sometimes used to search for changes. The silver crystals were given a light electropolish and chemically etched to check the dislocation density to see if it had remained constant during the reaction. Some specimens were further probed by measuring the Vickers Hardness; others had their distributions of defects investigated with a transmission electron microscope. The measured physical properties of

the silver crystals were saved for later correlation with the rate of the chemical reaction.

Analysis of Data

A chemical model was needed to calculate a rate constant that could be correlated with the different properties of the catalyst. Several nonlinear expressions from the assumed models were tested for the fit on a computer using the composition data from the reactor. The composition data were extracted from the chromatograms. Both the height of the carbon monoxide-oxygen peak and the carbon dioxide peak were stored on punched cards with other measurements from the experiment. The height of carbon monoxide at 750 mm pressure served as a standard for all experiments and was used to correct the value of the height of the carbon dioxide peak. An average temperature was obtained by integrating the thermalgram and dividing by the reaction time. The calculated rate constant from this work was later compared with the results of other investigators who studied the same reaction.

RESULTS AND INTERPRETATION

Independent Variables in the System

A rigorous interpretation of the results from the reaction studies was preceded by an understanding of the many parameters on which the rate constant depended. It was not possible to precisely control the parameters, so the effect which each of them had on the rate constant had to be known. For most parameters it was possible to estimate the sensitivity of the rate constant for a deviation of the parameter from its set point. The parameters of interest in this study were:

1. Temperature of the reactor and catalyst.
2. Flow rate through the reactor and catalyst.
3. Composition of the initial gas mixture.
4. Analysis of the products with gas chromatography.
5. Limitations of both heat and mass transfer in the reactor region.
6. Rate of the homogeneous reaction.
7. Purity of the materials of construction.
8. Purity of the reactant gases.
9. Effects related to the silver crystal:
 - a) Surface morphology.
 - b) Crystallographic plane exposed to the reactant gases.
 - c) Number of dislocations intersecting the surface.
 - d) Purity level of the silver surface.

It was ascertained for most parameters by either a calculation or experiment that the error in the measurement of the rate constant was less than three percent, thus little time was spent in refining the control of this group. From earlier trials it became evident that the silver catalyst was being rapidly poisoned by unknown impurities in the system and a search was made for them in both the supply gas and the materials of construction.

Hydrocarbons were suspected as being the most likely poison, since they could form a carbonaceous deposit on the silver. Methane and n-butane were found in the supply carbon monoxide, but only the butane was removed since the calculated rate of carbon formation from methane was too slow to affect the kinetics. The importance of removing the butane was once demonstrated when the molecular sieve column became saturated and the rate of reaction went to zero. Anxiety over the purity of the construction materials for the reaction was also warranted. It was shown that the use of either silicone grease on glass joints or plastics in the system would poison the catalyst in a matter of minutes. Only when the last Viton o-ring was removed from the apparatus did the reaction rate become reproducibly high.

Considering that Viton has a vapor pressure of 10^{-7} torr at room temperature and will poison the catalyst in a matter of minutes, it is apparent that the small area of the catalyst (10 cm^2) amplified the effect of impurities. Since the surface areas that are normally employed in catalytic studies are larger by factors of 10^3 - 10^5 times, the problem might not be observed, as the available working time would be multiplied by the same factor. It was interesting to notice that as

the poisons were removed the rate of reaction was increased by five orders of magnitude. Unfortunately, the experimental design afforded little opportunity to measure the purity of the catalyst surface, and only a high chemical rate constant assured one that the catalyst was not poisoned.

Catalyst Activation

Alternate treatments of hydrogen and oxygen were adopted to obtain a reproducible catalyst surface because of the success found by earlier researchers (3,24,25). Presumably, the high temperature treatments with hydrogen reduced both the oxides and sulfides on the catalyzed surface. The treatment with oxygen combusted the hydrocarbons and residual silver cyanide (from the electropolish), however, the silver was not catalytically active after an oxygen treatment. Kummer (3) had also noted a loss in catalyst activity after heating a silver catalyst in oxygen.

It was demonstrated that each time the pyrex system was opened to the atmosphere, a minimum number of cycles was necessary to clean the catalyst surface. Figure 3 presents a plot of chemical rate constant as a function of the oxidation-reduction cycle. Seven oxidation-reduction cycles were needed to remove impurities from the catalyst and reactor.

Reaction on First Single Crystal

Polycrystalline foils of silver were used during early trials as they were easier to handle and prepare. The results indicated that several data sets were required because the magnitude of the standard

error was about 20%. With some control over the problem of poisoning, a single crystal of silver with a low dislocation density ($5 \times 10^4 \text{ cm}^{-2}$) was prepared and carefully inserted into the reactor. Several experiments were carried out following the procedure already described. The crystal was removed from the reactor and it appeared shiny and clean to the eye. However, upon further examination it was evident that the surface was etched, the etch-pit density had increased four orders of magnitude, and the Vickers Hardness went from 18 to 24. Figure 4 shows a comparison between a polished crystal ready for use in the reactor and an etched surface after reaction. An etched surface was expected, as others (4,10) had noted the effect. The increase in the etch pit density was not anticipated, and several possible explanations were examined:

1. It was a surface effect and would disappear with polishing and etching in depth.
2. The pretreatment at high temperature had created thermal stresses which generated dislocations.
3. The single crystal was damaged by an applied stress.
4. Either there was no longer a one-to-one correspondence between the etch pits and the dislocations, or the dislocation density had increased by another mechanism.

The crystal was polished and etched in depth, but no change in etch pit density was found. A calculation of the thermal gradient was made and it indicated that thermal stresses were not the cause. Next, it was considered that dislocations were introduced while handling the soft crystal. Berg-Barrett X-ray topographs were taken to look for

slip bands near the edge of the crystal, but none were found. Thus it appeared that a change had occurred between the correspondence of etch pits and dislocations. The specimen was thinned and examined with a transmission electron microscope, and the dislocation density was less than 10^5 cm^{-2} . The result suggested the initial etch pit density was accurate and that there was no longer a correspondence between etch pits and dislocations after being in the reactor. Experiments were planned to investigate the effects of the pretreatment on the crystal.

Effects of Pretreatment

A second single crystal with a low dislocation density was heated in hydrogen, but the treatment changed neither the morphology nor the etch-pit density of the crystal. However, the results were different after the crystal was repolished and set in the furnace for one hour with an oxygen atmosphere. Upon removal of the crystal it was noted that the surface was etched and the etch pit density had increased by an amount similar to that of the first crystal from the reactor. It was now evident that the etch pit density did not correspond to the dislocation density after the oxygen treatment.

The second crystal was thicker than the first and was exposed to oxygen for a shorter time. Chemical etching was repeated in depth to measure the etch pit density and results are presented in Figure 5. The figures showed that the density of etch pits was reduced in depth and approached that of the initial dislocation density. The etch pits appeared larger than those of fresh dislocations and the variations are seen in Figure 5e.

Transmission electron micrographs were taken of the crystal that was heated in oxygen, and again the dislocation density was lower than the etch-pit count. The electron micrographs, Figures 6 and 7, were from two different treated crystals, and both exhibited many small black dots whose number per unit area was about the same as the number of chemical etch pits. It appeared as though the chemical solution was actually etching an inclusion in the silver matrix.

Justification for the Etch Pit Change

The following explanation was proposed to account for the observations after a crystal was heated in oxygen. While at 800°F, a gradient of oxygen was established in the crystal based on the solubility and diffusion coefficient. Then the silver was cooled rapidly as compared with the rate of oxygen diffusion out of the silver, and because the lattice had an excess of oxygen, a silver-oxide phase was nucleated. The second phase grew in the silver lattice with a different crystallographic structure and generated misfit dislocations on the interface of the oxide-silver matrix. The oxidized crystal was next heated in hydrogen, and the silver oxide particles were reduced. Even though the oxide was reduced, the silver lattice did not completely anneal, and interfacial dislocations remained where the particles were previously located. These dislocations were responsible for the observed increase in Vickers Hardness and were also probably the sites of the etch pits when the crystal was chemically etched after the oxygen pretreatment step.

As previously noted, the etch figures of the treated crystal were not the same as those of fresh dislocations, in fact, it appeared

as though the treated dislocations did not etch. When heated with oxygen, the dislocations in the crystal quickly became saturated with oxygen since they were paths for pipe diffusion. Upon cooling, the cores of the dislocations acted as one of the nucleation sites for the growth of an oxide particle, thus the pit revealed by the chemical dissolution was that of the oxide and not that of an undecorated dislocation. An indication that this process occurred was that the density of etch pits in an oxidized crystal was reduced to the original dislocation density when the crystal was etched in depth. Further tests were made to find support for the proposed growth of a silver-oxide phase.

A thin film X-ray diffraction camera was utilized to examine the changes in the diffraction pattern of silver before and after oxygen treatment. No oxides were indicated on the diffraction patterns even for an exposure to the CuK_{α} source of four times the normal rate. The result was interpreted to mean that the particles were too small to provide coherent scattering. In another experiment with an electron microprobe, an oxidized specimen was examined for the presence of the O K_{α} wavelength and a shift in wavelength for the silver M band. No new information was gained, however, since the resolution of the instrument was poor for wavelengths around 20\AA . Thus, the observed increase in Vickers Hardness and the black dots on the transmission electron micrographs were the best available physical evidence to justify that the growth of an oxide phase caused the change in the chemical etch.

The photomicrographs of the etch figures as a function of depth (Figure 5) were examined for additional information. A plot was

prepared of the relative concentration of oxygen in depth and of the relative etch pit density. The oxygen curve was calculated with the data of Verfurth (14) and plotted in Figure 8. The curves of Figure 8 were in the expected order, as they indicated that oxygen diffused faster than the oxide particles grew. No attempt was made to model the growth of the oxide phase because of the limited data.

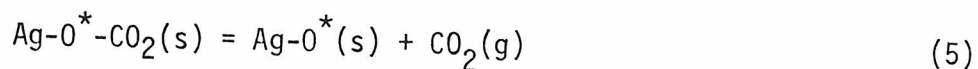
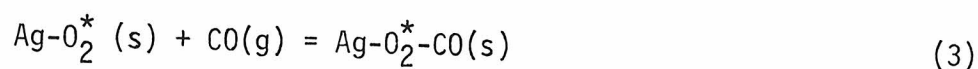
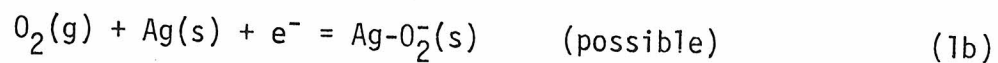
Oxidation of Carbon Monoxide

The question of why the density of etch pits changed during the reaction seemed answered by the discovered interactions between the silver catalyst and the oxygen atmosphere during pretreatment. However, it was not possible to achieve the highest catalytic activity from the silver without oxygen pretreatment. Thus the dislocation density was measured before the catalyst was treated with oxygen.

Catalysts with a dislocation density of either 10^4 - 10^5 cm^{-2} or 10^8 - 10^9 cm^{-2} were used in the experiments. Figure 9 is a photomicrograph showing both densities for comparison. A catalyst which was cold rolled prior to its use in the reactor is illustrated in a Berg-Barrett topograph (Figure 10) and the expected high number of slip bands was found in the figure. After the dislocation density of the silver crystal was established, the rate of oxidation of carbon monoxide was measured over the catalyst. Detailed results of the experiments were tabulated in Appendix E.

An attempt was next made to relate plausible kinetic mechanisms of the surface catalysis with the data from the reactor. A goal of the project was to elucidate the surface catalysis and to develop the role of the oxygen-silver bonds in the catalytic activity. The following

mechanism was proposed after a thorough review of the adsorption and kinetic behavior of the silver-oxygen system:



The mechanism presumed that both the carbon dioxide and carbon monoxide adsorbed on a silver surface already covered with oxygen, as had been observed in all previously reported adsorption studies. This set of chemical expressions were mathematically formulated so the rate of formation of carbon dioxide was calculated as being proportional to the fraction of the surface that was covered by the intermediate $Ag-O_2^*-CO(s)$. The fraction was calculated with the assumptions that the adsorbents did not interact and that equilibrium existed between the adsorbed and gaseous phases. The total fractional coverage was unity and equal to the sum of the individual coverages.

$$1 = \theta_{Ag-O_2^*-CO} + \theta_{Ag-O^*-CO_2} \quad (6)$$

The individual coverages were calculated with the mentioned assumptions and for the coverage of interest:

$$\theta_{\text{Ag-O}_2^*-\text{CO}} = \frac{K_{\text{CO}} n_{\text{CO}}}{(1 + K_{\text{CO}} n_{\text{CO}} + K_{\text{CO}_2} n_{\text{CO}_2})} \quad (7)$$

In equation (7), K_i was defined as the ratio of the adsorption rate constant to the desorption rate constant. The expression for the rate of formation of the carbon dioxide was:

$$\frac{dn_{\text{CO}_2}}{dt} = k_s \theta_{\text{Ag-O}_2^*-\text{CO}} = \frac{k_s K_{\text{CO}} n_{\text{CO}}}{(1 + K_{\text{CO}} n_{\text{CO}} + K_{\text{CO}_2} n_{\text{CO}_2})} \quad (8)$$

The three adjustable parameters in equation (8) were fitted to the experimental data with a computer program which used a non-linear least squares routine. The best-fit parameters indicated that the contribution of the term $K_{\text{CO}} n_{\text{CO}}$ in the denominator was less than 1% of the total sum. Since an additional degree of freedom did not seem justified, the term $K_{\text{CO}} n_{\text{CO}}$ was omitted in further calculations. The modified expression was:

$$\frac{dn_{\text{CO}_2}}{dt} = \frac{kn_{\text{CO}}}{1 + K_{\text{CO}_2} n_{\text{CO}_2}} \quad (9)$$

Equation (9) was integrated over the limits of the first measured concentration of carbon dioxide to the final value. The total conversion of carbon monoxide was less than 1%, so its concentration was assumed to remain constant in the integration. The integrated expression that was utilized in further curve fits was:

$$\frac{1}{k}(n_{\text{CO}_2} - n_{\text{CO}_2}^0) + \frac{K}{k}(n_{\text{CO}_2}^2 - n_{\text{CO}_2}^0{}^2) = tn_{\text{CO}}^0 \quad (10)$$

Composition and time data were entered into a computer, and the parameters (k, K) of equation (10) were calculated from the experimental data using a non-linear least squares analysis. When examining the best-fit parameters, it became apparent that the adsorption constant, K , was different for crystals with dissimilar areas. From a physical viewpoint, however, the adsorption constant should have been independent of area. The dependence of the adsorption constant on the area of the crystal occurred because the basis of the initial regression was the minimization of the likelihood function and not the physical situation. Thus, an average value of the adsorption constant was figured from the calculated values on the various crystals. The average value for the adsorption constant was substituted into equation (10) and values of the surface constant, k , were recomputed from the experimental data and are presented in Table 1.

In the calculations, the concentration of carbon monoxide was adjusted for a constant sample size by employing the peak height of the carbon monoxide-oxygen peak as a standard. Corrections to the surface rate constant, k , were made in order to account for the initial concentration of carbon monoxide and the area of the catalyst. No correction for the homogeneous reaction was required because its rate was negligible for the conditions of the study.

Effect of Oxygen and Temperature on the Chemical Rate

The effect of oxygen on the rate of reaction was tested by using a concentration of oxygen at 10.5% (molar) instead of the usual 25%. No change was found in the rate constant, thus the omission of oxygen in the rate expression appeared correct for the conditions of this study.

Results of the oxygen test are presented in Table 2.

The temperature of the reactor was difficult to set and it was established by allowing the reactor to cool after the hydrogen treatment to an equilibrium temperature for a fixed manual setting on the power control. As a result, rate data were commonly measured for several temperatures about a mean value. Values for the temperature were also purposely set higher and lower than the usual mean, in order to measure the effect of temperature on the rate. The calculated values of the adsorption constant, K , and the rate constant, k , were fit to an Arrhenius expression and the results are presented in Figures 12 and 13.

$$K = 1.11 \times 10^{-11} \exp(17,256/RT) \text{ mm}^{-1} \quad (11)$$

$$k = 0.272 \exp(-6,465/RT) \text{ min}^{-1} \text{ cm}^{-2} \quad (12)$$

Effects of Dislocations on the Chemical Rates

The role of dislocations in understanding mechanical strength and plasticity is well established, but only recently has the importance of dislocations on a catalyst surface been systematically explored. The catalysts used in this study were single crystals of silver with the (111) face exposed to the reactants and had two different dislocation densities. About 10^{15} atoms/cm² are found on a perfect (111) surface but many imperfections are part of a crystal surface. Two imperfections that might be possible active sites for catalysts to occur are the atoms on the edge of a step and the core atoms where a dislocation intersects the surface.

Some steps were formed on the surfaces of the crystals used in this study because it was not possible to precisely polish the crystal

on the (111) orientation. For example, a silver crystal whose orientation deviated by 0.25° from the (111) surface had about 6×10^{12} atoms/cm² on the edges of steps. An edge atom could exhibit a different chemical activity from the normal surface site because the edge atom had fewer nearest neighbors and more free bonds. Similarly, where a dislocation emerges to a free surface, the atoms had a different number of nearest neighbors and possibly a different chemical activity. However, one might question how a variation in the dislocation density from 10^4 /cm² to 10^8 /cm² as studied in this work would be noticed considering that 10^{12} atoms/cm² were on the edges of steps.

Dislocations are line defects that exist in crystals and are described by a variety of types. Two of the most common types are the edge dislocation and the screw dislocation. A screw dislocation results when the displacement of the lattice is parallel to the line of the dislocation. Notice that the intersection of a screw dislocation with a surface leads to the formation of a step that extends to the next boundary. Thus even a dislocation density of 10^6 /cm² will generate more than 10^{12} edge atoms/cm² on steps formed from the intersection of the screw dislocations with the surface.

Another difference between edge atoms and surface atoms near the core of a dislocation was demonstrated by the chemical activity of the core atoms in certain solutions. The enhanced activity at the core atoms lead to the formation of an etch pit at the point of emergence of either a screw or edge dislocation on the silver surface. Thus dislocations should be as important as edge atoms when considering active sites because of the equal numbers and because of the enhanced chemical activity

at the core of a dislocation. It was concluded that the number of edge atoms on surface steps would not suppress any possible effects of dislocations on the catalytic rate of reaction.

As mentioned previously, the dislocation density of the crystals used in the reactor was measured before the crystals were treated with oxygen, and in this work the dislocation density varied from 10^4 - 10^5 cm^{-2} to 10^8 - 10^9 cm^{-2} . It was assumed that the proposed mechanism of the surface catalysis would be independent of the dislocation density, and that the surface rate constant would differ if the number of dislocation sites was an important factor in the mechanism. The chemical rate data from the seven crystals used in the reactor was fitted to the proposed mechanism of the surface catalysis, and the surface rate constants were compared in Table 1 with the dislocation density of the crystal. In two instances a crystal with an initial low dislocation density was retested for its catalytic activity after being cold rolled and strained by five percent.

A comparison in Table 1 of the mean values of the rate constants did show some variation between the different crystals. However, it should be noted that because of the large standard error for the experimental data, the difference in the mean values was not statistically significant since the 95% confidence limits overlapped. Based on that fact, it was concluded that dislocations which were introduced by straining the silver crystal did not significantly alter the chemical activity of the catalyst and thus were not an important catalyst parameter in this particular reaction system. In reaching this conclusion, it was assumed that the microdislocations, which formed on the interface of the silver oxide particles and the silver matrix, did not mask the experimental

effects of the longer glissile dislocations that were introduced by straining the crystal.

COMPARISON BETWEEN THIS WORK AND PRIOR STUDIES

Oxidation of Carbon Monoxide

Earlier Benton and Bell (42), and Keulks and Chang (24) had studied the kinetics of the oxidation of carbon monoxide over silver for temperature and pressure conditions that were similar to those of this project. In both of their studies, the chemical rate data were empirically fitted to a mathematical expression of the power function type. Benton and Bell had found their data to best fit the rate expression:

$$\frac{dn_{CO_2}}{dt} = k_1 n_{CO} \quad (13)$$

But Keulks and Chang had fit their data to the equation:

$$\frac{dn_{CO_2}}{dt} = \frac{k_2 n_{CO}}{n_{CO_2}} \quad (14)$$

It is interesting to notice that both previous authors had selected expressions which were a special case of the kinetic formula developed in this work. Recall equation (9):

$$\frac{dn_{CO_2}}{dt} = \frac{kn_{CO}}{1 + Kn_{CO_2}} \quad (9)$$

Now, if the term $Kn_{CO_2} \ll 1$, then equation (9) is equivalent to equation (13) as found by Benton and Bell. However, if $Kn_{CO_2} \gg 1$, then equation (14) as determined by Keulks and Chang is similar to equation (9). The evidence of the experimental work in this investigation suggested that $Kn_{CO_2} \sim 1$, so

both terms were important in the denominator. Furthermore, the data of this study were fit to equations (14) and (9), and compared for fit on the basis of a Chi-square test. In all cases, the data fit better to the derived expression, equation (9), and a comparison of the curve between equations (9) and (14) is illustrated in Figure 11.

This comparison was extended by matching the calculated rate constants from equations (9) and (14) for the experimental data of Benton and Bell, Keulks and Chang, and this work. The calculated kinetic constants are compared in Table 3 and it is evident that better agreement is found for all sets of data when the derived expression, equation (9), is used instead of the power function model, equation (14). Differences which still exist might possibly be accounted for by impurities that were undetectable in their supply gases forty years ago.

Adsorption of Carbon Dioxide on Silver

A comparison was made between the value of the adsorption coefficient for carbon dioxide on a silver-oxygen surface which was calculated in this work, and the value which was determined from Czanderna's (26) experimental data. Czanderna had measured the coverage of carbon dioxide on a silver-oxygen surface as a function of carbon dioxide pressure. Results of this comparison are shown in Table 3 and appear to be in good agreement.

Silver-Oxygen Interactions

The observed changes in the Vickers Hardness and the etch-pit-count of a catalyst were explained by the proposed growth of silver oxide particles in the silver crystal during the oxygen treatment. Ehrlich (15)

also noticed an increase in the hardness of silver upon exposure to oxygen, but he was unable to explain that result. Most likely, oxide particles were also formed in his study.

Young (68) observed the etch-pit-count of a copper single crystal to increase upon continued exposure to oxygen. His study was comparable to this work since both silver and copper form similar metallic oxides, and in both studies the chemical etch-pit-count of the heated crystal had increased following an exposure to oxygen. Young explained his observations by proposing the growth of a copper oxide particle in the crystal matrix.

Effects of Dislocations

Some comparable results were found for the effects of dislocations on the rate of reaction. Woodward (69) had studied the effects of dislocations in silver on the catalytic oxidation of ethylene. He reported that "...a definite change in the manner in which etching solution attacked the crystal was noticed after the crystal was used in the reactor." Woodward noticed the number of etch pits on the silver surface had increased from $10^6/\text{cm}^{-2}$ to $10^7/\text{cm}^{-2}$ after exposure to a mixture of 80% oxygen and 20% ethylene at 260°C . The latter density was at the limit of resolution for his chemical solution. From similar results in this study, it can be presumed that Woodward's etching change was caused by the diffusion of oxygen into the silver lattice and the growth of an oxide particle. However, since oxygen and ethylene were always present together in the reactor, it may be inferred that the adsorbed oxygen may diffuse into silver even under some reducing atmospheres.

SUMMARY

1. The experimental evidence indicated that the concentration of hydrocarbons and silicones in the parts per million range decreased the catalytic rate of reaction by four orders of magnitude. Once these poisons to the silver catalyst were removed from the reactor, the catalyst was able to maintain its highest activity. However, alternate pretreatments at 800°F, first with oxygen and then with hydrogen, were still necessary to clean the surface of a crystal that had been exposed to the atmosphere. Hydrogen was employed in the final cycle since the silver exhibited no catalytic activity after an oxygen treatment.
2. Both the surface morphology and physical characteristics of the silver surface were modified by heating it in oxygen. After a crystal was heated in oxygen, it had a much higher etch-pit density and an increased Vickers Hardness. It was ascertained from electron micrographs that the number of dislocations in the crystal was much less than the number of etch pits, but the density of dots in the micrographs did somewhat correspond to the density of etch pits. The change in hardness and chemical etching of the silver surface was presumed to result from the growth of silver oxide particles inside the silver lattice, and the generation of misfit dislocations on the interface between the oxide particle and the silver lattice.
3. A kinetic model of the surface catalysis was proposed to explain the chemical rate data. The model was based on Langmuir-Hinshelwood

kinetics and was developed with the assumptions that the surface was in adsorption equilibrium, and that carbon monoxide and carbon dioxide competed for sites on the silver-oxygen surface. The chemical rate data of this study and that from earlier investigators were found to fit the mathematical expression for this proposed model. The adsorption coefficient for carbon dioxide on a silver-oxygen surface, which was calculated from the model, agreed with an experimental value measured in another study. The heat of adsorption was 17.2 Kcal per mole for the carbon dioxide adsorption on the silver-oxygen surface.

4. It was concluded that the dislocations which were introduced by straining the silver surface had little effect on the surface catalysis. This conclusion was reached after comparing the surface rate constants for silver surfaces where the only deliberate modification was a 10^4 difference in the number of dislocations which intersected the surface. The surface rate constant was the same within experimental error for the surfaces with either 10^4 or 10^8 dislocations per cm^2 . Thus, the number of dislocations that intersected a catalyst surface was not an important catalyst parameter in defining the activity of this reaction system.

One question which developed from the experimental results was the effects of the discovered oxide centers on the surface kinetics. These oxide sites were obviously reactive as evidenced by the attack of the chemical etching solution. First, it should be noted that the catalytic activity did not solely result because the oxide sites were

present. These sites were readily poisoned, and the catalytic activity of the surface was primarily dependent on the surface purity. Second, the interfacial dislocations which probably existed between the silver oxide and the silver matrix were shorter and of lower energy than the longer glissile dislocations which were introduced by straining the crystal. It was assumed that the surface kinetics would still have been affected by the density of the longer glissile dislocations if the catalytic activity was strongly dependent on them.

5. In reviewing the overall processes which occurred on the catalyst surface, it seems instructive to start by considering the silver-oxygen system. Oxygen was attracted to silver because of a strong chemical affinity - not merely because oxygen could be accommodated interstitially in the lattice (for example, oxygen is not soluble in gold which has a similar lattice spacing). The oxygen molecules chemisorbed onto the silver surface, dissociated into silver atoms, and diffused into the silver lattice to the extent of the equilibrium composition at the operating temperature. Presumably, dislocations could have increased the rate of oxygen diffusion into the bulk by acting as centers for pipe diffusion.

The introduction of carbon monoxide into the gas phase with oxygen created some changes on the silver surface. Oxygen still chemisorbed onto the silver, but the carbon monoxide now adsorbed on the chemisorbed oxygen and for certain conditions reacted with the oxygen to form carbon dioxide. Thus, a cross-sectioned view of the catalyst

system would have imaged a gaseous phase of carbon monoxide, carbon dioxide and oxygen; a solid phase of silver; and a gas-solid interfacial region. In the interfacial region, a layer of oxygen was chemisorbed to the silver, and multiple layers of carbon monoxide and carbon dioxide were adsorbed on the oxygen. Note that the chemisorbed oxygen was now chemically attracted by both the silver and the adsorbed gases, and this reduced the driving force for diffusion of oxygen into the silver lattice.

The chemisorbed layer of oxygen was the proposed intermediate complex which made the silver a good catalyst for the oxidation of carbon monoxide. Although the atomic stoichiometric ratio of silver-to-oxygen was about unity, the oxygen was coordinated to fewer silver atoms on the surface than in the recognized bulk oxides. Bulk silver oxides have a similar atomic ratio but are not catalytically active. The fewer number of silver-oxygen bonds on the surface also made the oxygen accessible for gases to adsorb on it, hence the catalytic oxidation of carbon monoxide. The gases adsorbed to the oxygen also inhibited the diffusion of oxygen into the bulk and the formation of bulk oxides. Finally, the oxygen layer was susceptible to poisoning by hydrocarbons and silicones. Product gases which adsorbed on the layer did inhibit the rate of reaction.

RECOMMENDATIONS FOR FURTHER STUDY

1. The change in the activity of the silver catalyst was more affected by impurities than by dislocations. Silver was easily contaminated and further work on dislocations should be made with a metal in an ultra-high vacuum system equipped with either an Auger-analyzer or an X-ray photoelectron spectroscope. Those apparatus would give the necessary consideration to impurities in the experiment. A refractory metal might be better, since many of the refractory metals have been extensively studied in previous experiments. Both the Auger and the X-ray spectroscope should allow one to gain some insight about the metal-adsorbed gas bonds that form on the surface.
2. The temptation of investigating the kinetics of a chemical reaction as well as dislocation effects adds a further complication to a difficult experiment. As a first trial, the scattering properties of a metal-gas system might be investigated as a function of the state of strain of the metal surface. Gases which adsorb on the surface should be considered.
3. The silver-oxygen-reducing gas system is commercially important and deserving of further study. Chemical rate data should be taken over a wider range of the concentration of oxygen and in temperature regions where the growth of silver oxide is thermodynamically stable. Results of this study suggested that the surface was not catalytically active after oxygen treatment. Additional information should improve the understanding of the kinetics and mechanism of the catalysis on silver.

REFERENCES

1. Twigg, G. H., Proc. Roy. Soc. (London), A188, 92,105,123 (1946).
2. Carberry, J. J., Kuczynski, G. C., Martinez, E., J. Catal. 26, 247 (1972).
3. Kummer, J. T., J. Phys. Chem., 60, 666 (1956).
4. Manara, G., Parravano, G., J. Catal., 23, 379 (1971).
5. Marcinkowsky, A. E., Berty, J. M., J. Catal., 29, 494 (1973).
6. Metcalf, P. L., Harriott, P., Ind. Eng. Chem. Process Design Develop., 11, 478 (1972).
7. Mikani, J., Satoh, S., Kobayashi, H., J. Catal., 18, 265 (1970).
8. Richey, W. F., J. Phys. Chem., 76, 213 (1972).
9. Menzel, E., Menzel-Kopp, Chr., Z. Naturforschg., 13a, 985 (1965).
10. Moore, A.J.W., Acta Met., 6, 293 (1958).
11. Ogilvie, G. J., Ridge, M. J., J. Phys. Chem. Solids, 10, 217 (1959).
12. McMillan, J. A., J. Inorg. Nucl. Chem., 13, 28 (1960).
13. Otto, E. M., J. Electrochem. Soc., 113, 643 (1966).
14. Verfurth, J. E., Rapp, R. A., Trans. AIME, 320, 1310 (1964).
15. Ehrlich, A. C., J. Mat. Sci., 9, 1064 (1974).
16. Benton, A. F., Drake, L. C., J. Am. Chem. Soc., 56, 266 (1934).
17. Smeltzer, W. N., Tollefson, E. L., Cambron, A., Can. J. Chem., 34, 1946 (1956).
18. Kummer, J. T., J. Phys. Chem., 63, 460 (1959).
19. Degeilh, R., Fourth International Congress on Catalysis, Moscow (1968), pg. 49.
20. Sandler, Y. L., Durigon, D. D., J. Phys. Chem., 69, 4201 (1965).
21. Sandler, Y. L., Durigon, D. D., J. Phys. Chem., 70, 3881 (1966).

22. Sandler, Y. L., Durigon, D. D., Trans. Far. Soc., 62, 215 (1966).
23. Boreskov, G. K., Khasin, A. V., Starostina, T. S., Dokk. Akad. Nauk. SSSR, 164, 606 (1965).
24. Keulks, G. W., Chang, C. C., J. Phys. Chem., 74, 2590 (1970).
25. Czanderna, A. W., J. Phys. Chem., 68, 2765 (1964).
26. Czanderna, A. W., J. Colloid and Interface Sci., 22, 482 (1966).
27. Czanderna, A. W., J. Colloid and Interface Sci., 24, 500 (1967).
28. Czanderna, A. W., Kollen, W., J. Colloid and Interface Sci., 38, 152 (1972).
29. Czanderna, A. W., Thin Solid Films, 12, S21 (1972).
30. Czanderna, A. W., J. Vac. Sci. Technol., 10, 295 (1973).
31. Czanderna, A. W., Chen, S. C., Biegen, J. R., J. Catal., 33, 163 (1974).
32. Steiger, R. T., Morabito, J. M., Somarjai, G. A., Muller, R. H., Surface Sci., 14, 279 (1969).
33. Bruce, L. A., Surface Sci., 20, 187 (1970).
34. Clarkson, R. B., Cirrillo, A. C., J. Catal., 33, 392 (1974).
35. Clarkson, R. B., Cirrillo, A. C., J. Vac. Sci. Technol., 9, 1073 (1972).
36. Schmidt, W. A., Frank, O., Block, J. H., Surface Sci., 44, 185 (1974).
37. Jansen, M.N.P., MooUryser, J., Sachtler, W.M.H., Surface Sci., 44, 553 (1974).
38. Roviada, G., Pratesi, F., Maglietta, M., Ferroni, E., J. Vac. Sci. Technol., 9, 796 (1972).
39. Bradshaw, A. M., Engelhardt, A., Menzel, D., Ber. Bunsenges., 76, 500 (1972).

40. Bradshaw, A. M., Engelhardt, A., Menzel, D., Surface Sci., 40, 410 (1973).
41. Dweyari, A. W., Mee, C.H.B., Phys. Stat. Sol. (a), 17, 247 (1973).
42. Benton, A. F., Bell, R. T., J. Am. Chem. Soc., 56, 501 (1934).
43. Yamada, N., Bull. Chem. Soc. Japan, 27, 36 (1954).
44. Allen, J. A., Scaife, P. H., Aust. J. Chem., 19, 715 (1966).
45. Keulks, G. W., Ravi, A., J. Phys. Chem., 74, 783 (1970).
46. Slager, T. L., Kindgren, B. J., Mallmann, A. J., Greenler, R. G., J. Phys. Chem., 76, 940 (1972).
47. Smith, A. W., J. Catal., 4, 172 (1965).
48. Robinson, W. H., "Techniques of Metals Research", Vol. II, Interscience, New York, 1968, pp. 291-340.
49. Eckell, J., Z. Elektrochem., 46, 369 (1940).
50. Cratty, L. E., Grant, A. V., J. Phys. Chem., 26, 96 (1957).
51. Kishimoto, S., J. Phys. Chem., 77, 1719 (1973).
52. Uhara, I., Kishimoto, S., Yoshida, Y., Hikino, T., J. Phys. Chem., 69, 880 (1965).
53. Uhara, I., Yanagimoto, S., Tani, K., Adachi, G., Teratani, S., J. Phys. Chem., 66, 269 (1962).
54. Uhara, I., Kishimoto, S., Hikino, T., Kageyama, Y., Hamada, H., Numata, Y., J. Phys. Chem., 67, 996 (1963).
55. Criado, J. N., Herrera, E. J., Trillo, J. M., Proc. 5th International Congress on Catalysis, Amsterdam (1972), p. 36.
56. Sosnovsky, H.M.C., J. Phys. Chem. Solids, 10, 304 (1959).
57. Thomas, J. M., Advances in Catalysis, 19, 293 (1969).
58. Bragg, J., Jaeger, H., Sanders, J. V., J. Catal., 2, 449 (1963).

59. Jaeger, H., J. Catal., 9, 237 (1967).
60. Perkins, T. D., PhD Thesis, "Effects of Dislocations upon the Catalytic Activity of Silver", University of Oklahoma (1963).
61. Robertson, A.J.B., "Catalysis of Gas Reactions by Metals", Springer-Verlag, New York, 1970.
62. Hall, J. W., Rase, H. F., Ind. Eng. Chem. Fund., 3, 159 (1964).
63. Woodward, J. W., Lindgren, R. E., Corcoran, W. H., J. Catal., 25, 292 (1972).
64. Wood, B. J., J. Phys. Chem., 75, 2186 (1971).
65. Smith, D. P., "Hydrogen in Metals", University of Chicago Press, 1949.
66. Bennett, C. O., Cutlip, M. B., Yang, C. C., Chem. Eng. Sci., 27, 2255 (1972).
67. Grenga, H. E., Lawless, K. R., J. Appl. Phys., 43, 1508 (1972).
68. Young, F. W., "Direct Observation of Imperfections in Crystals", J. B. Newkirk, J. H. Wernick, editors, Interscience, 1962, p. 103.
69. Woodward, J. W., PhD Thesis, "A Study of the Effects of Dislocation Density and Crystal Orientation on the Catalyzed Oxidation of Ethylene over a Single Crystal of Silver", California Institute of Technology (1965), p. 41.

NOMENCLATURE

k_1	Kinetic rate constant, model 1, $\text{min}^{-1}\text{cm}^{-2}$
k_2	Kinetic rate constant, model 2, $\text{moles min}^{-1}\text{cm}^{-2}$
k_s	Kinetic rate constant, model 3, $\text{moles min}^{-1}\text{cm}^{-2}$
K_1	Adsorption constant of carbon monoxide on a silver-oxygen surface, moles^{-1} or mm^{-1}
K_2	Adsorption constant of carbon dioxide on a silver-oxygen surface, moles^{-1} or mm^{-1}
K	Adsorption constant of carbon dioxide on a silver-oxygen surface, = K_2
k	Lumped constant = $k_s K_1$, $\text{min}^{-1}\text{cm}^{-2}$
n_i^0	Moles of component "i", initial
n_i	Moles of component "i" at time t
t	Time, min
T	Temperature, °R

Subscripts

CO	Pertains to carbon monoxide
CO ₂	Pertains to carbon dioxide

TABLE 1.

SUMMARY OF REACTION RATE CONSTANTS AT 175°F
FOR THE DIFFERENT SINGLE CRYSTALS OF SILVER

<u>Crystal</u>	<u>Area,</u> <u>CM. ²</u>	<u>k*10⁵,</u> <u>min.⁻¹ cm.⁻²</u>	<u>Condition</u> <u>Of Strain</u>	<u>Dislocation</u> <u>Density, cm.⁻²</u>
0	-	-	Non-Strained	10 ⁴ -10 ⁵
1	13.40	3.37	Strained 5%	10 ⁸ -10 ⁹
2	7.22	3.18	Non-Strained	10 ⁴ -10 ⁵
3	7.93	2.93	Non-Strained	10 ⁴ -10 ⁵
4	7.93	2.61	Strained #3 by 5%	10 ⁸ -10 ⁹
5	9.46	3.27	Non-Strained	10 ⁴ -10 ⁵
6	7.17	2.91	Non-Strained	10 ⁴ -10 ⁵
7	7.17	2.68	Strained #6 by 5%	10 ⁸ -10 ⁹

TABLE II

EFFECT OF THE CONCENTRATION OF OXYGEN ON
THE RATE OF OXIDATION OF CARBON MONOXIDE

	<u>% O₂, mole basis</u>	<u>k⁺ x 10⁴ min⁻¹</u>
1.	10.5%	3.64
2.	25.5	3.88

⁺ Calculated from Langmuir model and average of two experimental runs.

TABLE III
 COMPARISON OF KINETIC AND
 ADSORPTION CONSTANTS

A. Kinetic Constants at 100°C

	Power Function Model $k_2 \times 10^{12}$ <u>moles min.⁻¹ cm.⁻²</u>	Adsorption Model $k \times 10^6$ <u>min.⁻¹ cm.⁻²</u>
Benton, Bell* (3)	2.6	5.8
Keulks, Chang* (31)	1003.	17.7
This Work	2363.	44.3

* Catalyst area calculated from the mass of catalyst and the area per gram given in their articles.

B. Adsorption constant, K, for carbon dioxide on a silver surface
 Covered with oxygen.

Czanderna (13)	1.1 mm ⁻¹ 75-100°C ⁺
This Work	0.8 mm ⁻¹ @ 75°, 0.2 @ 100°C

⁺ Difficult to distinguish curves on graph

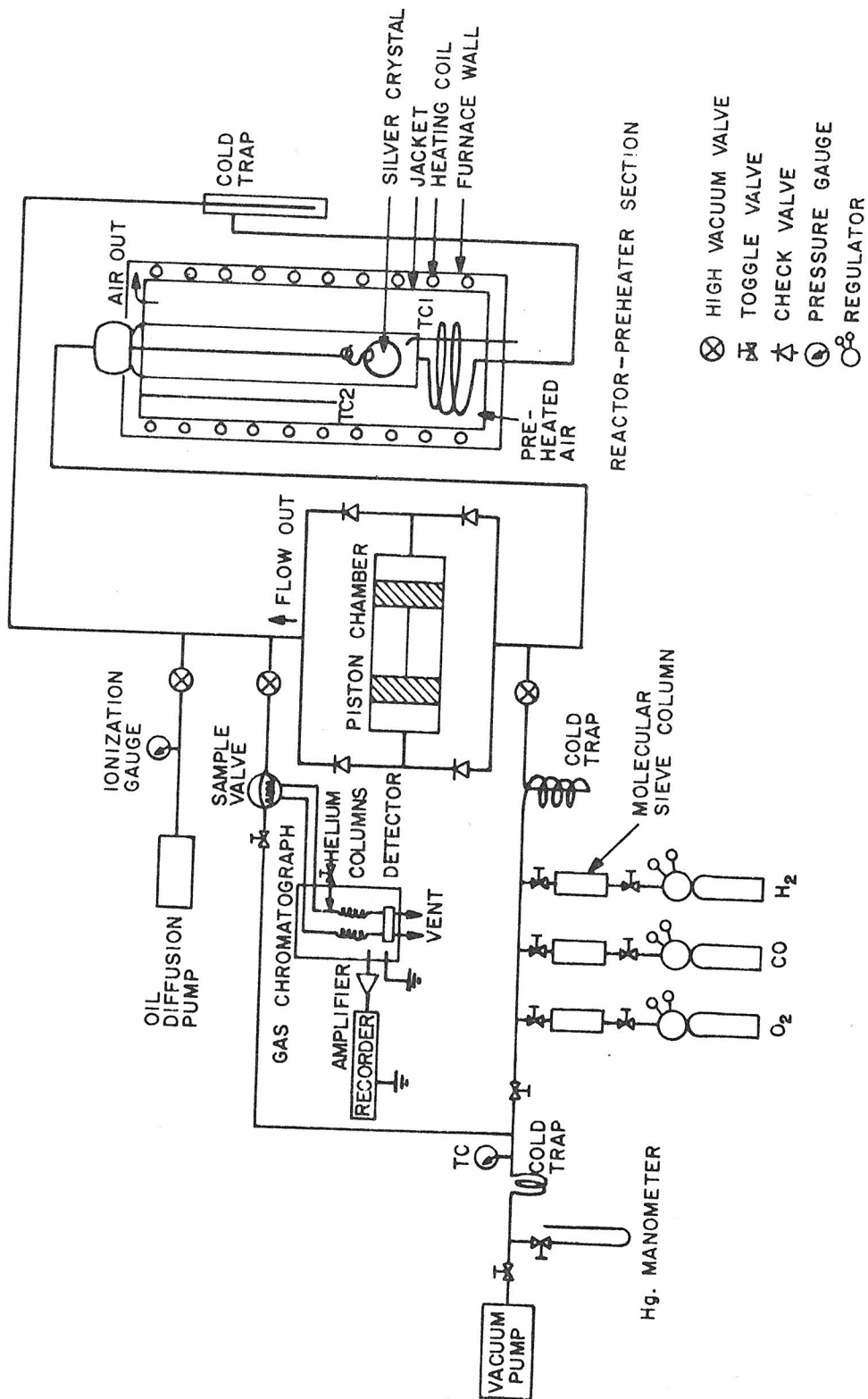


Figure 1. Schematic of experimental apparatus.

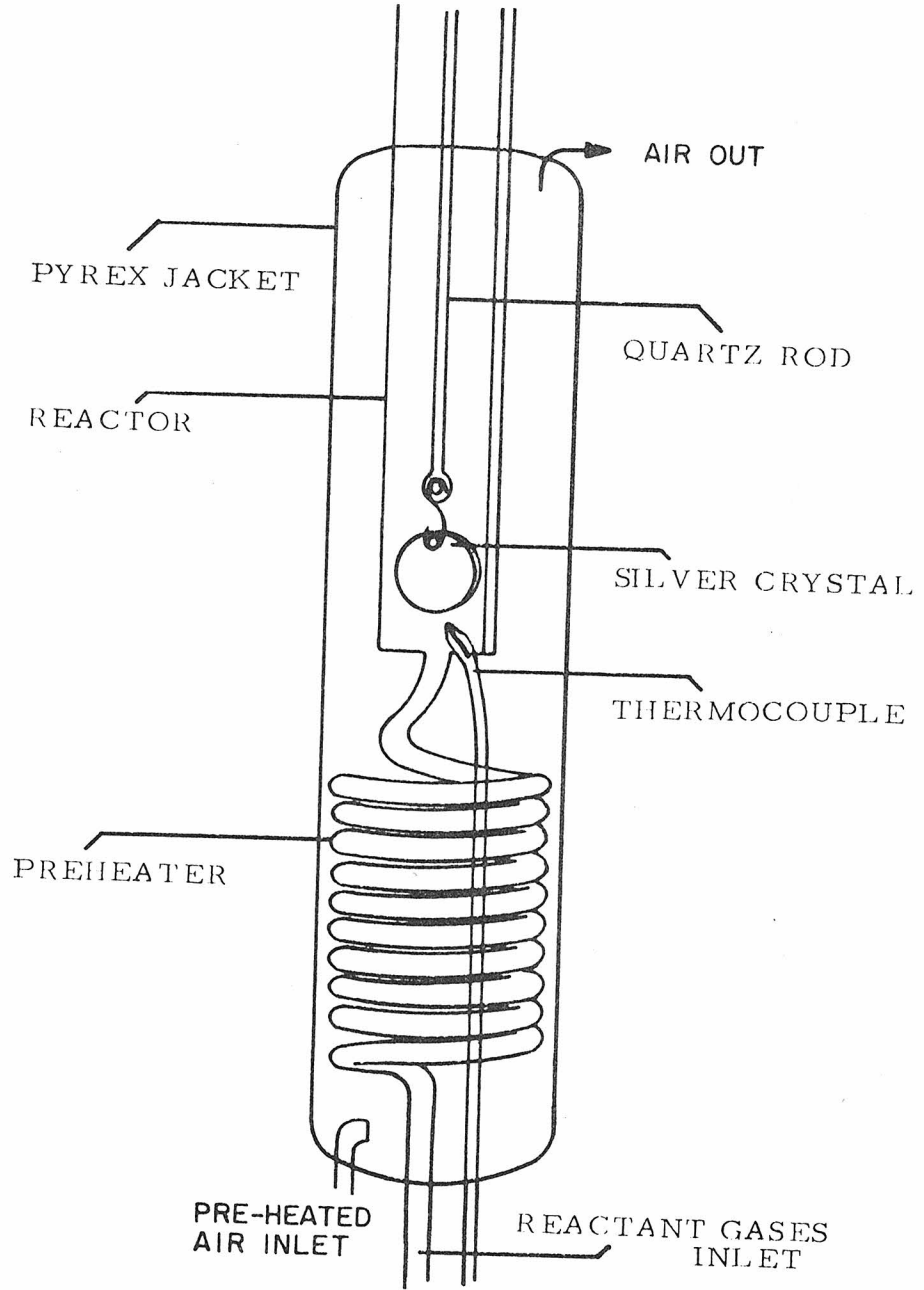


Figure 2. Schematic of heated reaction zone.

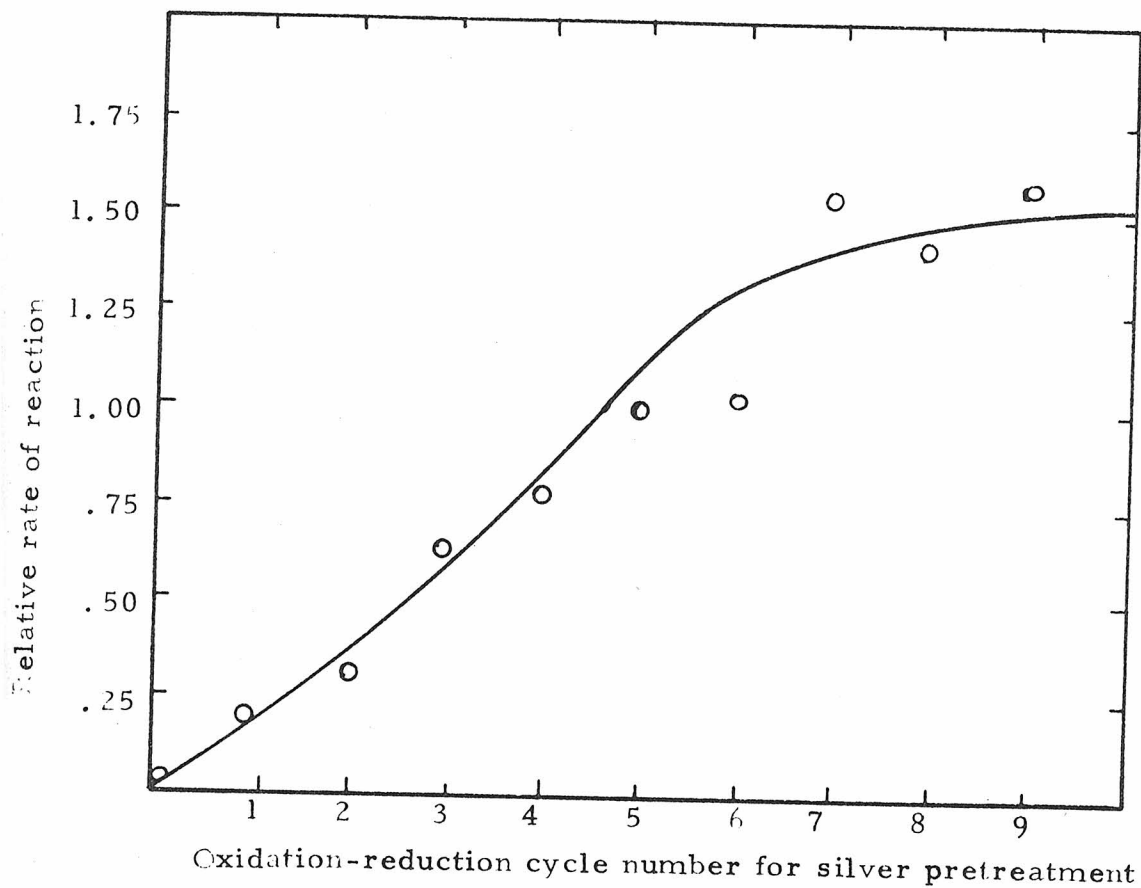
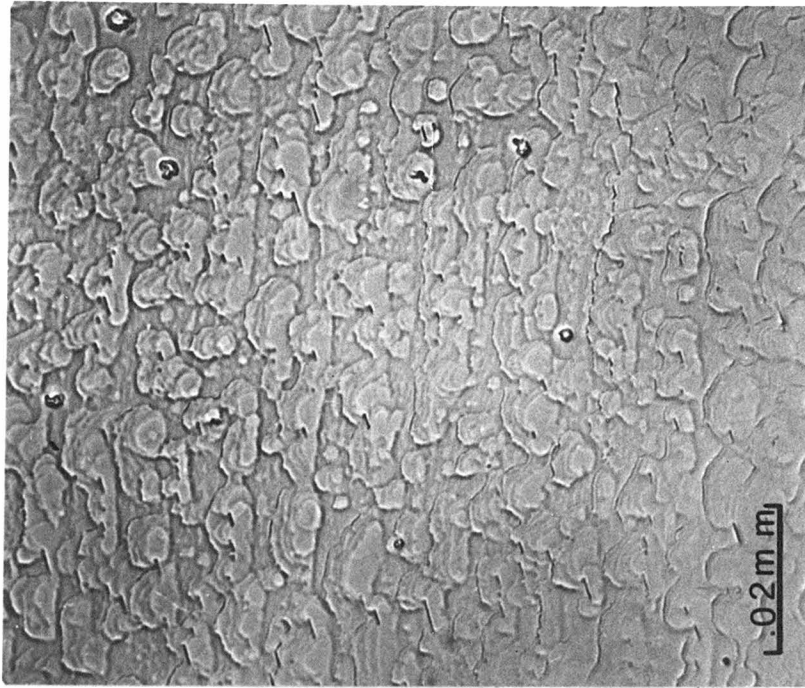
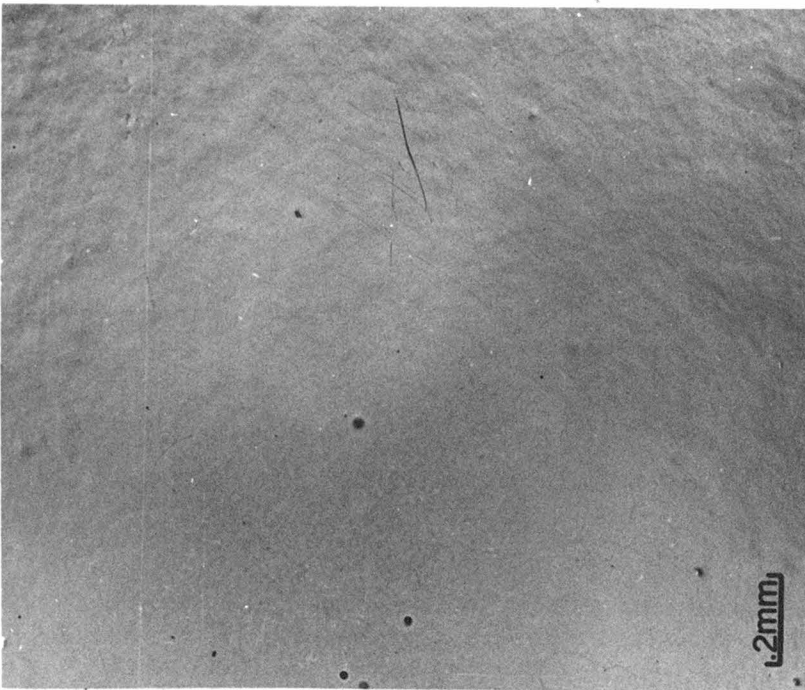


Figure 3. Rate of reaction as a function of the oxidation-reduction cycle number used in the pretreatment of the silver catalyst.



(a)



(b)

Figure 4 . Photomicrographs of the (111) surface of a silver crystal showing changes to morphology. (a) as polished (b) after use in reactor.

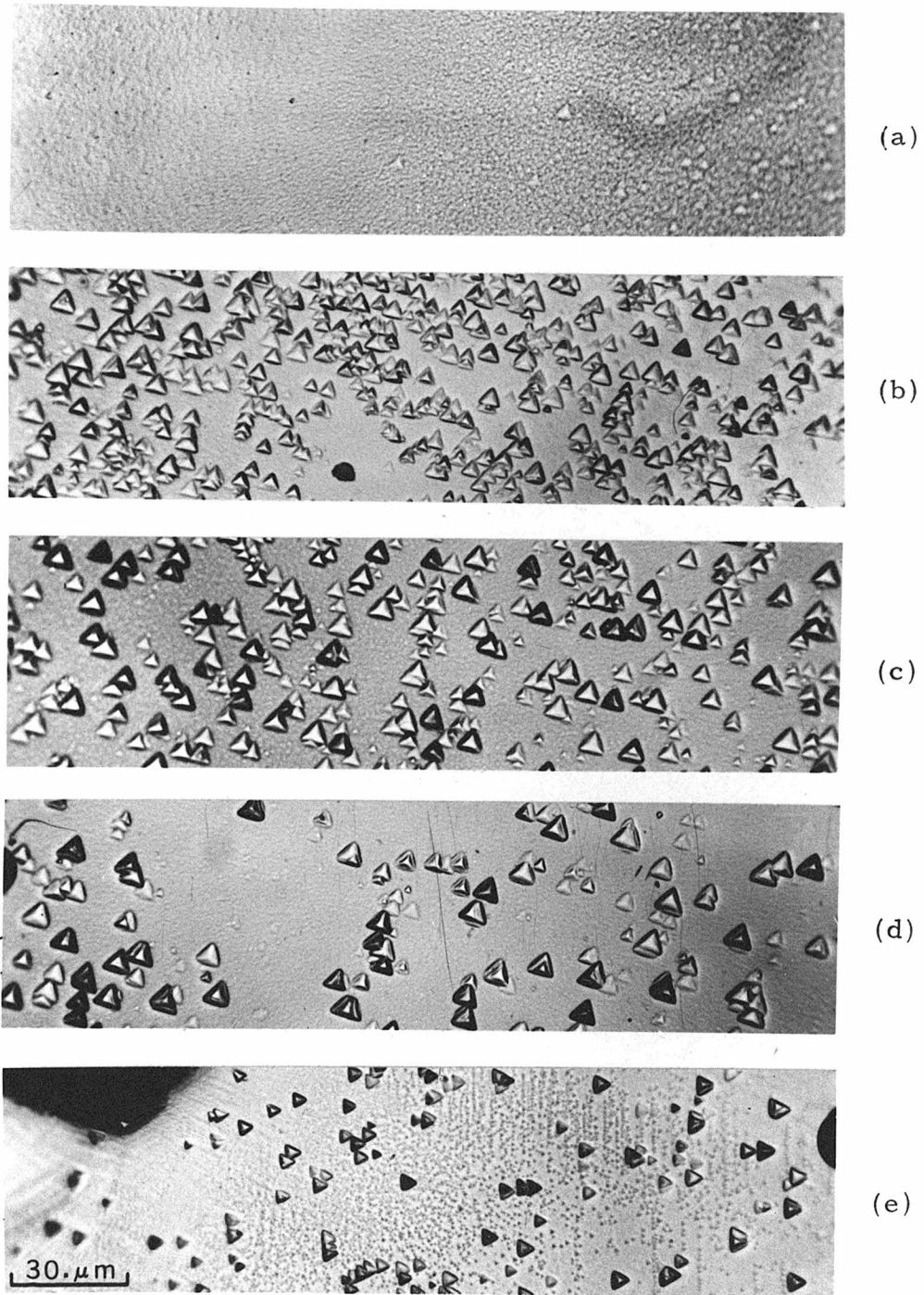


Figure 5. Photographs of etch pits as a function of depth on a (111) surface of a silver crystal heated in oxygen. Approximate depth: (a) surface, (b) $4.5\mu\text{ m}$. (c) $7.5\mu\text{ m}$. (d) $13.5\mu\text{ m}$. (e) crystal indented before etching - 500X.

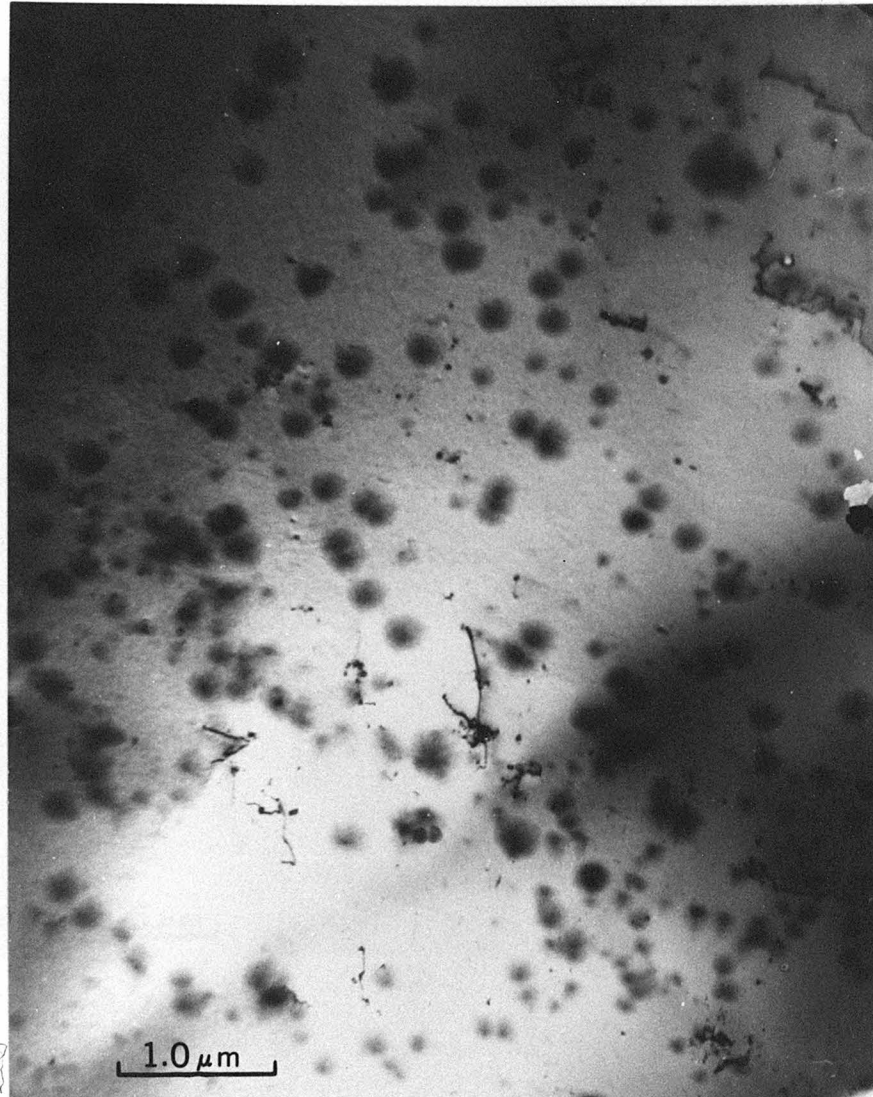


Figure 6 . Transmission electron micrograph of a foil made from a silver crystal which was heated in oxygen.

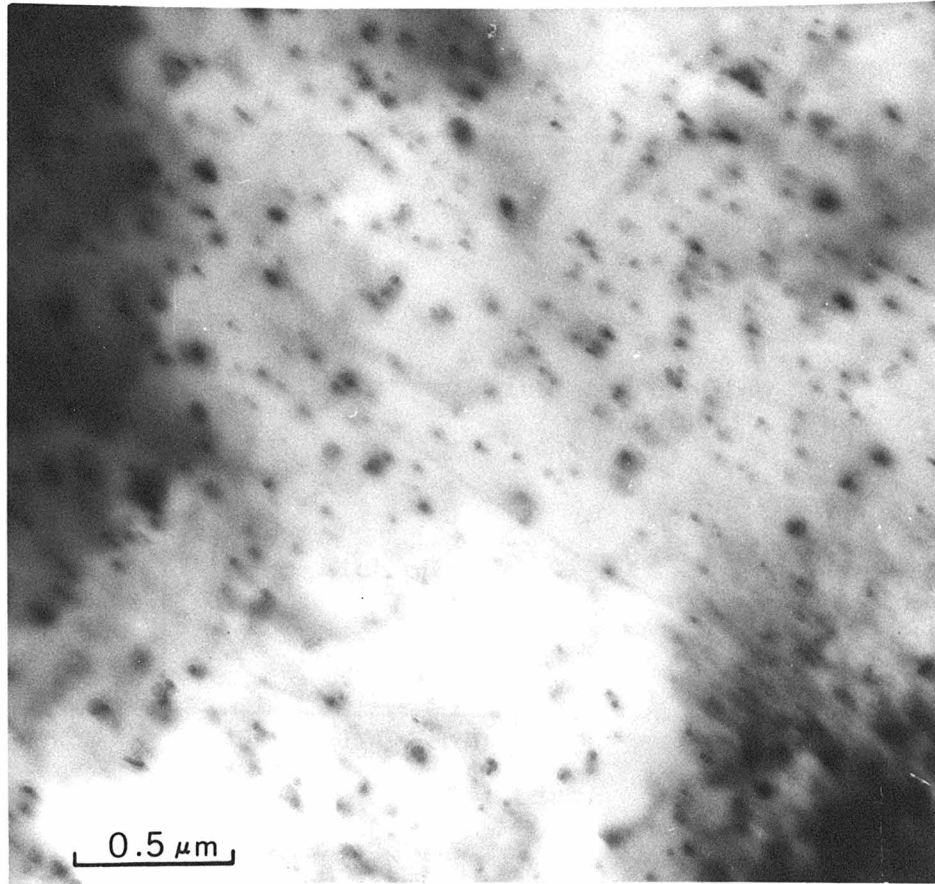


Figure 7. Transmission electron micrograph of a foil made from a silver crystal which was heated in oxygen.

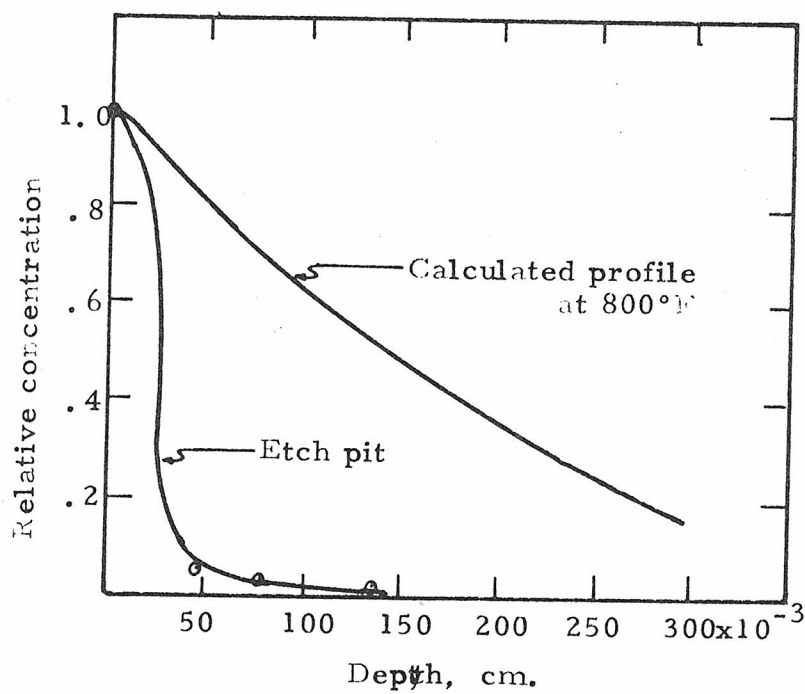
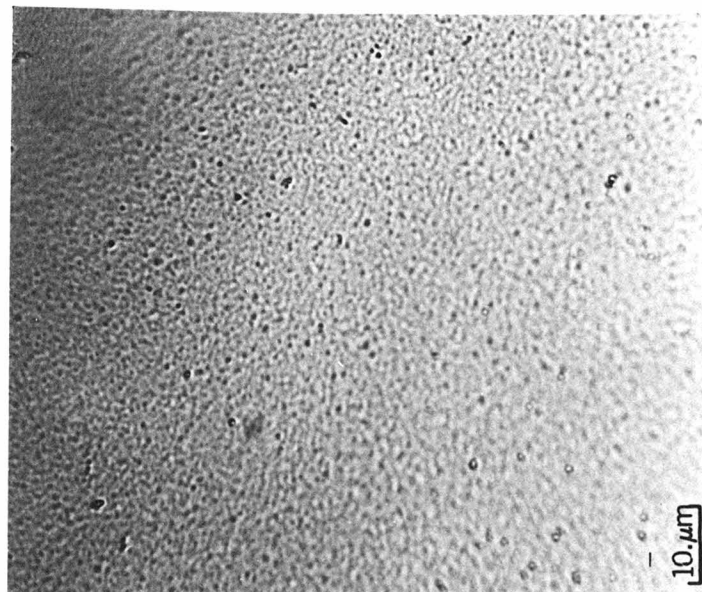
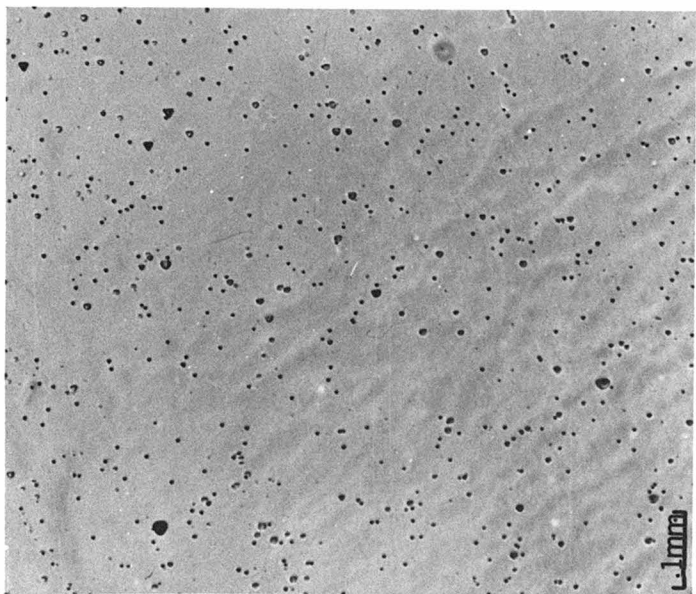


Figure 8. Comparison of the calculated concentration profile of oxygen diffusion into silver with the measured etch pit profile.



(a)



(b)

Figure 9. Photomicrographs of (111) surface as etched to reveal dislocations. (a) low density crystal (100X) (b) high density after 5% strain. (1000X)



Figure 10. X-ray diffraction topograph with CuK_α radiation of a (111) silver crystal which was strained 5%.

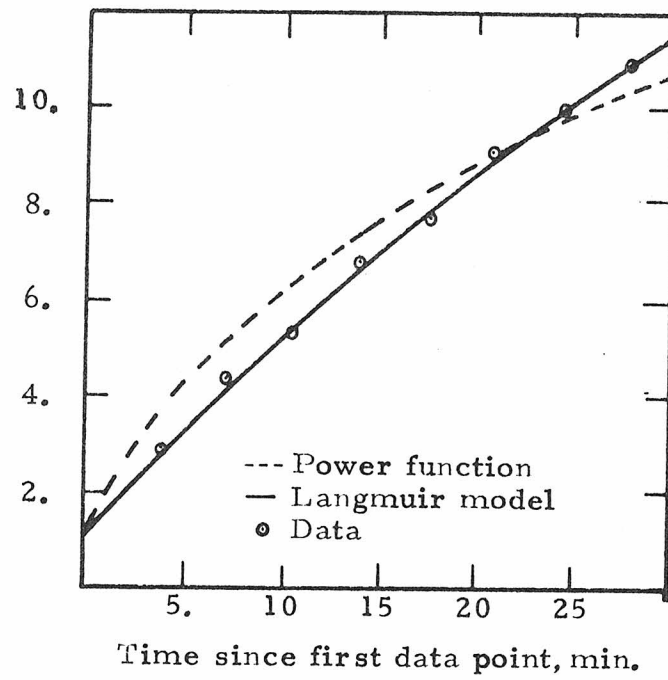


Figure 11. Graphical plot of experimental data fit to two different kinetic models.

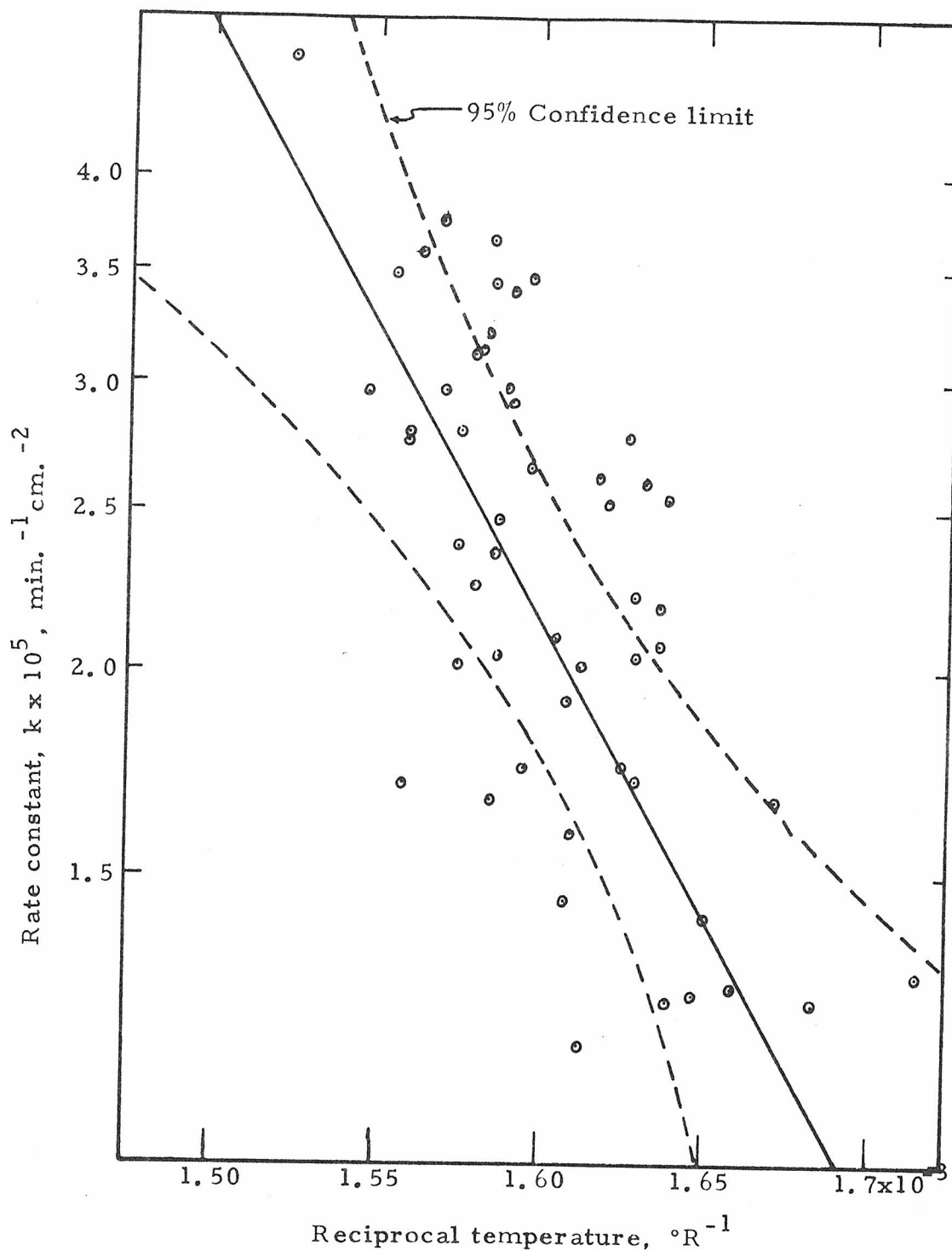


Figure 12. Temperature dependence of rate constant k from Langmuir model.

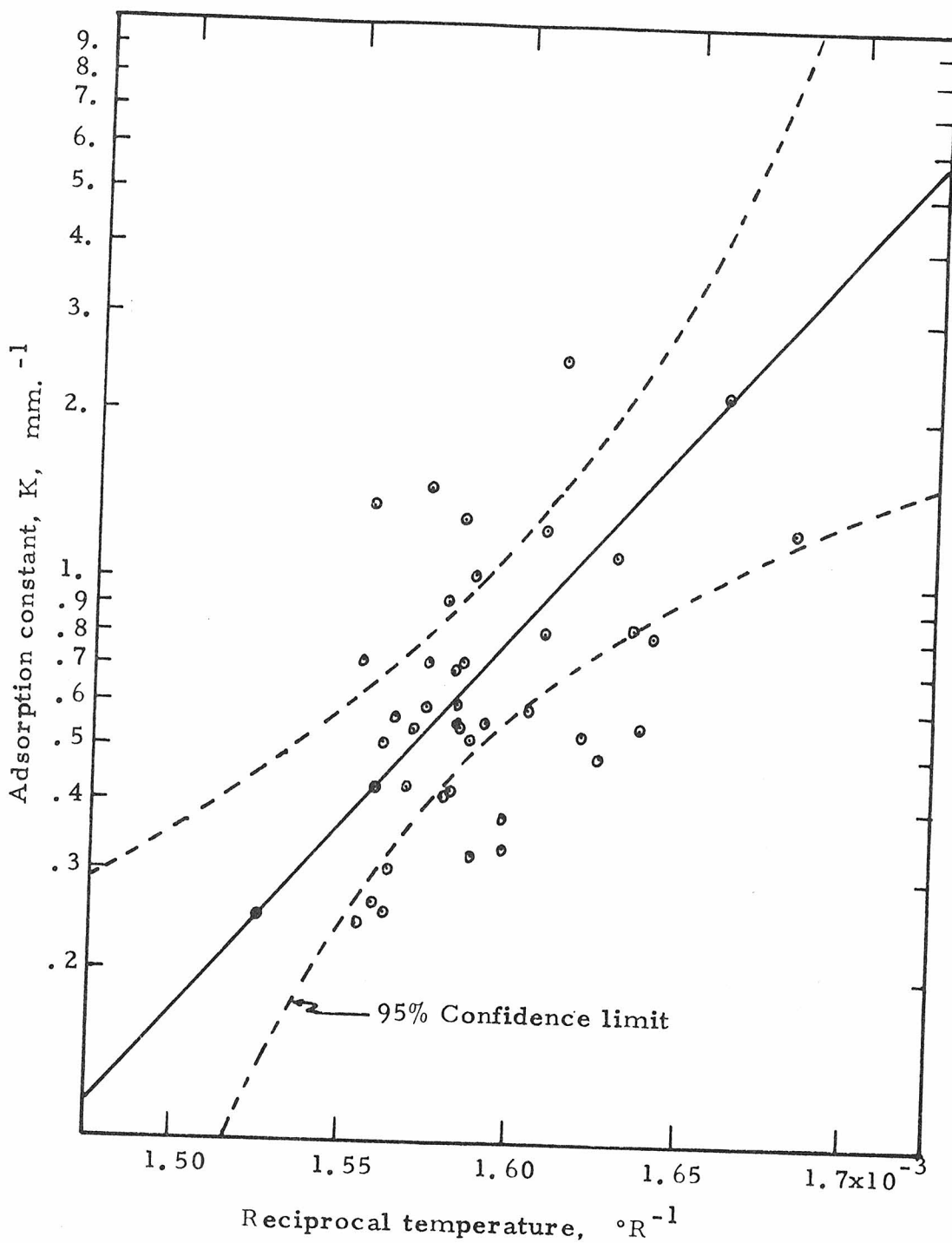


Figure 13. Temperature dependence of adsorption constant K for carbon dioxide on a silver surface with preadsorbed oxygen.

APPENDIX A
REACTOR DESIGN

The rate of reaction over single crystals of silver with different dislocation densities was measured in a batch recirculation system. Preliminary kinetic measurements, however, were made using a flow reactor with a large residence time. The chemical rates from the flow reactor were limited to an unknown extent because of concentration gradients in the reactor, but the results were useful in that unexpected problems arose from poisoning of the silver catalyst. It became apparent from the early measurements that the small area of the catalyst would not only amplify the problem of obtaining a measurable concentration change, but also the effect of a poison in the reactor. This appendix discusses the design of the recirculation reactor and its components with emphasis on the consideration that was given to minimize the effects of transport limitations and catalyst poisons on the chemical rate data.

Materials of Construction

In the initial design of the recycle-reactor, the glass tubing was interconnected by ball and socket joints. The joints used a Viton O-ring formed under the mild conditions in the reactor (A-2,4,5) and this problem was overcome by plating the Kovar connections with copper. As more possible poisons were identified and removed from the reactor, the rate of the chemical reaction became larger in magnitude and more reproducible.

Gas Recirculation Reactor

The experimental apparatus was divided into three components: A recirculating-gas reactor, a manifold for the mixing of gases, and a diffusion pump. A schematic of the apparatus is shown in Figure 1. The gas-recirculation reactor was composed of a pump, the reaction chamber, and a cold trap, and had a total volume of 350 cc. The different components of the reactor were connected with pyrex tubing (I.D. of 5 mm). The pump recirculated the gases and kept them well mixed. Details about the pump are presented in Appendix C. The gases went from the pump to a cold trap at -75°C which was placed in the line to lower the vapor pressure of the water in the loop and to trap any metal particles which might be carried over from the piston of the pump. The cold trap was 15 mm long and consisted of two concentric tubes of glass which had diameters of 5 and 10 mm. After the cold trap, the gases went to the preheater section.

The preheater was an 8-foot coil of pyrex tubing (5 mm) and was followed by the reaction chamber. The reaction chamber was a rectangular parallelepiped with dimensions of 1-1/8 in. by 1/16 in. in cross section and contained the silver catalyst. The catalyst was connected with a silver "S"-hook to a quartz rod which was suspended with a horizontal cross-bar from the top of the reactor. The rod was used to install or remove a catalyst from the reactor.

The preheater and reaction chamber were enclosed with a pyrex jacket before mounting them in a vertical tube furnace. In order to make the section isothermal, heated air flowed through the jacket at 18ℓ/min. Two thermocouples of chromel-alumel that were calibrated

against the freezing points of pure metals were utilized to monitor the temperature in the section. One couple was near the surface of the catalyst, and the other in the space between the jacket and the reactor. A proportioning controller (Leeds and Northrup Calibrated Azar with current control) regulated the temperature using the couple near the catalyst. Its value was also continuously recorded on a millivolt recorder. The other couple was connected to an "on-off" controller which was used in series as a reserve in order to prevent the temperature from going too high. The gas after passing through the reactor returned to the intake side of the pump and was recycled.

Mixing Manifold and Product Analysis Section

Purified gas supplies (Appendix B) were mixed and cold-trapped in the manifold before being admitted to the reactor where they were used either for studying the chemical reaction or for pretreating the catalyst. The manifold used lines of 0.25-inch copper tubing that were interconnected with soldered fittings. Two devices for measuring pressure were placed in the manifold section: A mercury manometer for pressures near atmospheric and a thermal conductivity gauge for those pressures less than 1 mm Hg. The possibility of contamination to the reactant gases by mercury was considered, so the valve to the manometer was kept closed unless measuring the pressure. Further precautions were taken by the installation of a small line (1/16-inch diameter) to the manometer to reduce the amount transferred by diffusion and by the addition of an extra cold trap at -75°C after the manometer line. The trap served a dual function in that it also slowed the rate diffusion

of oil from the vacuum pump into the manifold.

The vacuum pump attached to the manifold was used to remove the gases from: the manifold, the reactor, and the gas sample valve. Gas samples were withdrawn from the reactor by evacuating the collection loop of the gas sampling valve and then opening the line to the reactor. The sample was injected into the carrier gas of the chromatograph and analyzed. A special provision was made to remove a representative sample from the reactor in that a 0.0625-inch tube extended from the valve seat into the main flow stream.

Oil Diffusion Pump

The oil diffusion pump was connected to the reactor through a 0.50-inch copper line. The diffusion pump had a baffle plate at 77°K in order to prevent backstreaming of pump oil into the reactor system. The valve to the diffusion pump was opened after the roughing pump in the manifold section had reduced the pressure of the reactor to 100 μ m and the final pressure in the reactor section was about 5×10^{-6} torr.

Design Calculations

Transport limitations can produce large differences between the apparent and actual rate of a chemical reaction. The physical limitations are better controlled with the use of "gradientless reactors". A guideline for the minimization of material and thermal gradients was given by Chambers and Boudart (A-1) for a differential recycle reactor, as when the conversion-per-reactor pass was less than 0.2%. Although the reactor used in this study was operated below 0.2%, it still seemed necessary to demonstrate that transport limitations were not present.

This section presents the calculations for the transport effects in the reactor used in this study.

The maximum allowed reaction rate can be expressed in terms of the conversion-per-pass and other parameters of the system as:

$$\frac{\Delta n}{\Delta t} < 0.2\% (n_f g/v) = 3.6 \times 10^{-4} \text{ moles/min} \quad (1)$$

The rate of reaction was about 1.4×10^{-6} moles/min in the usual operating conditions of the reactor, and thus well below the recommended value for a gradientless system.

Estimates were made of the local heat and mass transfer from the surface of the catalyst to the recirculating gas. The temperature rise of the catalyst was calculated as the difference between the heat added by the exothermic reaction and that removed by the flowing gas stream:

$$\Delta T_c = ((\frac{\Delta n}{\Delta t}) \Delta H - h A_c T_{cg}) / (m_c \rho_c) \quad (2)$$

An estimate of the heat transfer coefficient was made from the appropriate empirical equation (A-3). The reaction rate when ΔT_c is zero was expressed in terms of the temperature gradient between the crystal and the gas phase as:

$$\Delta T_{cg} = (\Delta n / \Delta t) / 2.6 \times 10^{-4} = 5 \times 10^{-3} \text{ } ^\circ\text{C} \quad (3)$$

The calculation indicated that temperature gradients were small and should not have interfered with the accurate measurements of the rate of reaction. Similar calculations were made for mass transfer using the Colburn analogy, and they indicated the surface was uniformly accessible to the gas phase.

As a check on the validity of the calculations, the rate of reaction was measured as a function of the flow rate. The flow rate was varied by an order of magnitude with no effect found on the rate of reaction, and the results are presented in Figure 2. In summary, it became evident by the use of both calculations and experiments that transport limitations were minimized in the reactor design.

REFERENCES

- A-1. Chambers, R. P., Boudart, M., J. Catal., 5, 517 (1966).
- A-2. Durant, J. D., Durant, B., "Introduction to Advanced Inorganic Chemistry", John Wiley and Sons, New York, 1970.
- A-3. Foust, A. S., Wenzel, L. A., Clump, C. W., Maus, L., Anderson, L. B., "Principles of Unit Operations", John Wiley and Sons, New York, 1964.
- A-4. Spice, J. E., Staveley, L. A. K., Harrow, G. A., J. Chem. Soc. (London), 100 (1955).
- A-5. Sykes, K. W., Townshend, S. C., J. Chem. Soc. (London), 2528 (1955).

NOMENCLATURE

g	Volumetric flow rate, cm^3/min
ΔH	Heat of reaction, $\text{cal}/\text{gm}\cdot\text{mole}$
m	Mass of silver catalyst, grams
n	Moles of product
ρ	Density of silver, gm/cc
ΔT	Absolute temperature difference, $^{\circ}\text{K}$
t	Time, min
v	Volume of system, 349 cm^3

Subscripts

c	Refers to catalyst
cg	Refers to interface of crystal and gas
f	Refers to final state

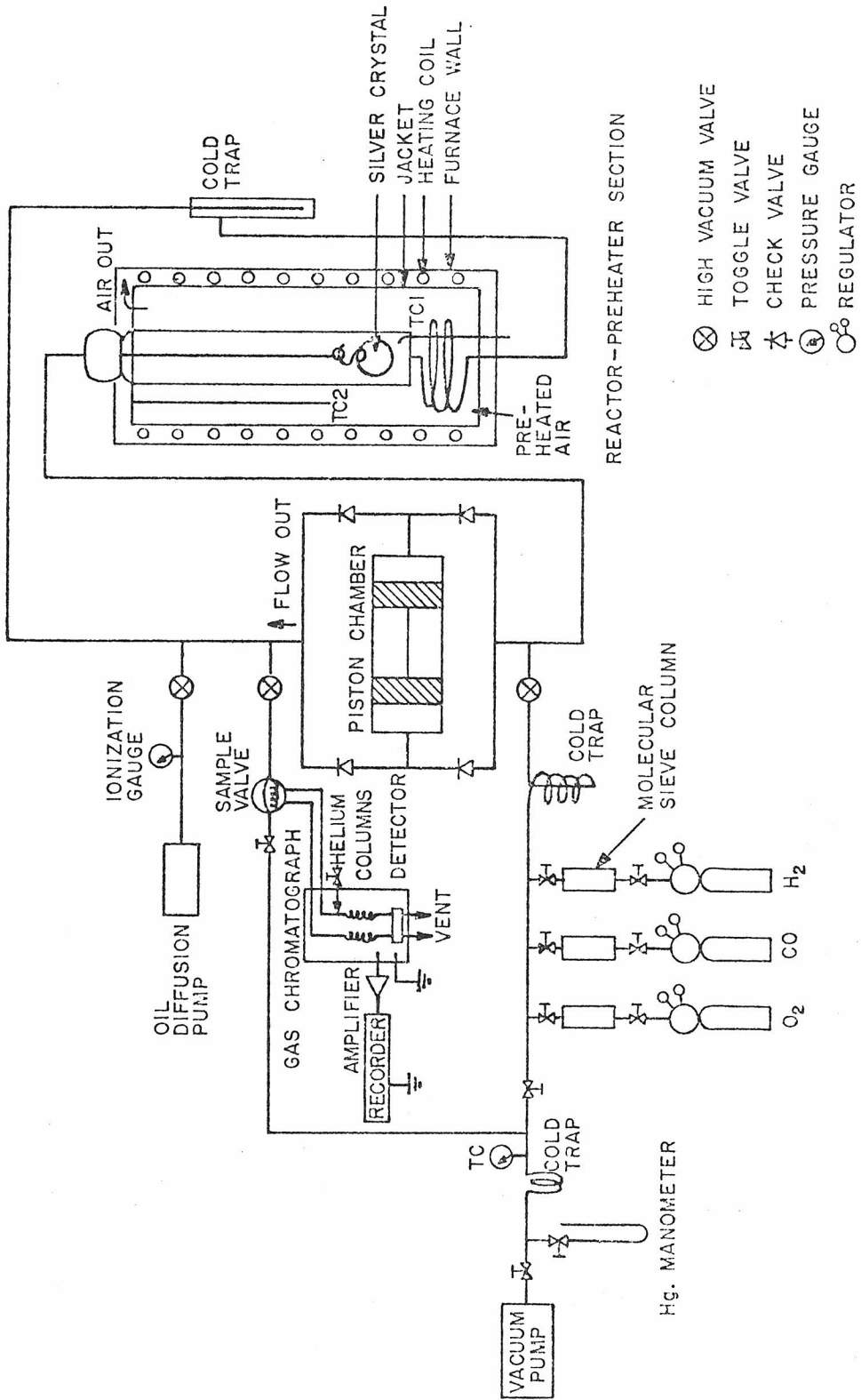


Figure A-1. Schematic of experimental apparatus

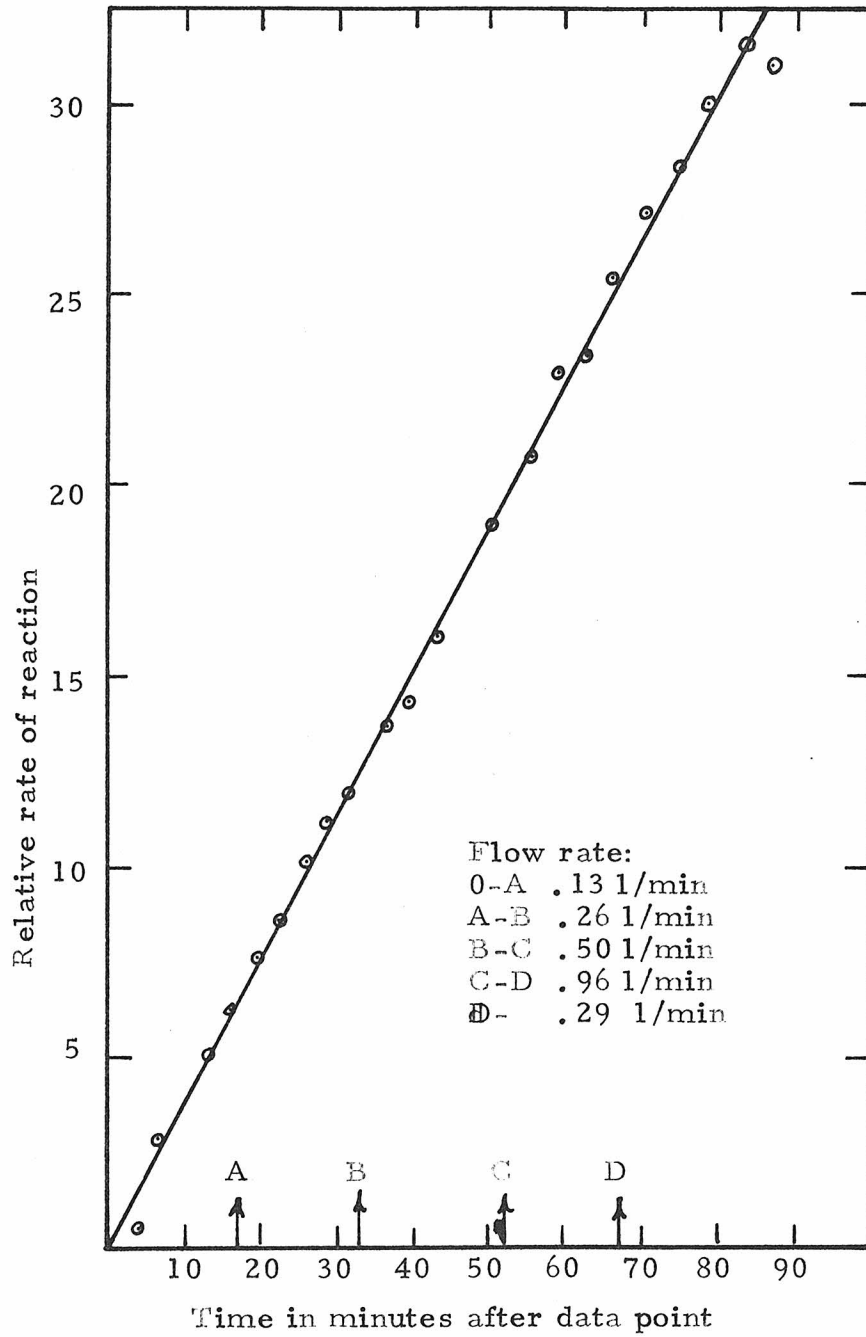


Figure A-2. Chemical rate as a function of time and flow rate through reactor.

APPENDIX B

PURIFICATION AND ANALYSIS OF GASES USED IN THE REACTOR

It was apparent from the experimental results that all sources of poisons to the silver catalyst either in the reactor or in the reactant gases needed to be removed. The identification and removal of the poisons in the reactant gases, and measurement of the concentration of products in the gas phase, are discussed in this appendix.

Carbon monoxide, oxygen and hydrogen were used in the reactor and a quantitative analysis is given in Table 1 for the as-supplied gas. Even though many impurities were present, only hydrocarbons, water, and chlorine might interfere with the catalytic properties of the silver and were of concern. A change to supply gas with a higher purity level would not have solved the problem, since in further purification the significant reduction in the concentration of impurities was in gases which did not poison the silver catalyst. It seemed that by making use of the chemical and physical properties of the impurity gases their concentration could be reduced to a non-interfering level.

A three-stage purification unit was constructed to purify the supply gases. The gases first passed through two columns with equal lengths of the 4\AA and 10\AA molecular sieves. The carbon monoxide cylinder had an additional column with 10\AA sieve placed before the dual molecular sieve column to aid in removing carbon dioxide. The molecular sieves regenerated with a helium purge stream at 600°F in eight hours time. The gases were also cold-trapped in the mixing manifold before entering the reactor with a dry-ice, acetone bath used for carbon monoxide and oxygen, and a liquid-nitrogen bath used for hydrogen.

Results

The traps removed the impurities to a low enough level as to not interfere with the reaction kinetics. N-butane was not detected (< 1 ppm) with a flame ionization detector. Similarly, the concentration of carbon dioxide was below 5 ppm, since it could not be measured with a thermal conductivity detector. The concentration of water was not measured but it was estimated at less than 0.1 ppm. Methane was not removed either by the molecular sieves or the cold trap. However, even if a pyrolysis side reaction was equal in rate to the reaction of methane with oxygen over silver*, methane would not present any problems at the temperatures used in the reactor. Experimental observations confirmed that when the impurities were removed from the supply gases the rate of reaction increased.

Analysis of Reactor Gases

Gas samples were periodically withdrawn from the reactor and quantitatively analyzed in order to determine the rate of reaction. Typical sample mixtures contained by volume about 80% carbon monoxide, 19% oxygen and 1% carbon dioxide. Concentrations of the components were determined by chromatographing the gases and then using a thermal conductivity detector. A Carle (Basic Model 8000) thermal conductivity chromatograph system was used with the modifications of a gas sample valve and a low noise power supply (Fairchild μ A723C chip) which replaced the standard mercury cells.

* Anderson, R. B., Stein, K. C., Feenan, J. J., Hofer, L.J.E., Ind. Eng. Chem., 53, 809 (1961).

Columns of activated charcoal, 5Å molecular sieve, and Porapak T were evaluated for chromatographing the gases. Based on the results in Table 2, Porapak T was selected since it was the best for analyzing the concentration of carbon dioxide. The electrical response of the thermal conductivity detector to standard mixtures of carbon dioxide and carbon monoxide was recorded for calibration curves (Figure 1).

Samples of gases in the reactor were withdrawn by first placing a gas sample loop (.6 cc) under vacuum and then opening a valve to the reactor. The position of the sample valve was changed to admit the sample to the chromatograph column which had a carrier-gas flow rate of 22.5 cc/min. Helium was chosen for the carrier gas because of its high thermal conductivity and since it would not interfere with the gas samples being analyzed. The electrical output of the thermal conductivity detector was amplified (Electro Model A-12) and recorded on a laboratory potentiometer with a mechanical integrator (Beckman Model 1005). The concentration of carbon dioxide in the sample was determined by comparing the as-recorded signal to those of the calibrated mixtures. Overall, gas analysis was accomplished with good precision for the range of concentrations of carbon dioxide found in the reactor. The level of precision was about $\pm 2\%$ above 1000 ppm and decreased to $\pm 7\%$ at 100 ppm.

TABLE B-1

APPROXIMATE COMPOSITION OF CYLINDER GASES
WITH CONCENTRATION OF IMPURITIES IN
PARTS PER MILLION (ppm)

<u>Cylinder Gas</u>	<u>Impurities</u>
1. Carbon Monoxide (99.5%)	CO ₂ (2,000 ppm), N ₂ (75 ppm), O ₂ (20 ppm), n-butane (60 ppm)
2. Helium (99.995%)	Ne (10 ppm), N ₂ (8 ppm), O ₂ (5 ppm), H ₂ (2 ppm), CO ₂ (1 ppm)
3. Hydrogen (99.95%)	N ₂ (400 ppm), O ₂ (8 ppm), Cl ₂ (1 ppm), CO & CO ₂ (1 ppm), Hydrocarbon (1 ppm)
4. Oxygen (99.5%)	A (3500 ppm), N ₂ (200 ppm), Hydrocar- bons--mostly as CH ₄ (20 ppm), CO ₂ (5 ppm)

TABLE B-2
CHROMATOGRAPHY COLUMNS

<u>Column</u>	<u>Results</u>
1. Loosely packed nine foot 1/8" column of 80/90 mesh activated charcoal (Analabs, Inc.). Conditioned at 600°F for six hours.	Column gave poor separation and poor reproducibility for peak heights.
2. Five foot 1/8" column of 5Å molecular sieve. Conditioned twelve hours at 550°F.	Column had good separation of carbon monoxide and oxygen. There was excellent agreement with literature values for response ratio (within 2.5%), but carbon dioxide is absorbed on the molecular sieve.
3. Five feet of 1/8" tubing packed with Porapak T. Conditioned at 350°F for six hours.	Column gave good separation of carbon dioxide from carbon monoxide and oxygen but did not separate carbon monoxide from oxygen.

NOTE: All columns used at room temperature.

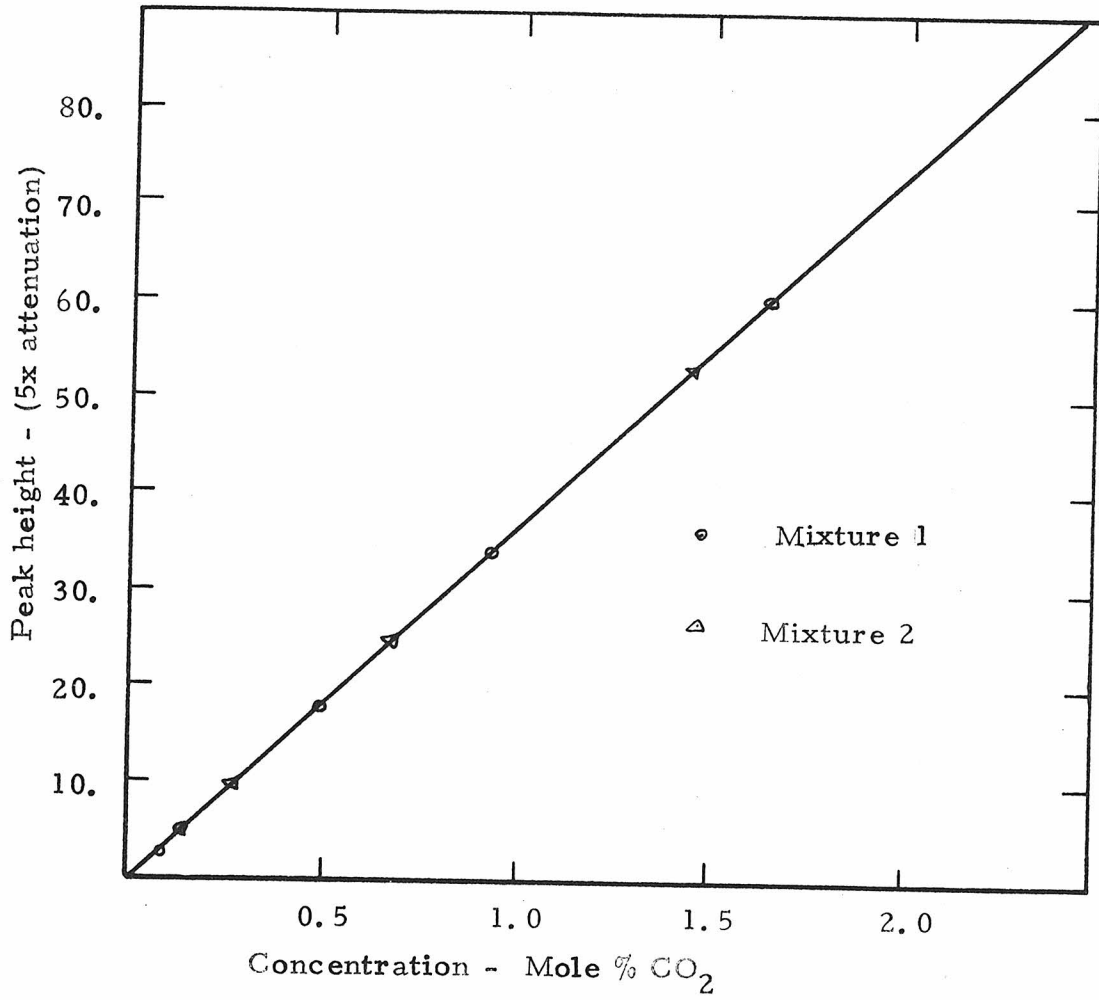


Figure B-1. Calibration curve for the concentration of carbon dioxide as a function of detector response (peak height).

APPENDIX C

PUMP DESIGN FOR THE RECIRCULATION OF GASES

A recirculating pump for a gas-phase chemical reactor was needed to maximize reliability and minimize contamination. Commercial designs were not found, and so one was designed and constructed. It was based upon designs found in the literature (1-5), and analysis of these designs showed several areas for improvement. This appendix describes some of the details of improvement and operation.

Pump Design

The mechanism selected was a double-acting piston inside a cylindrical chamber where each end was connected to the midpoint of a pair of check valves. The piston moved alternately between two electromagnetic coils located outside of the cylindrical tube. Each stroke displaced the volume of gas in front of the piston into the reactor system. Check valves allowed gas flow only in one direction. In essence then, the system represented the mechanical analog of an electrical circuit used to rectify an alternating current. There was a minimum of dead space in order to eliminate incomplete mixing.

Materials which were relatively inert were chosen for construction of the pump because of the sensitivity of the silver catalyst used in the experiments to impurities. Ground-glass balls with ground-glass seats served as check valves, and the cylindrical piston was machined from iron (99%). An early design incorporated Teflon bearings on the piston but was abandoned because the Teflon apparently caused poisoning of the silver catalyst. Teflon was transported to the catalyst surface

as fine particles from the abrasion of the Teflon on the glass, and as monomer vapor.

An electrical circuit was designed which alternately energized the coils in order to move the piston back and forth. It employed solid-state components in order to eliminate wear associated with electrical relays, as is shown in Figure 1. Principal elements of the circuit were a power supply for the coils and a trigger circuit to turn on the silicon-controlled rectifiers (SCR's). The trigger circuit used a unijunction transistor to pulse a bistable multivibrator, the output of which was reshaped by a "one-shot" before triggering the SCR. Components associated with the unijunction and "one-shot" allowed the circuit to have two adjustable time constants. In the use of the two adjustable time constants, one determined the frequency of pumping and therefore the flow rate, and the other controlled the on-time of the coils. The minimum time required for the piston to move was 80 milliseconds, and that number established the minimum setting of the time constants. Although the second time constant allowed some control over the heat generated, there was still need to cool the coils with water. The electrical circuit functioned well and was developed to limit the piston stroke.

Insertion of a variable resistor (R_1) between the coils altered the magnetic force as shown in Figure 2. With both coils energized, there was an electromagnetic braking force which limited the piston stroke. The optimum value of R_1 was a function of the gas being recirculated. For example, while recirculating hydrogen a larger braking force was required as compared to recirculation of oxygen. Thus, with

recirculation of hydrogen, the value of RI was decreased and collisions no longer occurred between the piston and the ends of the glass cylinder in which it traveled. Dimensions of the pump parts were selected after the breakage problem was solved.

Before sizing the pump, an estimate was made of the minimum flow rate required in order to minimize the effects of transport limitations on the chemical rate data. This value was then compared with the estimated maximum flow rate from the pump. The maximum flow rate was estimated to be the product of three terms: the minimum response time of the piston (80 msec), the diameter of the piston, and the length of the coil. We found that a piston diameter of 22 mm and a coil length of 7.7 cm were adequate, and that 34 mm was the optimum distance between the coils for the largest displacement of the piston. Our measured flow rates were about 80% of the estimated values. The difference between the estimated and measured flow rates was due to leakage through the clearance between the piston and the glass cylinder. The range of flow rates for the pump used in this study is shown in Figure 3.

Summary

Overall performance of the pump in two years of use was excellent. The only difficulty was the occasional maintenance required because of the wear of the iron piston on the glass. This problem probably could be reduced by a chrome plating of the piston. For situations where there must be a trouble-free system for the recirculation of gases in a non-reactive and non-contaminating atmosphere, the pump appears to be very useful. Specific advantages of the system are:

1. It gave a flow rate large enough to minimize transport limitations on the chemical rate data from the reactor.
2. Bearings and piston rings were eliminated because of their material possibly causing poisoning of the catalyst.
3. A solid-state electronic circuit eliminated problems of electrical relays and provided a better control of the flow rate from the pump and heat generated by the coils.
4. An electromagnetic braking force was incorporated into the electronics to stop the metal piston at the end of its stroke without breakage of the glass.

REFERENCES

- C-1. Bennett, C. O., Cutlip, M. B., Yang, C. C., Chem. Eng. Sci., 27, 2255 (1972).
- C-2. Chambers, R. P., Daugharty, N. A., Boudart, M., J. Catal., 4, 625 (1965).
- C-3. Kallo, D., Preszler, I., Payer, K., J. Sci. Instr., 41, 338 (1964).
- C-4. Otto, K., Shelef, M., Kimmner, J. T., J. Phys. Chem., 74, 2690 (1970).
- C-5. Sterner, C. J., Rev. Sci. Instr., 31, 1159 (1960).

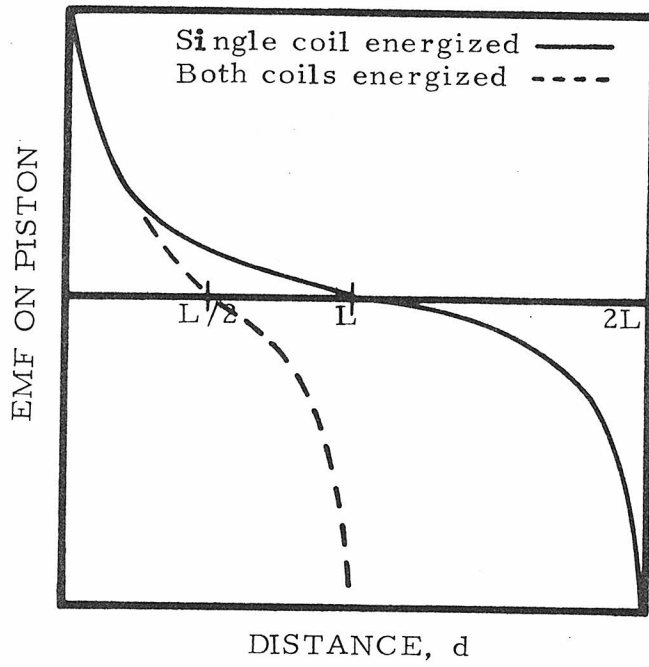


Figure C-2. Electromagnetic force (EMF) on the pump piston as a function of its distance into a coil of length L . (Arbitrary units)

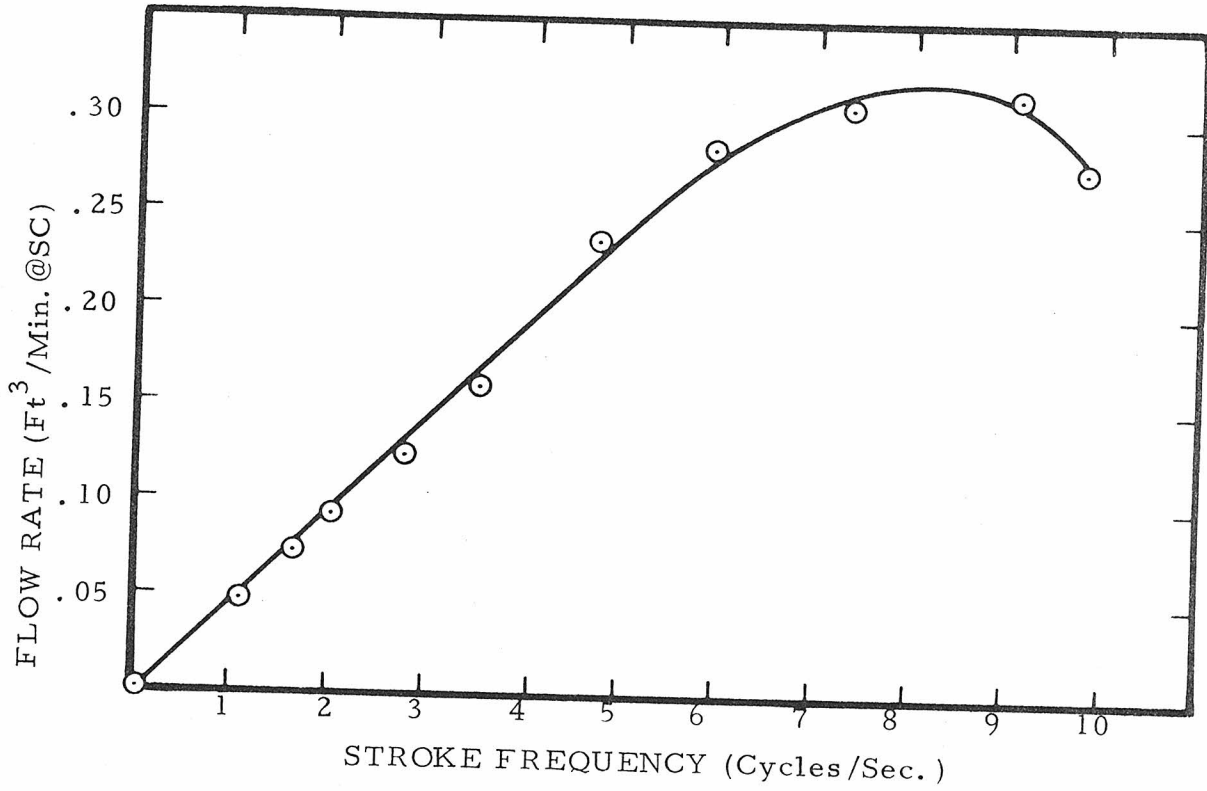


Figure C-3. Pump output as a function of stroke frequency of piston.

APPENDIX D
SPECIMEN PREPARATION

Both foils and single crystals of silver were used as catalysts at various stages of the work. The single crystals were disk-shaped and had a controlled dislocation density. The single crystal specimens were prepared with some of the special techniques and instruments developed by earlier scientists (4-6) in the Materials Science Department at the California Institute of Technology. This appendix describes the transition steps in changing from a polycrystalline silver rod to the single crystal used in the chemical reactor.

Growth of Single Crystals

Early work with silver was on the development of techniques for the introduction and observation of dislocations. During the preliminary effort, it was not considered important that the crystals be of a high purity, have a low dislocation density, or have the proper crystallographic face exposed. It soon became evident, however, that single crystals of high purity silver were required with a low density of dislocations. Single crystals with a specified dislocation density were not found commercially, so they were prepared locally.

The single crystals were grown from polycrystalline rods that were purchased from the United Mineral and Chemical Corporation. The silver was of a high purity (99.999+%) and the major impurities in parts per million as revealed by spectrographic analysis were copper (2 ppm), iron (2 ppm), silicon (.2 ppm) and magnesium (< .1 ppm). From the rods several single crystals of silver were grown under vacuum ($< 10^{-6}$ torr)

with a modified Bridgman method. The molten silver was contained during the growth by graphite molds of ultra-high purity. The crystals were cylindrical in shape and were grown with a diameter of either 1/2 inch or 1-1/8 inch. The single crystals produced in this manner had a high purity, a large sub-grain size, and a low dislocation density.

Machining of Silver

Some experiments did not require the silver to be a single crystal, and for these experiments the silver was prepared with standard methods. For example, early measurements on the catalytic activity of the silver used foils that were prepared by cold-rolling and by cutting the foil to the desired shape. The silver "S"-hook employed in later work to suspend the single crystals was prepared by cold-rolling the silver into a 1 mm square cross-section and bending with pliers into the desired geometry. Other non-strain-free methods such as spark cutting and mechanical polishing with abrasives were found acceptable during early work, but were abandoned with the more precise work needed on the single crystals.

The crystallographic orientation of the single crystals of silver was determined with the back-reflected Laue method. The equipment was accurate to $\pm 0.1^\circ$. After interpretation of the results on the film, the crystal was sliced perpendicular to the desired direction with a wire saw. The saw utilized a stainless steel wire which moved over the single crystal and between two reservoirs of 90 percent nitric acid by volume in water. During sawing the dislocation density did not increase, and two parallel cuts produced an oval disk which needed

further machining.

In order to facilitate handling, the disks were glued to brass buffers with a low melting paraffin wax (45°C) of high purity. Brass was selected for the buffer material because its thermal conductivity was similar to that of silver and thereby minimized any thermal strain on the mounted surface. After mounting, a dab of electrically conductive butyl acetate was placed across the silver crystal and the buffer, and a 1.6 mm hole was trepanned into the crystal using a spark discharge machine with low energy sparks. The site for the hole was selected along the major axis of the disk and near the edge of the crystal. The hole was later used to suspend the polished crystal in the reactor.

Initially, the crystals were polished with the chemical solutions reported by Gilpin and Wozala (3), but later electropolishing was utilized. The change in polishing technique was made because of a concern that some chromium salts would remain on the surface after the chemical polish and interfere with the catalysis. Also, Edmonds (2) had indicated the advantages of electropolishing while preparing specimens for low-energy-electron diffraction. Several electropolishing solutions (1,9) were found useful for different operations, and information is compiled in Table 1.

The face of the mounted silver specimen was electropolished with a special facing machine. The apparatus had two parallel shafts that were electrically isolated. One shaft supported a stainless steel wheel which was covered with a soft wool cloth and rotated in a reservoir of the electrolyte. The other shaft held the crystal face exactly perpendicular to the cloth. After one side of the crystal was polished,

it was remounted on the polished face, and the other side was polished. The polished face was protected with a thin layer of a lacquer while polishing the second side. After polishing the second side, the crystal was rinsed in methyl ethyl ketone to remove the lacquer and reagent grade chloroform to remove the residual paraffin. It was then dried with a stream of air. The resultant surface of the crystal was smooth and film-free, and with careful handling the crystal had the same dislocation density as when the machining was begun. The crystal was ready for use in the reactor after the dislocation density was measured.

Introduction of Dislocations

Several techniques were investigated for introducing dislocations into silver and especially isolated dislocations that would be visible with X-ray diffraction. Initially, it was hoped that the position movement of isolated dislocations could be studied before and after the silver was used as a catalyst. Dislocations were introduced into the single crystals with bursts of laser radiation, and by scratching with an alumina whisker or iron razor blade. Previously, these techniques had proved successful for producing isolated dislocations (4-6). The forces employed in the scratching experiments were from 50-300 dynes on the alumina whiskers and 100-3000 dynes on the razor blades. In the laser trials, a Q-switched laser with an approximate power of one megawatt for ten picoseconds was line focussed on the surface of the silver. Although the procedures of earlier workers were followed, it did not seem possible to produce isolated dislocations in silver. All the methods introduced dislocations (Figure 1), but only the laser pulse appeared to produce what might be single dislocations which could

be observed with X-ray diffraction. The scratching procedures produced only slip bands that were observed as individual dislocation loops which did not move away from the scratch (Figure 1a). The poor results in obtaining isolated dislocations might be attributed to an incomplete understanding of the methods that were tested. Solution of the stress-strain relationships with either a moving point load (scratch) or steep temperature gradient (laser gap) are difficult problems.

The dislocation density of the silver was reduced by annealing. The crystals were placed in a quartz tube which contained a purified argon atmosphere, and the temperature was periodically varied between 1700° and 1350°F. Cyclic annealing was to improve the results and the furnace was "on" for 45 minutes and "off" for 16 minutes. The anneal procedure continued for a week and then the temperature was lowered at 3°C/min to room temperature.

Observation of Dislocations

Although limited success was obtained for introducing isolated dislocations, progress was made in the observation of dislocations. This section describes the Berg-Barrett X-ray-diffraction technique and a chemical-etch pit method. Two methods were needed because the Berg-Barrett method did not image all the dislocations in a crystal and allow a measurement of the dislocation density.

The equipment and analysis for the Berg-Barrett method reported by Turner et al. (10) was used in the experiments. The X-ray diffraction method did not damage the imaged surface, and it was used to view slip bands and the surface topography of the crystals. The penetration

depth of X-rays in silver was limited by the high absorption coefficient. In order to increase the penetration depth, copper $K\alpha$ radiation was diffracted off the (113) plane of silver. A calculation indicated most information would come from a depth within 1 μm of the surface if the intensity of the incident beam was reduced by 85 percent. Nickel filters were placed between the recording film and the crystal in order to improve the signal/noise ratio.

Results recorded with the Berg-Barrett method were satisfactory but there was a problem due to the small penetration depth. For example, compared to aluminum, silver had 1/50th of the X-ray penetration depth. This meant that the signal/noise ratio had to be maximized in order to view isolated dislocations, and that the surfaces of the crystals had to be oriented within 0.25° of the [111] direction in order to image dislocation segments of 500 μm in length. The Berg-Barrett method worked successfully for revealing dislocations in grain boundaries and slip bands as seen in X-ray topographs of Figure 1.

Chemical Etching

The basic etching solution of Robinson and Levinstein (8) was found to be effective for silver, but other additives were necessary to selectively etch dislocations on the (111) face. Addition of a small amount of chromic acid to the basic etching solution gave an indication of the beginnings of a selective etch, and improved results were obtained after halide ions were also added. The effective concentrations of the halide ions in etch developed in this study were either 60 ppm chloride ion or 600 ppm of fluoride ion. A concentration of 60 ppm for

the bromide and iodide ions was too high and formed a film on the silver surface. It seemed evident that a correlation existed between the optimum concentration of the halide ion for a successful etch and the equilibrium constant for the solubility products of the silver halide. The etching solution that was developed for etching the (111) face of silver contained: 20 ml of concentrated NH_4OH , 2 ml of 30 percent hydrogen peroxide, 0.05 ml of chromic acid and 5 ml of 0.2 F NaF solution. The chromic acid solution consisted of 5 g CrO_3 , 25 ml H_2O and 0.5 ml HCl . Newly polished crystals were etched with this solution for twenty seconds and the resulting etch figures on the (111) surface were equilateral triangles with a side length of about $1\mu\text{m}$. Examples of slip bands, grain boundaries and other dislocations as revealed with this solution are shown in Figure 2.

Dislocations which intersected the (111) plane of an unoxxygenated silver crystal were reliably etched by the above chemical etch pit method. The small size of the etch pit enabled crystals with dislocation densities up to 10^8 per cm^2 to be etched. A one-to-one correspondence between etch pits and dislocations was not conclusively proved, but there was strong evidence to suggest such a case:

1. The crystals deformed with increased strain had increased etch pit densities and the pits were observed to be along the $\langle 110 \rangle$ directions.
2. Fresh dislocations introduced into the silver by the scratching methods were etched with this procedure.
3. Observations indicated that sub-boundaries observed in Berg-Barrett topographs were also revealed by this etch-pit

technique. Etch pits which appear between sub-boundaries of as-grown crystals were presumably grown-in dislocations.

Transmission Electron Microscopy

Some experiments were done with transmission electron microscopy to examine the silver crystals for evidence of point defects and/or new phase formation and to compute the actual density of dislocations in a crystal. Only this instrument had the resolving power capable of performing the experiments and in this work a Siemens Eliskop I microscope was used. In order to view a specimen in the electron microscope there are three desired conditions: First, that the specimens be thin ($\sim 1000\text{\AA}$), second, that they be free of films, and finally, that the distribution of defects in the foil was not changed during its preparation.

Specimens were prepared for observation with the following procedure. First, bulk specimens were thinned to 0.25 mm and then a 2.3 mm disk was trepanned from the thinned specimen with a rotating copper electrode on an Agietron spark-discharge machine. In order to limit damage to the specimen during the cutting, low values were used for the capacitance and charging current. Damage from the operation was measured by chemically etching a specimen, and was found to extend less than 0.25 mm from the specimen edge.

The cut and thinned specimens were next jet polished with an electrolyte solution of 7-1/2 percent KCN by weight at 60 ma. The polishing equipment used a single jet of fluid which had a column of light centered on the solution stream. When the foil was perforated,

the column of light illuminated a phototransistor beneath the foil and a relay was triggered to halt the flow of the solution. Hole sizes 20 μm in diameter were obtainable, but it was found necessary to thin both sides in order to have a gradual slope and more thinned areas. While polishing the reverse side, the already polished side was protected by lacquer to prevent the formation of a film. Control of flow rate of the electrolyte, jet diameter, anode to cathode distance, and polishing voltages were all found to be important parameters for successfully polishing foils. Good foils were observed in the microscope on a tilting stage and the usual precautions were taken to insure that number of defects was not changed by handling or from the heat of the electron beam. Magnifications between 5000 and 80,000X were routinely used in this work.

Recording of Surface Topography

Several methods were used for retaining information about the topography of the specimens. In early work acetate replicas were made of the chemically etched surfaces. The replicas later had aluminum flashed onto them but the procedure was replaced with the use of photomicrographs at low magnifications. The Berg-Barrett method allowed a record to be made of grain boundaries and the larger surface features. Results from the Berg-Barrett method were recorded on the following Kodak films: High Resolution Plates, Minicard #6451, and Industrial X-ray film--Type R. Various films were used because of the trade-off between exposure time and resolution.

Other work involved photomicrographs of transparent slides and the crystal surfaces. Photomicrographs of the transparencies were made with a Unitron Model BU-11, and the photomicrographs of the solids with the Bausch and Lomb Model L with reflexback, and Bausch and Lomb Research Metallograph. The two metallographs used for the solids were employed in different ranges of magnification with the former used at 10X and the latter utilized for 50-1500X. Results of metallography were recorded on Kodak Process Ortho, which was developed in DK-41 to improve the resolution. Other recommendations of Kodak were followed during the processing of films and printing to obtain consistently good results.

REFERENCES

- D-1. Baily, J. E., Hirsch, P. B., Phil. Mag., 5, 485 (1960).
- D-2. Edmonds, T., BP Research Center Report #10. 142, March 29, 1967.
- D-3. Gilpin, O. B., Wozala, F. J., Rev. Sci. Instr., 35, 229 (1964).
- D-4. Gorman, J. A., PhD Thesis, "The Mobility of Dislocations in High Purity Aluminum," California Institute of Technology, 1968.
- D-5. Jassby, K. M., PhD Thesis, "An Experimental Study of the Mobility of Edge Dislocations in Pure Copper Single Crystals," California Institute of Technology, 1970.
- D-6. Pope, D. P., PhD Thesis, "The Mobility of Edge Dislocations in the Basal Slip System of Zinc," California Institute of Technology, 1967.
- D-7. Robinson, W. H., Levinstein, H. J., AIME Symposium, "Direct Observation of Imperfections in Crystals", Interscience, 1962, p. 561.
- D-8. Robinson, W. H., Levinstein, H. J., J. Appl. Phys., 33, 3149 (1962).
- D-9. Robinson, W. H., Moon, D. M., Can. J. Phys., 45, 1017 (1967)
- D-10. Turner, A.P.L., Vreeland, T., Jr., Pope, D. P., Acta Cryst., A24, 452 (1968).

TABLE D-1

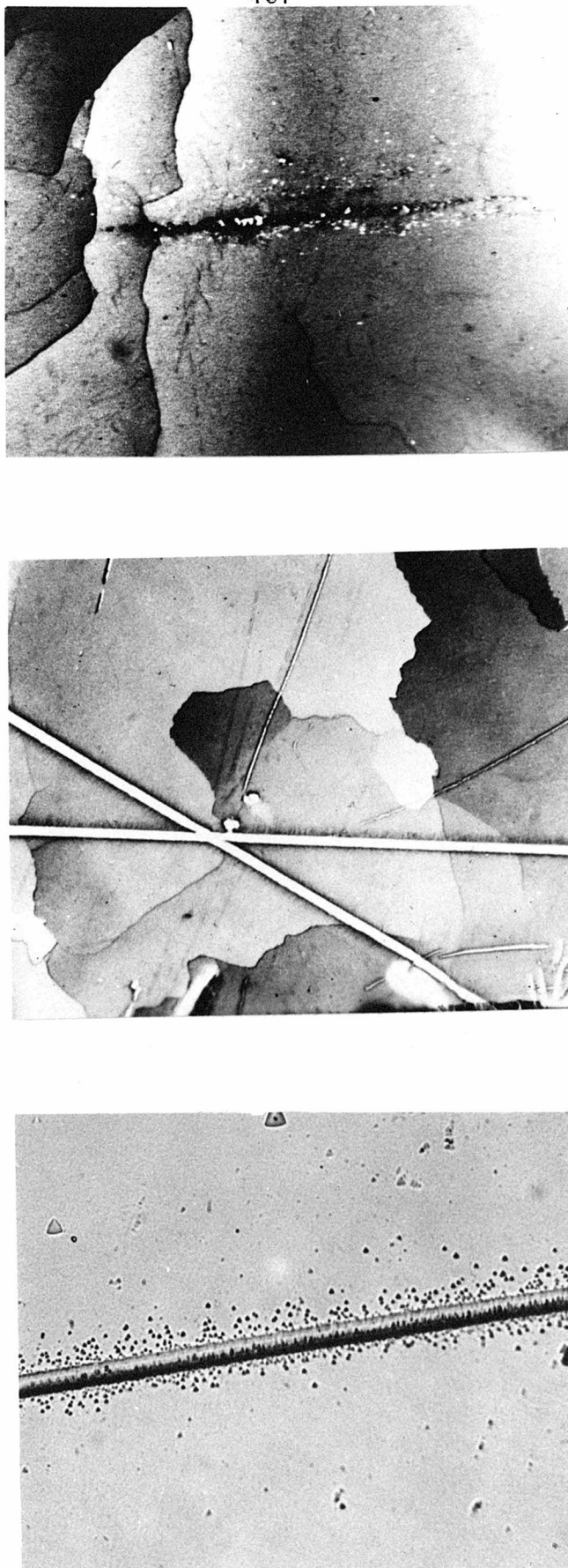
ELECTROPOLISHING SOLUTIONS FOR SILVER

1. 9% KCN (by weight) in water.

This electrolyte was used for rapid silver removal at about 4-5 Volts and 2 amps/cm². The calculated removal rate was 0.005 in/min.

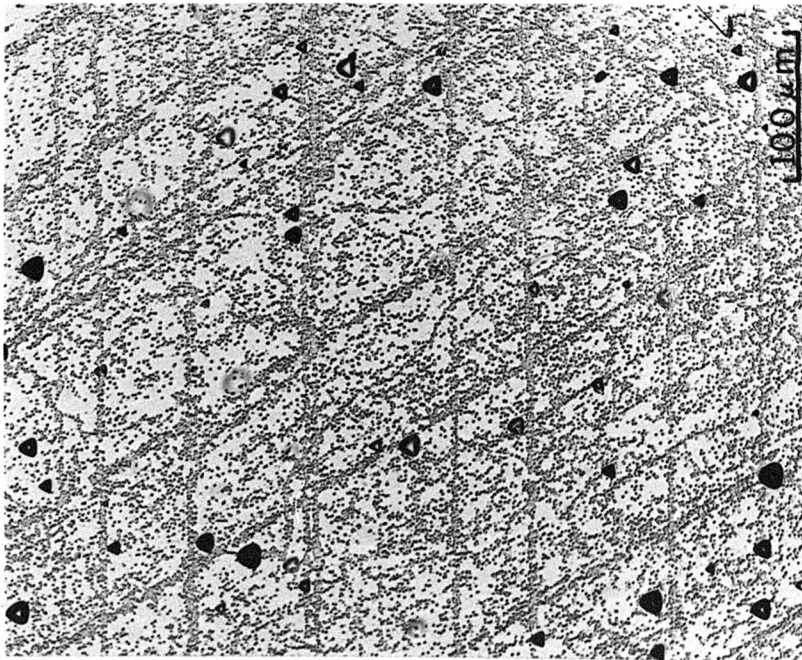
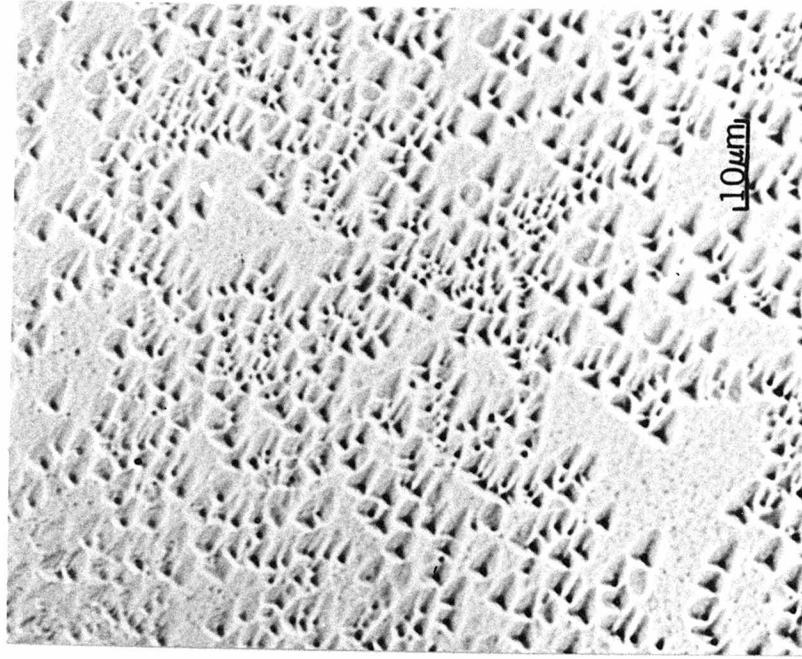
2. 67.5g KCN, 15g KNaC₄H₄O₆ · 4H₂O, 19.5 cc conc. H₃PO₄, 25 cc conc. NH₄OH, 15g K₄Fe(CN)₆ · 3H₂O, 1ℓ H₂O.

This electrolyte was used for final surface polishing at about 4 Volts and 475 ma/cm². Its removal rate for silver was 0.0012 in/min and worked best with some pressure on the wiper wheel of the facing machine.



(a) (b) (c)

Figure 1. Methods attempted to introduce isolated dislocations into silver and view them on the (111) plane (a) Alumina whisker scratch with dislocations revealed by chemical etching, 300X, (b) A razor blade scratch with slip bands and sub-boundaries revealed by the Berg-Barrett method, 50X, (c) A laser pulse in the [112] direction as revealed by the Berg-Barrett method, 50X.



(a)

(b)

Figure 2. Photo micrographs of dislocations intersecting the (111) surface of silver as revealed by the chemical-etch-pit technique (a) Area with slip bands and sub-boundaries at 150X, (b) Area of a high density of pits at 1000X.

APPENDIX E

The change in chemical composition of the reactor gases as a function of time is tabulated in this appendix. Included are the heights of the carbon monoxide-oxygen peak and the carbon dioxide peak from the response of the thermal conductivity detector. Kinetic constants were later obtained by fitting the data to the expression that was developed in the main section of the thesis. The best-fit parameters were then used to calculate the concentration of carbon dioxide in the reactor for the times when a sample was withdrawn. The calculated values were included in the tables for comparison with the measured values. In general, good agreement was found between the calculated and measured concentration of carbon dioxide as a function of time.

-104-
TABLE E-1

DATA ABSTRACTED FROM FIGURE 1 IN PAPER BY KEULKS AND CHANG*
AND USED FOR COMPARISON WITH THIS WORK

Initial conditions in their study:

<u>Temperature</u>	100°C
P_{CO}°	30 torr
$P_{O_2}^{\circ}$	10 torr
π	200 torr

Time (min)	Abscissa F(C)	f	P_{CO_2} (torr)
2.73	.15	.145	2.90
6.0	.45	.245	4.90
10.45	.91	.339	6.79
14.09	1.25	.392	7.84
18.45	1.64	.443	8.86
22.64	1.89	.472	9.44
32.0	2.86	.563	11.26
43.64	3.75	.630	12.61
50.0	4.43	.675	13.50

*Keulks, G. W., Chang, C. C., J. Phys. Chem. 74, 2590 (1970).

TABLE E-2

CRYSTAL # 1 RUN 1

Temperature: 147°F
K = 100236 moles⁻¹
k = 1.707 x 10⁻⁴ min⁻¹

<u>Time (min)</u>	<u>EXPERIMENTAL</u>		<u>CALCULATED</u>
	<u>Peak Height of CO-O₂</u>	<u>Peak Height of CO₂</u>	<u>Peak Height of CO₂</u>
1.0	77.9	1.16	1.16
7.0	79.0	1.70	2.56
10.0	77.5	3.35	3.07
13.0	76.5	3.80	3.52

TABLE E-3

CRYSTAL #1 RUN 2

Temperature: 186°F

$K = 21,174 \text{ moles}^{-1}$

$k = 3.95 \times 10^{-4} \text{ min}^{-1}$

<u>Time (min)</u>	<u>EXPERIMENTAL</u>		<u>CALCULATED</u>
	<u>Peak Height of CO-O₂</u>	<u>Peak Height of CO₂</u>	<u>Peak Height of CO₂</u>
1.0	80.0	1.75	1.75
4.0	80.2	3.18	4.06
7.0	80.4	5.30	6.10
10.0	80.0	7.55	7.87
13.0	80.0	10.16	9.51
16.0	78.8	11.20	10.87

TABLE E-4

CRYSTAL # 1 RUN 3

Temperature: 151°F

$K = 84,684 \text{ moles}^{-1}$

$k = 2.78 \times 10^{-4} \text{ min}^{-1}$

<u>Time (min)</u>	<u>EXPERIMENTAL</u>		<u>CALCULATED</u>
	<u>Peak Height of CO-O₂</u>	<u>Peak Height of CO₂</u>	<u>Peak Height of CO₂</u>
1.0	80.5	2.0	2.0
8.0	80.0	3.77	4.26
12.0	81.5	4.96	5.37
15.0	82.0	5.55	6.12
20.0	79.6	6.30	6.97
25.0	80.1	7.41	7.96
35.0	78.0	9.00	9.37
40.0	78.2	9.60	10.14
45.0	78.5	10.64	10.88
58.0	78.3	13.70	12.52
65.0	77.8	14.14	13.26

TABLE E-5

CRYSTAL #1 RUN 4

Temperature: 150°F

 $K = 88,311 \text{ mole}^{-1}$ $k = 3.57 \times 10^{-4} \text{ min}^{-1}$

<u>Time (min)</u>	<u>EXPERIMENTAL</u>		<u>CALCULATED</u>
	<u>Peak Height of CO-O₂</u>	<u>Peak Height of CO₂</u>	<u>Peak Height of CO₂</u>
1.0	80.8	1.59	1.59
4.0	79.0	2.58	2.96
10.0	79.5	4.40	5.08
17.0	77.6	6.32	6.80
25.0	77.0	7.80	8.48
32.0	77.5	9.38	9.86
40.0	76.8	10.56	11.12
50.0	76.5	12.80	12.59
60.0	76.3	14.50	13.93
70.0	75.5	15.26	15.03
80.0	75.6	16.8	16.23

TABLE E-6

CRYSTAL #1 RUN 5

Temperature: 158°F

$K = 63,379 \text{ moles}^{-1}$

$k = 3.52 \times 10^{-4} \text{ min}^{-1}$

<u>Time (min)</u>	<u>EXPERIMENTAL</u>		<u>CALCULATED</u>
	<u>Peak Height of CO-O₂</u>	<u>Peak Height of CO₂</u>	<u>Peak Height of CO₂</u>
1.0	79.8	2.28	2.28
5.0	79.6	4.00	4.13
10.0	79.8	5.52	5.98
20.0	79.9	8.30	8.90
25.0	80.3	9.26	10.18
30.0	77.7	10.54	10.95
35.0	77.4	11.70	11.93
40.0	78.6	12.90	13.08
45.0	78.0	14.10	13.89
50.0	76.5	14.96	14.47
55.0	76.0	15.40	15.18
60.0	74.8	16.44	15.70

TABLE E-7

CRYSTAL # 1 RUN 6

Temperature: 157°F

$K = 66,032 \text{ moles}^{-1}$

$k = 3.38 \times 10^{-4} \text{ min}^{-1}$

<u>Time (min)</u>	<u>EXPERIMENTAL</u>		<u>CALCULATED</u>
	<u>Peak Height of CO-O₂</u>	<u>Peak Height of CO₂</u>	<u>Peak Height of CO₂</u>
1.0	78.0	2.02	2.02
5.0	79.5	3.83	3.87
10.0	78.6	5.14	5.59
15.0	79.4	6.86	7.13
20.0	77.8	7.85	8.27
25.0	78.1	9.40	9.46
30.0	76.7	10.00	10.34
35.0	78.0	11.14	11.50
40.0	77.7	12.40	12.38
45.0	76.6	12.90	13.06
50.0	75.7	13.90	13.72
55.0	75.1	14.70	14.38
60.0	75.4	15.8	15.17

TABLE E-8

CRYSTAL #2 RUN 1

Temperature: 160°F

$K = 58,413 \text{ moles}^{-1}$

$k = 1.45 \times 10^{-4} \text{ min}^{-1}$

<u>Time (min)</u>	<u>EXPERIMENTAL</u>		<u>CALCULATED</u>
	<u>Peak Height of CO-O₂</u>	<u>Peak Height of CO₂</u>	<u>Peak Height of CO₂</u>
1.0	80.9	1.56	1.56
5.0	80.0	2.50	2.50
10.0	79.0	3.90	3.48
15.0	78.5	4.55	4.35
20.0	79.0	5.35	5.19
25.0	76.3	5.89	5.73
30.0	78.5	6.65	6.58
35.0	79.5	7.30	7.32
40.0	77.4	7.85	7.73
45.0	76.2	8.19	8.18
50.0	75.2	8.46	8.60
55.0	76.0	9.09	9.21
60.0	75.2	9.36	9.60

TABLE E-9

CRYSTAL #2 RUN 2

Temperature: 152°F

K = 81,217 moles⁻¹k = 1.39 x 10⁻⁴ min⁻¹

<u>Time (min)</u>	<u>EXPERIMENTAL</u>		<u>CALCULATED</u>
	<u>Peak Height of CO-O₂</u>	<u>Peak Height of CO₂</u>	<u>Peak Height of CO₂</u>
1.0	81.0	1.50	1.50
5.0	81.0	2.35	2.34
10.0	79.4	3.18	3.17
15.0	79.5	3.88	3.94
20.0	80.0	4.63	4.66
25.0	80.0	5.30	5.29
30.0	78.5	5.67	5.77
35.0	78.3	6.00	6.30
40.0	77.0	6.54	6.70
45.0	77.0	6.92	7.16
50.0	77.0	8.00	7.63
55.0	75.0	8.18	7.86

TABLE E-10

CRYSTAL #2 RUN 3

Temperature: 155°F

$K = 71,703 \text{ moles}^{-1}$

$k = 1.29 \times 10^{-4} \text{ min}^{-1}$

<u>Time (min)</u>	<u>EXPERIMENTAL</u>		<u>CALCULATED</u>
	<u>Peak Height of CO-O₂</u>	<u>Peak Height of CO₂</u>	<u>Peak Height of CO₂</u>
1.0	80.0	2.28	2.28
5.0	80.0	3.29	2.90
10.0	78.4	3.90	3.70
15.0	78.3	4.66	4.40
20.0	78.0	5.17	5.01
25.0	78.3	5.90	5.62
30.0	77.6	6.40	6.12
35.0	77.5	6.82	6.63
40.0	77.6	7.05	7.14
45.0	77.0	7.65	7.55
50.0	77.2	7.58	8.02
55.0	77.0	8.28	8.43
60.0	76.6	8.60	8.80

TABLE E-11

CRYSTAL #2 RUN 4

Temperature: 154°F
 $K = 74,734 \text{ moles}^{-1}$
 $k = 2.01 \times 10^{-4} \text{ min}^{-1}$

<u>Time (min)</u>	<u>EXPERIMENTAL</u>		<u>CALCULATED</u>
	<u>Peak Height of CO-O₂</u>	<u>Peak Height of CO₂</u>	<u>Peak Height of CO₂</u>
1.0	80.3	1.80	1.80
5.0	80.0	2.92	2.93
10.0	80.3	4.23	4.12
15.0	80.1	5.05	5.13
20.0	80.8	6.03	6.08
25.0	80.3	7.05	6.87
30.0	78.6	7.25	7.47
35.0	79.4	8.10	8.25
40.0	77.2	8.38	8.67
45.0	77.7	9.40	9.34
50.0	77.7	10.09	9.93
55.0	76.5	10.24	10.33
60.0	77.7	11.34	11.03

TABLE E-12

CRYSTAL #2 RUN 5

Temperature: 154°F

$K = 74,734 \text{ moles}^{-1}$

$k = 1.61 \times 10^{-4} \text{ min}^{-1}$

<u>Time (min)</u>	<u>EXPERIMENTAL</u>		<u>CALCULATED</u>
	<u>Peak Height of CO-O₂</u>	<u>Peak Height of CO₂</u>	<u>Peak Height of CO₂</u>
1.0	78.0	1.48	1.48
5.0	80.0	2.54	2.49
10.0	78.0	3.78	3.42
15.0	76.6	3.85	4.21
20.0	77.5	5.24	5.03
25.0	77.5	5.80	5.73
30.0	78.2	6.45	6.44
35.0	75.3	7.00	6.79
40.0	77.6	7.80	7.57
45.0	76.8	8.05	8.03
55.0	75.2	8.60	8.85
60.0	74.7	9.00	9.26

TABLE E-13

CRYSTAL #3 RUN 1

Temperature: 183°F

K = 23,704 moles⁻¹k = 1.30 x 10⁻⁴ min⁻¹

<u>Time (min)</u>	<u>EXPERIMENTAL</u>		<u>CALCULATED</u>
	<u>Peak Height of CO-O₂</u>	<u>Peak Height of CO₂</u>	<u>Peak Height of CO₂</u>
1.0	89.0	1.30	1.30
5.0	92.2	2.62	2.59
8.0	88.8	3.43	3.34
11.0	88.7	4.35	4.12
14.0	89.0	4.90	4.90
18.0	86.5	5.80	5.69
22.0	89.0	6.60	6.76
25.0	87.0	7.28	7.24
28.0	85.0	7.58	7.68

TABLE E-14

CRYSTAL #3 RUN 2

Temperature: 161°F

$K = 56,089 \text{ moles}^{-1}$

$k = 7.93 \times 10^{-5} \text{ min}^{-1}$

<u>Time (min)</u>	<u>EXPERIMENTAL</u>		<u>CALCULATED</u>
	<u>Peak Height of CO-O₂</u>	<u>Peak Height of CO₂</u>	<u>Peak Height of CO₂</u>
1.0	81.4	0.93	0.93
5.0	81.2	1.45	1.54
8.5	81.3	2.02	2.03
12.0	83.0	2.44	2.53
15.5	80.1	2.78	2.87
19.0	80.0	3.2	3.26
22.5	80.0	3.76	3.63
26.0	81.0	4.13	4.04

TABLE E-15

CRYSTAL # 3 RUN 3

Temperature: 162°F

$K = 53,865 \text{ moles}^{-1}$

$k = 1.14 \times 10^{-4} \text{ min}^{-1}$

<u>Time (min)</u>	<u>EXPERIMENTAL</u>		<u>CALCULATED</u>
	<u>Peak Height of CO-O₂</u>	<u>Peak Height of CO₂</u>	<u>Peak Height of CO₂</u>
3.0	80.0	1.64	1.64
6.5	80.0	2.38	2.31
10.0	80.0	7.87	2.93
13.5	78.0	3.40	3.41
17.0	79.0	4.08	3.98
20.5	79.5	4.53	4.50
24.0	78.7	4.95	4.93
27.5	79.0	5.32	5.39

TABLE E-16

CRYSTAL # 3 RUN 4

Temperature: 172.5°F

$K = 35,490 \text{ moles}^{-1}$

$k = 1.79 \times 10^{-4} \text{ min}^{-1}$

<u>Time (min)</u>	<u>EXPERIMENTAL</u>		<u>CALCULATED</u>
	<u>Peak Height of CO-O₂</u>	<u>Peak Height of CO₂</u>	<u>Peak Height of CO₂</u>
3.5	81.8	1.48	1.47
7.0	81.8	2.60	2.67
10.5	80.8	3.76	3.70
14.0	81.2	4.95	4.68
17.5	81.6	5.60	5.60
21.0	80.7	6.38	6.36
24.5	81.0	7.00	7.17
28.0	80.8	7.90	7.89

TABLE E-17

CRYSTAL #3 RUN 5

Temperature: 161°F

$K = 56,089 \text{ moles}^{-1}$

$k = 1.25 \times 10^{-4} \text{ min}^{-1}$

<u>Time (min)</u>	<u>EXPERIMENTAL</u>		<u>CALCULATED</u>
	<u>Peak Height of CO-O₂</u>	<u>Peak Height of CO₂</u>	<u>Peak Height of CO₂</u>
5.5	82.0	2.56	2.56
9.0	81.8	2.82	3.21
13.0	84.7	3.43	4.04
16.5	81.4	4.28	4.45
20.0	81.4	4.75	4.97
23.5	81.5	5.40	5.48
27.0	82.0	6.17	5.99
30.5	79.5	6.70	6.25

TABLE E-18

CRYSTAL #3 RUN 6

Temperature: 163°F

K = 51,735 moles⁻¹

k = 1.66 x 10⁻⁴ min⁻¹

<u>Time (min)</u>	<u>EXPERIMENTAL</u>		<u>CALCULATED</u>
	<u>Peak Height of CO-O₂</u>	<u>Peak Height of CO₂</u>	<u>Peak Height of CO₂</u>
2.5	82.5	1.40	1.40
6.0	82.2	2.47	2.43
9.5	81.7	3.38	3.32
13.0	81.8	4.12	4.14
16.5	90.0	5.10	5.38
20.0	83.1	5.70	5.67
23.5	83.0	6.29	6.33
27.0	81.3	7.00	6.81

TABLE E-19

CRYSTAL # 3 RUN 7

Temperature: 134°F

$K = 176,116 \text{ moles}^{-1}$

$k = 1.00 \times 10^{-4} \text{ min}^{-1}$

<u>Time (min)</u>	<u>EXPERIMENTAL</u>		<u>CALCULATED</u>
	<u>Peak Height of CO-O₂</u>	<u>Peak Height of CO₂</u>	<u>Peak Height of CO₂</u>
1.0	82.4	0.6	0.60
4.5	80.8	1.10	1.12
8.0	81.1	1.43	1.56
11.5	80.0	1.96	1.92
15.0	79.6	2.22	2.25
18.5	79.7	2.48	2.56
22.0	78.5	2.85	2.81
25.5	79.0	3.20	3.09

TABLE E-20

CRYSTAL #3 RUN 8

Temperature: 138°F

$K = 147,690 \text{ moles}^{-1}$

$k = 1.33 \times 10^{-4} \text{ min}^{-1}$

<u>Time (min)</u>	<u>EXPERIMENTAL</u>		<u>CALCULATED</u>
	<u>Peak Height of CO-O₂</u>	<u>Peak Height of CO₂</u>	<u>Peak Height of CO₂</u>
1.5	82.0	0.48	0.48
5.0	82.7	1.43	1.25
8.5	83.0	1.91	1.87
12.0	91.0	2.38	2.62
15.5	83.0	2.76	2.85
19.0	80.3	3.22	3.17
22.5	80.8	3.59	3.56
26.0	81.0	4.00	3.92

TABLE E-21

CRYSTAL #3 RUN 9

Temperature: 196°F

$K = 14,642 \text{ moles}^{-1}$

$k = 3.75 \times 10^{-4} \text{ min}^{-1}$

<u>Time (min)</u>	<u>EXPERIMENTAL</u>		<u>CALCULATED</u>
	<u>Peak Height of CO-O₂</u>	<u>Peak Height of CO₂</u>	<u>Peak Height of CO₂</u>
1.0	82.7	1.94	1.94
4.5	83.0	4.73	4.72
8.0	83.0	7.10	7.19
11.5	80.5	9.05	9.14
15.0	80.4	11.10	11.13
18.5	79.6	13.12	12.87
22.0	80.5	14.80	14.77
25.5	80.0	16.24	16.33

TABLE E-22

CRYSTAL #3 RUN 10

Temperature: 166°F

 $K = 45,873 \text{ moles}^{-1}$ $k = 2.10 \times 10^{-4} \text{ min}^{-1}$

<u>Time (min)</u>	<u>EXPERIMENTAL</u>		<u>CALCULATED</u>
	<u>Peak Height of CO-O₂</u>	<u>Peak Height of CO₂</u>	<u>Peak Height of CO₂</u>
1.0	80.5	0.92	0.92
4.5	81.2	1.96	2.32
8.0	85.5	3.28	3.69
11.5	82.3	4.20	4.60
15.0	80.0	5.30	5.40
18.5	78.4	6.19	6.13
22.0	78.0	6.75	6.87
25.5	77.0	7.50	7.51
29.0	77.4	8.16	8.23
32.5	77.0	9.27	8.83
36.0	76.5	9.55	9.39

TABLE E-23

CRYSTAL #3 RUN 11

Temperature: 171.5°F

 $K = 36,906 \text{ moles}^{-1}$ $k = 2.55 \times 10^{-4} \text{ min}^{-1}$

<u>Time (min)</u>	<u>EXPERIMENTAL</u>		<u>CALCULATED</u>
	<u>Peak Height of CO-O₂</u>	<u>Peak Height of CO₂</u>	<u>Peak Height of CO₂</u>
1.0	82.7	1.05	1.05
4.5	81.5	2.72	2.76
8.0	81.3	4.12	4.21
11.5	81.3	5.40	5.49
15.0	80.5	6.50	6.58
18.5	79.8	7.80	7.57
22.0	80.0	8.59	8.57
25.5	79.0	9.35	9.37

TABLE E-24

CRYSTAL #3 RUN 12

Temperature: 170°F
K = 39,147 moles⁻¹
k = 2.73 x 10⁻⁴ min⁻¹

<u>Time (min)</u>	<u>EXPERIMENTAL</u>		<u>CALCULATED</u>
	<u>Peak Height of CO-O₂</u>	<u>Peak Height of CO₂</u>	<u>Peak Height of CO₂</u>
1.0	82.2	1.02	1.02
4.5	82.5	2.95	2.86
8.0	83.4	4.28	4.44
11.5	90.0	5.75	6.25
15.0	81.6	6.77	6.86
18.5	82.0	8.05	8.00
22.0	84.0	9.04	9.24
25.5	80.0	10.25	9.73

TABLE E-25

CRYSTAL # 3 RUN 13

Temperature: 166°F

K = 45,873 moles⁻¹k = 2.58 x 10⁻⁴ min⁻¹

<u>Time (min)</u>	<u>EXPERIMENTAL</u>		<u>CALCULATED</u>
	<u>Peak Height of CO-O₂</u>	<u>Peak Height of CO₂</u>	<u>Peak Height of CO₂</u>
1.0	80.8	1.00	1.00
4.5	82.5	2.42	2.71
8.0	82.5	3.87	4.10
11.5	80.5	5.00	5.19
15.0	83.0	6.08	6.45
18.5	79.8	7.03	7.17
22.0	81.0	7.82	8.19
25.5	79.4	9.10	8.87
29.0	80.0	9.80	9.73
32.5	80.0	10.70	10.48
36.0	78.5	11.36	11.00

TABLE E-26

CRYSTAL # 3 RUN 14

Temperature: 170°F

K = 39, 147 moles⁻¹k = 2.74 x 10⁻⁴ min⁻¹

<u>Time (min)</u>	<u>EXPERIMENTAL</u>		<u>CALCULATED</u>
	<u>Peak Height of CO-O₂</u>	<u>Peak Height of CO₂</u>	<u>Peak Height of CO₂</u>
1.0	81.6	1.04	1.04
4.5	81.1	2.97	2.84
8.0	82.3	4.45	4.42
11.5	83.8	5.60	5.86
15.0	81.2	6.85	6.87
18.5	81.3	7.73	7.97
22.0	81.4	8.95	8.99
25.5	80.5	10.0	9.84
29.0	79.6	10.80	10.61

TABLE E-27

CRYSTAL # 3 RUN 15

Temperature: 168°F
K = 42,366 moles⁻¹
k = 2.69 x 10⁻⁴ min⁻¹

<u>Time (min)</u>	<u>EXPERIMENTAL</u>		<u>CALCULATED</u>
	<u>Peak Height of CO-O₂</u>	<u>Peak Height of CO₂</u>	<u>Peak Height of CO₂</u>
1.0	82.8	1.35	1.35
4.5	82.9	3.83	3.08
8.0	83.0	4.32	4.54
11.5	85.0	5.65	5.96
15.0	81.0	6.82	6.80
18.5	81.3	7.56	7.86
22.0	81.9	8.60	8.88
25.5	80.8	9.85	9.66
29.0	79.8	10.74	10.38

TABLE E-28

CRYSTAL # 4 RUN 1

Temperature: 167°F
K = 44,082 moles⁻¹
k = 1.38 x 10⁻⁴ min⁻¹

<u>Time (min)</u>	<u>EXPERIMENTAL</u>		<u>CALCULATED</u>
	<u>Peak Height of CO-O₂</u>	<u>Peak Height of CO₂</u>	<u>Peak Height of CO₂</u>
1.0	81.4	0.81	0.81
4.5	80.9	1.72	1.77
8.0	81.0	2.54	2.63
11.5	79.5	3.44	3.34
15.0	79.8	4.50	4.05
18.5	80.0	5.05	4.72
22.0	79.5	5.30	5.30
25.5	90.0	6.04	6.66

TABLE E-29

CRYSTAL #4 RUN 2

Temperature: 175°F

$K = 32,300 \text{ moles}^{-1}$

$k = 1.89 \times 10^{-4} \text{ min}^{-1}$

<u>Time (min)</u>	<u>EXPERIMENTAL</u>		<u>CALCULATED</u>
	<u>Peak Height of CO-O₂</u>	<u>Peak Height of CO₂</u>	<u>Peak Height of CO₂</u>
1.0	88.0	0.68	0.68
4.5	80.5	2.29	2.00
8.25	79.5	3.47	3.25
11.5	78.8	4.33	4.21
15.0	80.0	5.52	5.26
18.5	77.1	6.10	5.95
22.0	85.5	6.95	7.52
25.5	80.0	7.82	7.85

TABLE E-30

CRYSTAL #4 RUN 3

Temperature: 180°F

$K = 26,566 \text{ moles}^{-1}$

$k = 1.96 \times 10^{-4} \text{ min}^{-1}$

<u>Time (min)</u>	<u>EXPERIMENTAL</u>		<u>CALCULATED</u>
	<u>Peak Height of CO-O₂</u>	<u>Peak Height of CO₂</u>	<u>Peak Height of CO₂</u>
1.0	82.6	1.30	1.30
4.5	94.0	2.68	3.10
8.0	82.0	4.02	3.97
11.5	8.15	4.99	5.09
15.0	80.5	6.12	6.08
18.5	80.3	7.09	7.04
22.0	79.0	7.90	7.84

TABLE E-31

CRYSTAL # 4 RUN 4

Temperature: 179°F

$K = 27,601 \text{ moles}^{-1}$

$k = 2.36 \times 10^{-4} \text{ min}^{-1}$

<u>Time (min)</u>	<u>EXPERIMENTAL</u>		<u>CALCULATED</u>
	<u>Peak Height of CO-O₂</u>	<u>Peak Height of CO₂</u>	<u>Peak Height of CO₂</u>
1.0	80.0	1.05	1.05
4.5	80.0	2.73	2.71
8.0	80.0	4.08	4.16
11.5	78.6	5.40	5.37
15.0	83.5	6.55	6.95
18.5	78.2	7.60	7.59
22.0	78.5	8.70	8.64
25.5	78.3	9.80	9.58

TABLE E-32

CRYSTAL # 4 RUN 5

Temperature: 178.5°F

$K = 28,135 \text{ moles}^{-1}$

$k = 2.31 \times 10^{-4} \text{ min}^{-1}$

<u>Time (min)</u>	<u>EXPERIMENTAL</u>		<u>CALCULATED</u>
	<u>Peak Height of CO-O₂</u>	<u>Peak Height of CO₂</u>	<u>Peak Height of CO₂</u>
1.0	78.8	0.79	0.79
4.5	82.0	2.54	2.52
8.0	80.0	3.93	3.90
11.5	78.5	5.24	5.09
15.0	78.0	6.20	6.21
18.5	78.0	7.05	7.28
22.0	79.0	8.50	8.38

TABLE E-33

CRYSTAL #4 RUN 6

Temperature: 174°F

$K = 33,474 \text{ moles}^{-1}$

$k = 2.48 \times 10^{-4} \text{ min}^{-1}$

<u>Time (min)</u>	<u>EXPERIMENTAL</u>		<u>CALCULATED</u>
	<u>Peak Height of CO-O₂</u>	<u>Peak Height of CO₂</u>	<u>Peak Height of CO₂</u>
1.0	80.0	1.21	1.21
4.0	80.1	2.62	2.64
7.0	79.5	3.73	3.87
10.0	78.8	5.34	4.94
13.0	83.0	5.76	6.27
16.0	78.8	7.50	6.90
19.0	80.0	7.79	7.90
22.0	78.0	8.38	8.52
25.0	77.8	9.25	9.28

TABLE E-34

CRYSTAL #4 RUN 7

Temperature: 183°F

$K = 23,704 \text{ moles}^{-1}$

$k = 2.77 \times 10^{-4} \text{ min}^{-1}$

<u>Time (min)</u>	<u>EXPERIMENTAL</u>		<u>CALCULATED</u>
	<u>Peak Height of CO-O₂</u>	<u>Peak Height of CO₂</u>	<u>Peak Height of CO₂</u>
1.0	80.8	1.40	1.40
4.5	79.8	3.36	3.30
7.5	80.3	4.95	4.78
11.2	78.9	6.05	6.29
14.5	79.8	7.78	7.68
17.5	87.0	8.42	9.60
20.5	79.5	9.81	9.82
23.5	77.5	10.88	10.55
27.0	77.5	11.44	11.63
30.0	77.3	12.76	12.49
33.0	76.9	13.64	13.27

TABLE E-35

CRYSTAL # 5 RUN 1

Temperature: 154°F
K = 74,734 moles⁻¹
k = 1.93 x 10⁻⁴ min⁻¹

<u>Time (min)</u>	<u>EXPERIMENTAL</u>		<u>CALCULATED</u>
	<u>Peak Height of CO-O₂</u>	<u>Peak Height of CO₂</u>	<u>Peak Height of CO₂</u>
1.5	81.5	1.80	1.80
5.0	80.8	3.30	2.77
10.0	80.0	4.70	3.90
15.0	80.0	5.10	4.91
20.0	80.8	5.78	5.85
25.0	80.4	6.82	6.64
30.0	78.9	7.50	7.25
35.0	79.0	7.89	7.95
40.0	78.3	8.14	8.53
45.0	77.8	8.78	9.08

TABLE E-36

CRYSTAL #5 RUN 2

Temperature: 154°F

$K = 74,734 \text{ moles}^{-1}$

$k = 1.62 \times 10^{-4} \text{ min}^{-1}$

<u>Time (min)</u>	<u>EXPERIMENTAL</u>		<u>CALCULATED</u>
	<u>Peak Height of CO-O₂</u>	<u>Peak Height of CO₂</u>	<u>Peak Height of CO₂</u>
1.0	80.0	1.50	1.50
5.0	79.5	2.50	2.47
10.0	79.5	3.80	3.49
15.0	80.6	4.50	4.43
20.0	79.2	5.80	5.15
25.0	78.6	5.93	5.83
30.0	77.0	7.00	6.36
35.0	80.0	7.43	7.24
40.0	78.0	7.65	7.64
45.0	77.1	7.86	8.10
50.0	79.8	8.48	8.92
55.0	77.5	8.94	9.16
60.0	76.0	9.20	9.46

TABLE E-37

CRYSTAL #5 RUN 3

Temperature: 151°F

 $K = 84,684 \text{ moles}^{-1}$ $k = 2.06 \times 10^{-4} \text{ min}^{-1}$

<u>Time (min)</u>	<u>EXPERIMENTAL</u>		<u>CALCULATED</u>
	<u>Peak Height of CO-O₂</u>	<u>Peak Height of CO₂</u>	<u>Peak Height of CO₂</u>
1.0	79.5	1.32	1.32
5.0	82.0	2.40	2.59
10.0	79.0	3.40	3.68
15.0	81.8	4.50	4.86
20.0	81.0	5.68	5.72
25.0	79.5	6.40	6.41
30.0	78.4	6.48	7.06
35.0	78.6	7.60	7.75
40.0	78.8	8.21	8.42
45.0	77.8	8.80	8.91
50.0	77.7	9.74	9.46
55.0	77.5	10.50	9.98
60.0	77.2	10.76	10.46

TABLE E-38

CRYSTAL #5 RUN 4

Temperature: 150°F
K = 88,311 moles⁻¹
k = 1.13 x 10⁻⁵ min⁻¹

<u>Time (min)</u>	<u>EXPERIMENTAL</u>		<u>CALCULATED</u>
	<u>Peak Height of CO-O₂</u>	<u>Peak Height of CO₂</u>	<u>Peak Height of CO₂</u>
1.0	80.0	0.91	0.91
5.0	80.0	1.26	1.66
10.0	80.0	2.40	2.45
15.0	79.1	2.90	3.10
20.0	79.1	3.46	3.71
25.0	78.3	3.95	4.22
30.0	79.3	4.60	4.79
35.0	79.2	5.28	5.26
40.0	78.6	5.73	5.68
45.0	78.6	5.99	6.10
50.0	78.8	6.45	6.53
55.0	77.7	7.53	6.82

TABLE E-39

CRYSTAL # 5 RUN 5

Temperature: 152°F

$K = 81,217 \text{ moles}^{-1}$

$k = 2.74 \times 10^{-4} \text{ min}^{-1}$

<u>Time (min)</u>	<u>EXPERIMENTAL</u>		<u>CALCULATED</u>
	<u>Peak Height of CO-O₂</u>	<u>Peak Height of CO₂</u>	<u>Peak Height of CO₂</u>
1.0	77.5	1.05	1.05
5.0	77.5	2.90	2.60
10.0	78.0	3.80	4.15
15.0	77.5	5.10	5.36
20.0	76.9	6.50	6.37
25.0	77.7	6.94	7.40
30.0	77.2	7.90	8.23
35.0	77.0	9.35	9.01
40.0	77.0	9.76	9.77
45.0	76.4	10.48	10.40
50.0	76.2	11.40	11.04

TABLE E-40

CRYSTAL #6 RUN 1

Temperature: 182°F

$K = 24,619 \text{ moles}^{-1}$

$k = 1.25 \times 10^{-4} \text{ min}^{-1}$

<u>Time (min)</u>	<u>EXPERIMENTAL</u>		<u>CALCULATED</u>
	<u>Peak Height of CO-O₂</u>	<u>Peak Height of CO₂</u>	<u>Peak Height of CO₂</u>
1.0	80.0	1.18	1.18
4.5	79.4	1.97	2.07
8.0	80.2	3.07	2.94
11.5	78.4	5.20	3.65
15.0	79.0	4.30	4.42
18.5	80.6	4.90	5.23
22.0	77.0	5.61	5.66
22.5	79.0	6.32	6.45
29.0	77.0	7.00	6.89
32.5	75.6	7.15	7.34
36.0	75.5	7.75	7.88

TABLE E-41

CRYSTAL # 6 RUN 2

Temperature: 180°F

 $K = 26,566 \text{ moles}^{-1}$ $k = 2.57 \times 10^{-4} \text{ min}^{-1}$

<u>Time (min)</u>	<u>EXPERIMENTAL</u>		<u>CALCULATED</u>
	<u>Peak Height of CO-O₂</u>	<u>Peak Height of CO₂</u>	<u>Peak Height of CO₂</u>
1.0	79.5	0.96	0.96
4.5	79.5	2.92	2.77
8.0	79.2	4.70	4.32
11.25	78.5	5.70	5.57
14.5	79.8	6.80	6.87
21.0	78.3	8.40	8.87
24.0	76.1	9.60	9.50
27.25	76.7	10.30	10.49
30.5	76.2	11.32	11.28
33.75	76.3	12.36	12.13
37.0	75.8	12.86	12.84

TABLE E-42

CRYSTAL #6 RUN 3

Temperature: 177°F

$K = 29,804 \text{ moles}^{-1}$

$k = 2.69 \times 10^{-4} \text{ min}^{-1}$

<u>Time (min)</u>	<u>EXPERIMENTAL</u>		<u>CALCULATED</u>
	<u>Peak Height of CO-O₂</u>	<u>Peak Height of CO₂</u>	<u>Peak Height of CO₂</u>
1.0	80.0	1.10	1.10
4.0	79.3	2.76	2.67
7.0	84.5	4.25	4.31
10.0	80.0	5.25	5.33
13.0	78.7	6.30	6.36
16.0	78.5	7.55	7.38
19.0	87.5	8.90	9.31
22.0	79.8	9.26	9.43
25.0	77.0	9.96	9.95
28.0	76.8	10.80	10.74
31.0	76.2	11.60	11.43
34.0	76.0	12.28	12.14

TABLE E-43

CRYSTAL #6 RUN 4

Temperature: 172.5

$K = 35,490 \text{ moles}^{-1}$

$k = 2.23 \times 10^{-4} \text{ min}^{-1}$

<u>Time (min)</u>	<u>EXPERIMENTAL</u>		<u>CALCULATED</u>
	<u>Peak Height of CO-O₂</u>	<u>Peak Height of CO₂</u>	<u>Peak Height of CO₂</u>
1.0	79.1	1.54	1.54
4.0	79.8	2.76	2.78
7.0	85.0	3.90	4.13
10.0	81.5	4.54	4.98
13.0	78.7	5.50	5.71
16.0	78.5	6.50	6.53
19.0	76.6	7.35	7.14
22.0	75.2	7.88	7.73
25.0	77.8	8.78	8.70
28.0	75.5	9.60	9.09
31.0	77.0	9.50	9.92

TABLE E-44

CRYSTAL #6 RUN 5

Temperature: 171°F

$K = 37,638 \text{ moles}^{-1}$

$k = 2.63 \times 10^{-4} \text{ min}^{-1}$

<u>Time (min)</u>	<u>EXPERIMENTAL</u>		<u>CALCULATED</u>
	<u>Peak Height of CO-O₂</u>	<u>Peak Height of CO₂</u>	<u>Peak Height of CO₂</u>
1.0	80.2	1.24	1.24
4.0	83.1	2.76	2.81
7.0	80.0	3.90	3.97
10.0	77.9	5.05	4.96
13.0	78.7	5.76	6.02
16.0	79.6	7.60	7.04
19.0	77.8	7.50	7.74
22.0	80.0	8.24	8.79
25.0	78.0	9.70	9.34
28.0	76.9	9.80	9.94
31.0	75.0	10.54	10.37
34.0	75.0	11.08	11.02

TABLE E-45

CRYSTAL # 6 RUN 6

Temperature: 174°F

$K = 37,639 \text{ moles}^{-1}$

$k = 1.19 \times 10^{-4} \text{ min}^{-1}$

<u>Time (min)</u>	<u>EXPERIMENTAL</u>		<u>CALCULATED</u>
	<u>Peak Height of CO-O₂</u>	<u>Peak Height of CO₂</u>	<u>Peak Height of CO₂</u>
1.0	79.0	1.00	1.00
4.0	79.2	1.72	1.72
7.0	78.0	2.36	2.34
10.0	81.5	3.00	3.07
13.0	79.8	4.30	3.59
16.0	81.2	4.00	4.21
19.0	77.0	4.50	4.49
22.0	80.0	5.13	5.16
25.0	77.0	5.53	5.43
28.0	76.5	5.75	5.83
31.0	76.6	6.07	6.27
34.0	75.9	6.86	6.62
37.0	76.9	6.90	7.10

TABLE E-46

CRYSTAL # 7 RUN 1

Temperature: 170°F

$K = 39,148 \text{ moles}^{-1}$

$k = 1.46 \times 10^{-4} \text{ min}^{-1}$

<u>Time (min)</u>	<u>EXPERIMENTAL</u>		<u>CALCULATED</u>
	<u>Peak Height of CO-O₂</u>	<u>Peak Height of CO₂</u>	<u>Peak Height of CO₂</u>
1.0	80.5	0.88	0.88
4.5	81.0	2.12	1.91
8.0	80.0	2.92	2.79
11.5	80.6	3.66	3.64
15.0	79.5	4.53	4.35
18.5	79.3	4.90	5.04
22.0	79.5	5.70	5.71
25.5	78.9	6.24	6.29
29.0	78.6	6.90	6.86
33.0	78.0	7.38	7.44

TABLE E-47

CRYSTAL # 7 RUN 2

Temperature: 171°F

 $K = 37,639 \text{ moles}^{-1}$ $k = 2.80 \times 10^{-4} \text{ min}^{-1}$

<u>Time (min)</u>	<u>EXPERIMENTAL</u>		<u>CALCULATED</u>
	<u>Peak Height of CO-O₂</u>	<u>Peak Height of CO₂</u>	<u>Peak Height of CO₂</u>
1.0	78.8	1.17	1.17
4.0	90.0	3.03	3.14
7.0	79.0	4.18	4.13
10.0	78.5	5.23	5.31
13.0	79.4	6.29	6.49
16.0	85.0	7.38	8.05
19.0	75.6	8.32	8.08
22.0	77.5	8.90	9.16
25.0	76.5	10.20	9.88
31.0	75.4	11.32	11.26
34.0	75.2	11.90	11.94
37.0	75.2	12.90	12.63

TABLE E-48

CRYSTAL # 7 RUN 3

Temperature: 175°F
 $K = 32,200 \text{ moles}^{-1}$
 $k = 1.43 \times 10^{-4} \text{ min}^{-1}$

<u>Time (min)</u>	<u>EXPERIMENTAL</u>		<u>CALCULATED</u>
	<u>Peak Height of CO-O₂</u>	<u>Peak Height of CO₂</u>	<u>Peak Height of CO₂</u>
1.0	80.0	1.02	1.02
4.25	80.8	1.98	1.99
7.5	80.0	3.08	2.83
10.75	80.6	3.70	3.66
14.0	79.5	4.18	4.35
17.25	79.8	5.21	5.06
20.5	79.4	5.47	5.69
23.75	78.7	6.20	6.27
27.0	78.0	6.88	6.80
30.25	78.4	7.56	7.40
33.5	78.0	7.90	7.91

TABLE E-49

CRYSTAL # 7 RUN 4

Temperature: 181°F

$K = 25,573 \text{ moles}^{-1}$

$k = 2.01 \times 10^{-4} \text{ min}^{-1}$

<u>Time (min)</u>	<u>EXPERIMENTAL</u>		<u>CALCULATED</u>
	<u>Peak Height of CO-O₂</u>	<u>Peak Height of CO₂</u>	<u>Peak Height of CO₂</u>
1.0	100.0	1.67	1.67
4.5	100.0	2.70	3.43
7.75	78.7	3.90	3.86
11.0	77.9	5.00	4.87
14.25	77.5	5.91	5.82
17.5	78.3	6.84	6.81
20.75	77.6	7.56	7.61
24.0	77.1	8.45	8.38
27.25	77.8	9.30	9.25
30.5	77.0	9.80	9.90
33.75	76.7	10.60	10.58
37.0	75.8	11.16	11.52

TABLE E-50

CRYSTAL # 7 RUN 5

Temperature: 181°F

K = 25,573 moles⁻¹

k = 2.04 x 10⁻⁴ min⁻¹

<u>Time (min)</u>	<u>EXPERIMENTAL</u>		<u>CALCULATED</u>
	<u>Peak Height of CO-O₂</u>	<u>Peak Height of CO₂</u>	<u>Peak Height of CO₂</u>
1.0	80.0	1.40	1.40
4.25	80.0	2.54	2.72
7.50	80.0	4.03	3.92
10.75	79.5	5.00	4.99
14.0	79.1	5.76	5.97
17.25	78.5	6.80	6.86
20.5	78.5	7.55	7.75
23.75	78.6	8.30	8.61
27.0	78.7	9.24	9.43
30.25	78.0	10.28	10.11
33.5	77.0	10.96	10.71
36.75	77.0	11.70	11.41

TABLE E-51

CRYSTAL # 7 RUN 6

Temperature: 175°F

$K = 32,200 \text{ moles}^{-1}$

$k = 2.00 \times 10^{-4} \text{ min}^{-1}$

<u>Time (min)</u>	<u>EXPERIMENTAL</u>		<u>CALCULATED</u>
	<u>Peak Height of CO-O₂</u>	<u>Peak Height of CO₂</u>	<u>Peak Height of CO₂</u>
1.0	77.9	1.42	1.42
4.0	77.9	2.58	2.54
7.0	77.0	3.80	3.51
10.0	77.0	4.64	4.42
13.0	77.0	5.38	5.26
16.0	77.1	5.90	6.06
19.0	76.8	6.67	6.79
22.0	75.8	7.30	7.40
25.0	76.0	8.00	8.08
28.0	75.0	8.66	8.61
31.0	74.5	9.15	9.16

TABLE E-52

CRYSTAL # 7 RUN 7

Temperature: 177°F

K = 29,805 moles⁻¹

k = 2.12 x 10⁻⁴ min⁻¹

<u>Time (min)</u>	<u>EXPERIMENTAL</u>		<u>CALCULATED</u>
	<u>Peak Height of CO-O₂</u>	<u>Peak Height of CO₂</u>	<u>Peak Height of CO₂</u>
1.0	79.0	1.26	1.26
4.0	79.4	2.49	2.51
7.0	78.3	3.64	3.57
10.0	77.6	4.61	4.54
13.0	78.6	5.40	5.53
16.0	78.2	6.28	6.37
19.0	77.6	6.95	7.13
22.0	76.8	7.80	7.82
25.0	75.5	8.54	8.40
28.0	76.9	9.28	9.26
31.0	76.4	9.80	9.87
34.0	75.8	10.60	10.43

TABLE E-53

CRYSTAL # 7 RUN 8

Temperature: 170.5°F

K = 38,385 moles⁻¹k = 1.68 × 10⁻⁴ min⁻¹

<u>Time (min)</u>	<u>EXPERIMENTAL</u>		<u>CALCULATED</u>
	<u>Peak Height of CO-O₂</u>	<u>Peak Height of CO₂</u>	<u>Peak Height of CO₂</u>
1.0	79.5	1.64	1.64
4.25	79.5	2.59	2.62
7.50	78.8	3.42	3.48
10.75	78.0	4.31	4.25
14.0	77.6	4.97	4.97
17.4	77.0	5.68	5.65
20.75	76.0	6.30	6.29
24.0	77.0	6.99	6.93
27.25	76.4	7.50	7.46
30.5	76.6	80.3	8.04
33.75	76.0	8.50	8.51
37.0	75.2	8.90	8.94

II. A MECHANISM FOR THE FORMATION OF DISLOCATIONS DURING
THE OXIDATION OF ZINC

INTRODUCTION

The results of the first study on silver indicated that oxidation of the silver changed both the physical properties and chemical reactivity of the catalyst. This section is again about the oxidation of a metal, but the metal is zinc. First, it should be noted that the mechanism of oxidation for zinc is different from silver. Silver oxidation occurs by the diffusion of oxygen through the oxidized lattice, whereas for zinc oxidation, the zinc atoms migrate through the oxide layer leaving a vacancy behind. This work discusses a mechanism to explain the increased rate of oxidation and the production of loop and spiral dislocations from the vacancies.

It is well known that dislocation loops may be formed in close packed metals by the condensation of vacancies which are present in excess of the equilibrium concentration (1-14). Spiral dislocations were also observed but less frequently (15). Some investigators (1-8) examined the dislocation loops in thin crystals ($\sim 1000\text{\AA}$) under a transmission electron microscope while others (9-14) employed X-ray diffraction methods. The diameter of a loop in thin film studies was of the order of $1\ \mu\text{m}$, and in the bulk specimens it was often as large as $100\ \mu\text{m}$. During many of the studies, the diameter of the loop changed during the observation period.

Many of the observations with both transmission electron microscopy and X-ray diffraction were identical for studies of thick and thin samples; thus it appeared as though a common mechanism existed for the growth of loops in zinc. Several theories were proposed by earlier scientists to explain the development of loops:

1. The dislocation loops resulted from the motion of a glissile dislocation which was pinned to an inclusion on neighboring slip planes. A loop was formed as the pinned dislocation acted as a Frank-Read source.

2. The loops were the outgrowth from the bombardment damage by negative ions in the transmission electron microscope.

3. The loops were formed under the electron beam by aggregation of small vacancy clusters. The clusters were placed into the specimen during growth from the vapor phase.

4. Loops were formed because an oxide film existed which prevented quenched-in vacancies from diffusing to a free surface. The vacancies then collected into loops.

5. Dislocation loops were produced while an oxide formed on the metal surface. The metal-metal oxide interface became a source of vacancies. The vacancies diffused into the metal and coalesced into loops.

The Burgers Vector of the loop and spiral dislocations was investigated in thin crystals by earlier scientists with the use of a transmission electron microscope since that instrument provided an exact routine for determining it. Identification of the Burgers Vector in thick samples was more difficult because the X-ray diffraction technique used in this study did not allow the contrast from all Burgers Vectors to be extinguished.

In this study large loop dislocations (diameter $\sim 100 \mu\text{m}$) were observed in annealed zinc specimens with the Berg-Barrett X-ray diffraction method. It was learned that if the zinc was chemically treated before the anneal, the formation of loop dislocations was reproducible. Loop dislocations were also observed with a much lower frequency in as-grown crystals and along cleavage steps. The crystallographic

structure of the dislocations is ascertained by a study of contrast extinction of various Burgers Vectors with X-ray diffraction, and by calculations of the minimum line energy for the loops.

EXPERIMENTAL METHOD

Specimen Preparation

Monocrystals of 99.999% zinc were grown by the Bridgman method in pyrex molds coated with graphite. The specimens were machined (16) from the as-grown crystal into right circular cylinders (.5 inch diameter) with its axis parallel to the [0001] direction. The orientation of the end surfaces of the cylinder was established by cleaving the crystals in liquid nitrogen. After the crystal was cleaved, it was annealed in a pyrex tube which had a controllable temperature and atmosphere.

During the annealing process the specimens were heated from room temperature to 700°F at 3°F/min, remained at 700°F for 30 min, and then were cooled at 3°F/min. Hydrogen, argon and air were tested as the atmosphere in the pyrex tube both as dry gases and as saturated with water at room temperature. These tests were to measure the correlation between the annealing atmosphere and the frequency of observation of the loop and spiral dislocations. High purity argon (99.996%) was used as the annealing atmosphere in most of the study. It was further purified by passing it through a column of molecular sieves and manganese oxide before reaching the pyrex tube. Following the anneal, the specimen was examined for loop and spiral dislocations.

Observations of Dislocations

Chemical etching and Berg-Barrett X-ray topography are two different techniques for observing dislocations. A chemical etching procedure was developed and it proved useful for measuring the number of dislocations which intersected the basal plane. It is described

in Appendix A. Berg-Barrett X-ray topography (17) was employed to observe the loop and spiral dislocations beneath the basal plane. Topographs were recorded on Kodak Minicard 6451 film by diffraction from selected planes with either CoK_{α} (4 hr) or NiK_{α} (8 hr) radiation. Both X-ray tubes were operated at 40 kV and 8 ma. The signal to noise ratio was improved by placing a 0.001 inch metal foil in front of the film. An iron foil was used for CoK_{α} and a cobalt foil was used for NiK_{α} . The developed films were viewed with an optical microscope when searching for the loop and spiral dislocations. Stereoscopic measurements (18) were made with pairs of topographs to learn the apparent depth of the dislocations beneath the surface.

Measurement of Oxide Thickness

The thickness of the zinc oxide on the zinc crystal was determined by measuring the capacitance of the oxide film. A capacitor was constructed across the film by first vacuum evaporating a grid of gold dots (150 μm diameter) onto the oxide. Next, 13 millivolts was applied across a gold dot and the zinc crystal, and the capacitance of the circuit was measured with a capacitance meter. The values were recorded and later used to calculate the oxide thickness.

EXPERIMENTAL RESULTS

Observations of Dislocations

Initial results on the formation of loop and spiral dislocations were not very reproducible in this study. It was first noticed that the dislocations were observed in the X-ray topographs only after annealing the crystal. The first tests checked the effect of various gaseous atmospheres in the annealing tube. Changing the atmosphere from hydrogen to air to argon had little effect on the production of the desired dislocations. The gases were tested either dry or saturated with water at room temperature and results were the same. Thus, it seemed as though another process was responsible for the loop and spiral dislocations.

It became apparent that loop and spiral dislocations were usually generated when water reached the zinc surface during the cleavage operation, so an interaction between water and the zinc surface was suspected as the cause for observing the dislocations in the annealed crystal. The frequency for observing the dislocations was further improved by placing an annealed crystal in water (tap or deionized) and reannealing it. The treatment consisted of immersing the crystal in water for fifteen minutes and then drying the basal surface with a stream of air. Later, it was noted that the addition of a few drops of sodium hydroxide to the water seemed to improve the chances of finding the dislocations. Figure 1 is an X-ray topograph of loop and spiral dislocations in a bulk zinc crystal after a water treatment and second anneal. Stereoscopic measurements of the spiral dislocations were made with some topographs and the measurements indicated that the

end with the large radius was near the surface and that the center of the spiral was several microns deeper into the crystal.

Thickness of Zinc Oxide

A zinc oxide film was assumed to grow on a freshly cleaved zinc surface on exposure to oxygen. The thickness of the oxide film was determined by substituting the measured value of the capacitance between a gold dot and the zinc crystal into the expression

$$d = \kappa \epsilon_0 A/c$$

In the formula ϵ_0 is the permittivity (19), A is the area of the gold dot, c is the measured capacitance, and κ is the dielectric constant (20). The formula was used to calculate the oxide thickness for three different samples: a cleaved and annealed crystal; a cleaved, annealed, and water treated crystal; and a cleaved, annealed, water treated, and reannealed crystal. The calculated thickness of the first sample was about 90°A . For the second sample no thickness was ascertained since all the tested capacitors were shorted; and in the third case, the thickness was calculated as 1436°A . It was apparent that the thickness of the films was different in each stage of preparation for the growth of the loop and spiral dislocations.

DISCUSSION

Growth of Oxide Film

The results indicated that during the first anneal a thin film ($\sim 90\text{\AA}$) of zinc oxide grew on the cleaved zinc surface. The small value for the thickness was compared with a value which was calculated with the reported kinetic data on the oxidation of zinc. The data of Nwoko and Uhlig (21) were utilized in the calculation and were first fit on the basis of least squares to a parabolic growth curve rather than their two-stage logarithmic function. Their data at 125°C and 206°C were fit to the expression:

$$\text{time, min} = (\text{constant, k})(\text{thickness, } \overset{\circ}{\text{\AA}})^2$$

A change in the functional form was made to facilitate the integration of the oxide thickness over the time-temperature curve of the anneal cycle. After integrating the expression, a value for the oxide thickness of $153\overset{\circ}{\text{\AA}}$ was calculated which was in good agreement with the measured value of $90\overset{\circ}{\text{\AA}}$. The closeness in the results implied that the value of the film after a second anneal ought to be predictable. The functional form of the oxide growth kinetics indicated that the rate will decrease during the second anneal and the expected film thickness was about $200\overset{\circ}{\text{\AA}}$. This value was well below the measured value of $1450\overset{\circ}{\text{\AA}}$ and it was an indication that some changes must have occurred to the thin zinc oxide film when it was immersed in water.

Effect of Water Treatment

Both tap and deionized water were used in the study, and in most cases several drops of concentrated sodium hydroxide were added to the solution. The zinc oxide film, ZnO, is almost insoluble in water (~ 5 ppm) and sparingly soluble in dilute solutions of alkalies. ZnO was reported to dissolve by forming zinc hydroxide and two types of acidic ions, monobasic, Zn(OH)_3^- and dibasic Zn(OH)_4^{2-} according to the following reactions (22):

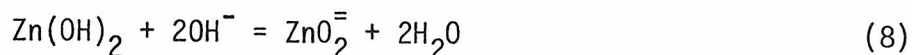


The addition of hydroxide ion should increase the dissolution rate of the zinc oxide film and expose the zinc surface to further attack by the aqueous solution. Gilbert (23) investigated with X-ray diffraction methods the nature of the corrosion products formed on zinc when immersed in water. He identified zinc oxide and several forms of zinc hydroxide as products of the corrosion. He presumed the reactions were



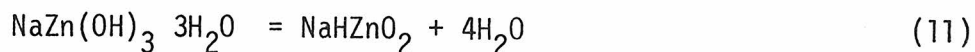
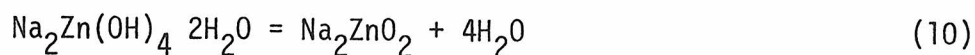
Dirkse (24) stated that the thermodynamic driving forces for reactions (4) and (5) are favorable and practically identical. However, the compounds once formed on the zinc surface will begin to dissolve in the solution. ZnO would dissolve as in equations (1)-(3).

The dissolution of zinc hydroxide was studied by Fulton and Swinehart (25). They found the hydroxide was dissolved according to the following reactions:



Reactions (1)-(3) and (6)-(8) would remove the film and leave the zinc susceptible to further erosion. Presumably, the total amount of corrosion was determined by the porosity of the film and by the dissolution kinetics. The film on the water-treated zinc crystal was a mixture of zinc oxide, zinc hydroxides and zincates. On the basis of the capacitance measurements, it was suspected that the film was porous, as the gold had simply diffused to the zinc surface.

The second anneal of a crystal began with a corrosion film on the zinc surface rather than with a thin (150\AA) zinc oxide film. As the temperature was raised, some of the compounds in the corrosion film were dehydrated, for example,



The water evaporated and left a porous film. Zinc metal which was beneath the film was still liable to oxidation at the elevated temperature during the anneal. It was learned from the capacitance measure-

ment that the film thickness after the second anneal was 1450\AA as compared to the 200\AA which was calculated based on the oxidation of a 150\AA film. The difference between the expected film thickness of 200\AA and the observed value of 1450\AA was because the zinc oxide film was thicker than 150\AA after exposure to water. Furthermore, it was possible that the oxidation kinetics might not be the same, since the film was porous. Others (26) have demonstrated with silicon that trace amounts of water increased the oxidation rate and many of the zinc corrosion products were dehydrated during the annealing process.

Formation of Loop and Spiral Dislocations

The results, already discussed, were concerned with the effect of a water treatment on the properties of the zinc oxide film. It was learned that the water caused the growth of a much thicker oxide film than was expected and that the treatment significantly improved the chances for observing loop and spiral dislocations. Figure 4a shows an example of the distribution of loop and spiral dislocations near a water droplet on a reannealed zinc crystal. The discussion in this section focuses on the vacancies that were formed during the formation of the oxide layer. It is reported (27) that zinc oxide contains excess metal atoms, and grows by zinc atoms entering the oxide in interstitial positions and diffusing to the oxide/oxygen interface where further oxidation occurs.



As the zinc atoms migrated to the oxide layer, vacancies were injected into the bulk. The concentration of the vacancies became

larger than the equilibrium value at the anneal temperature, so they either diffused to available sinks or coalesced into a lower energy configuration (Figure 1). Dislocations were one sink to which the vacancies diffused, and the interaction resulted in the climb of the dislocation. The high density of basal dislocations, which were introduced during the cleaving process, were effective sinks. They eliminated most of the vacancies injected from the oxide layer, and as a result, loop dislocations were scarcely seen after the first anneal.

A spiral dislocation was produced by the climb of a screw dislocation and some examples are presented in Figure 3. The spirals seen in this study were not perfect helices as compared to those observed by Amelinckx et al (15) since the flux of vacancies was parallel to the axis of the spiral instead of perpendicular as in their studies. Figure 3 also depicts the competition between a spiral dislocation and a sub-boundary for the vacancies of the oxidation process. The rate of growth of the spiral was reduced in the vicinity of the boundary.

Identification of the Burgers Vector

The excess vacancies, which did not diffuse to sinks, coalesced into loop dislocations. Figure 5 presents a review of the common dislocations and Burgers vectors in zinc. The Burgers vector of the loop dislocation was investigated by two methods: First, it was selected on the basis of that Burgers vector which had the lowest calculated configurational energy in the lattice, and second, the Burgers vector was determined by the extinction of dislocation contrast in X-ray topographs. A comparison was later made of the results of the two methods.

Previous studies on the energetics of a coalescence of the vacancies into loops were reported by Schoeck (28) and Bolling (29). In their work, the free energy of the dislocation loop was established as the sum of the line energy, the stacking fault energy and an entropy term for the atoms in the dislocation core. Both the entropy and the core energy terms were small as compared with the total energy of the loop dislocation, and thus were neglected from further consideration. Using the remaining terms in the energy equation, Bolling (29) demonstrated that the transitional radius from vacancy clusters to prismatic loops was small enough that the notion of the dislocation was suspect. Thus, a prismatic loop was considered to be the initial geometry of the coalesced vacancies.

The prismatic loop or Frank partial has a very high energy of the stacking sequence, ABAB/BAB, and two crystallographic transitions (1,30) were proposed to lower the configurational energy. The first modification is depicted in Figure 5b(3) and shows the creation of an extrinsic stacking fault of high energy that is bounded by low energy Frank partial dislocations of the type σS . The second possible change is the creation of an intrinsic stacking fault of a low energy that is bounded by a high energy Frank-Shockley composite partial of the type AS. It is shown in Figure 5b(4).

When considering the latter case, there is a value for the radius when the high stacking fault energy of the prismatic loop is reduced by the dislocation reaction:



The energy of the loop was considered equal to the sum of the energy of the stacking fault and the elastic energy of the strain field. The stacking fault energy, E_{SF} , varied as the square of the radius of the loop (R_L)

$$E_{SF} = \pi R_L^2 \gamma_{SF} \quad (14)$$

The expressions derived by Chou and Eshelby (31) were used to calculate the elastic energy of a dislocation loop on the basal plane of a hexagonal metal. The total elastic energy was the sum of a term with the Burgers vector parallel to the loop and another term with the Burgers vector perpendicular to the loop

$$E_{\parallel} = \frac{1}{4} (K_e + K_s) b_{\parallel}^2 R_L \left(\ln \frac{8R}{r_0} - 2 \right) \quad (15)$$

$$E_{\perp} = \frac{1}{2} K_n b_{\perp}^2 R_L \left(\ln \frac{8R}{r_0} - 2 \right) \quad (16)$$

The K's in equations (15) and (16) were defined in their article (31) and computed for this study with the elastic constants of zinc that were measured by Alers and Neighbours (32). Other values used in the energy calculation were $a = 2.66\text{\AA}$, $c = 4.94\text{\AA}$ and $\gamma_{AS} = \frac{1}{3} \gamma_{\sigma S} = 140$ dynes/cm (2). After substituting the values in the energy equations, a value of 15\AA was found for the radius when a loop with either dislocation AS or σS had the same energy. The calculated radius for when reaction (13) occurred was so small that the expressions used for the line energy of the dislocations were not completely valid. It was clear, however, that the transition took place for small loop radii. Further evidence to support that conclusion was ascertained from examination of thin foils with the electron microscope, in that, no loops with dislocation σS were found.

It seemed evident that for a loop with a big radius the stacking fault energy could become large enough to cause the formation of a

perfect dislocation according to the dislocation reaction:



The energy equations for loop dislocations with a Burgers vector of either AT or ST were equated and solved for the value of the radius when the stacking fault would disappear. A value of 250\AA was calculated and, as before, it was compared with experimental observations.

Harris (6) examined dislocation loops in zinc which had a diameter of about $1\ \mu\text{m}$ and found both the Burgers vectors ST and SA. The energy calculation had predicted the existence of the perfect dislocation for that size loop. Presumably the difference can be explained by assuming that the dislocation reaction of equation (17) was an activated process and not all loops had sufficient energy to change. One possible process for the reaction to occur was by the nucleation of a second loop on a neighboring basal plane above a large established loop. However, no attempt was made to model the formation of a second loop but, as the loops in this study were large, their Burgers vectors were checked using X-ray diffraction.

X-ray diffraction was employed by assuming certain Burgers vectors for the loops and then obtaining a suitable diffraction topograph from a plane which contained the Burgers vector. The method was based upon contrast extinction of a Burgers vector in the diffraction plane and can be fully justified by calculation for only electron diffraction. It was used in this work with X-rays since no complete theory of X-ray diffraction was available, and the simple rules for dislocation

visibility given by the electron diffraction analysis frequently have provided a useful guide in topography, particularly when X-ray adsorption was low (33).

The Burgers vector of the loops that were checked in this study were: \bar{a} , $\bar{c} + \bar{a}$, and $\bar{c}/2 + \bar{a}/\sqrt{3}$, as these were considered the most probable. No plane was found which contained all the Burgers vectors, but at least one normal of a $\{20\bar{2}3\}$ was within 10° of being perpendicular to them. Diffraction topographs were recorded from the $\{20\bar{2}3\}$ planes and the results in a small area of a crystal are presented in Figure 2. As seen in the figure, there was no contrast change to the dislocations due to extinction of a Burgers vector. The data obtained from loops in this crystal were reproducible, hence it was determined that the Burgers vector was not one of the three tested for, but instead probably a full \bar{c} . The selection of that Burgers vector was in agreement with the energy calculations.

SUMMARY

Before this study was initiated, the observation of loop and spiral dislocations in zinc crystals was of a random nature, as compared to a controlled and well understood situation. It was demonstrated during the experimental phase of the project that the loop and spiral dislocations appeared if the zinc crystal was oxidized after being exposed to an aqueous environment. The aqueous exposure created many micro-cracks in the epitaxial oxide layer and these cracks provided low energy paths for the zinc to reach the surface. Subsequently, the rate of oxidation of the zinc crystal was increased and the vacancies that remained in the metal either coalesced into loop and spiral dislocations or moved to vacancy sinks.

The Burgers Vector of the dislocations was investigated and it was concluded that the most likely Burgers Vector was a full \bar{c} . This decision was reached by first finding the crystallographic structure with the lowest calculated energy, and second, by searching for contrast extinction with the Berg-Barrett method.

The results from this work should help to explain many of the previous observations of loop dislocations in hexagonal metals that were left unexplained. Furthermore, it was evident that the rate of oxidation of the zinc metal was rapidly increased when in an aqueous environment since the zinc oxide film which formed on the metal was not epitaxial but had many micro-cracks.

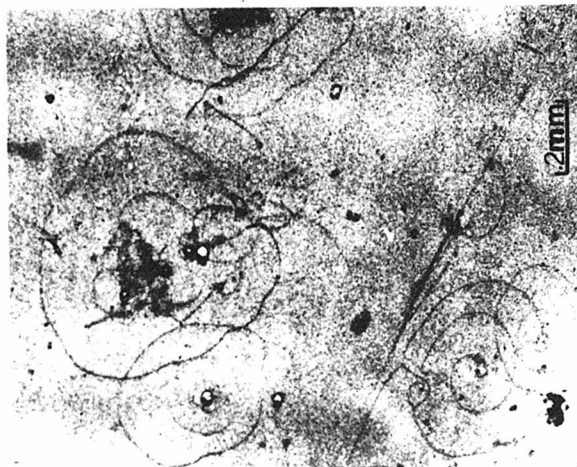
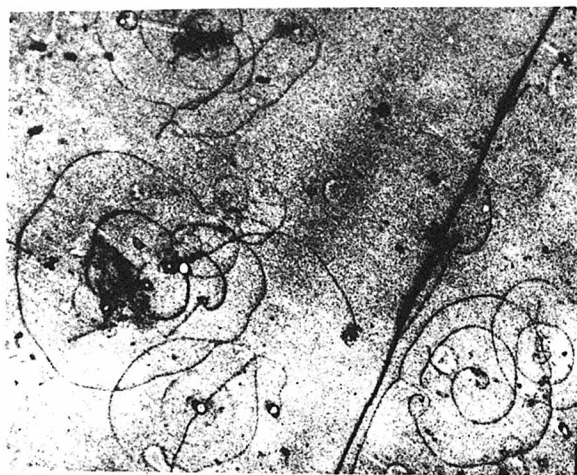
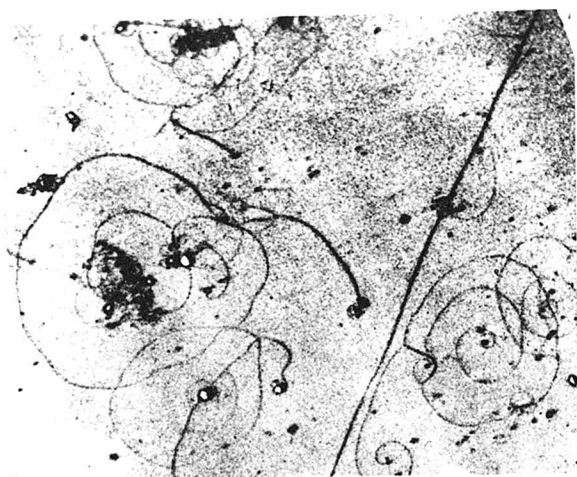
REFERENCES

1. Berghezan, A., Fourdeux, A., Amelinckx, S., Acta Met., 9, 464 (1961).
2. Hales, R., Smallman, R. E., Dobson, P. S., Proc. Roy. Soc. (A), 307, 71 (1968).
3. Dobson, P. S., Smallman, R. E., Proc. Roy. Soc. (A), 293, 423 (1966).
4. Hales, R., Dobson, P. S., Smallman, R. E., Metal. Sci. J., 2, 224 (1968).
5. Harris, J. E., Masters, B. C., Phys. Stat. Sol., 9, K181 (1965).
6. Harris, J. E., Masters, B. C., Proc. Roy. Soc. (A), 292, 240 (1966).
7. Harris, J. E., Masters, B. C., Phil. Mag., 13, 963 (1966).
8. Crump, J. C., Mitchell, J. W., Phil. Mag., 8, 59 (1963).
9. Roessler, B., Burns, S. J., Phys. Stat. Sol. (a), 24, 285 (1974).
10. Roessler, B., Phys. Stat. Sol. (a), 17, K85 (1973).
11. Mitchell, D., Ogilvie, G. J., Phys. Stat. Sol., 15, 83 (1966).
12. G'Sell, C., Champier, G., Iwaski, Y., J. Crys. Growth, 24/25, 527 (1974).
13. Armstrong, R. W., Schultz, J. M., Surface Sci., 12, 19 (1968).
14. Armstrong, R. W., Schultz, J. M., Acta Met., 14, 436 (1966).
15. Amelinckx, S., Bontinck, W., Dekeyser, W., Seitz, F., Phil. Mag., 2, 355 (1957).
16. Pope, D. P., Vreeland, Jr., T., Trans. AIME, 245, 2447 (1969).
17. Turner, A.P.L., Vreeland, Jr., T., Pope, D. P., Acta Cryst., A24, 452 (1968).
18. Vreeland, Jr., T., to be published in Acta Cryst.

19. Collins, R. J., Kleinman, D. A., Phys. Chem. Solids, 11, 190 (1959).
20. Hutson, A. R., Phys. Rev. Letters, 4, 505 (1960).
21. Nwoko, V. O., Uhlig, H. H., J. Electrochem. Soc., 112, 1181 (1965).
22. Dirkse, T. P., Postmus, Jr., C., Vanderbosch, R., J. Am. Chem. Soc., 76, 6022 (1954).
23. Gilbert, P. T., J. Electrochem. Soc., 99, 16 (1952).
24. Dirkse, T. P., Timmer, R., J. Electrochem. Soc., 116, 162 (1969).
25. Fulton, J. W., Swinehart, D. F., J. Am. Chem. Soc., 76, 804 (1954).
26. Irenc, E. A., J. Electrochem. Soc., 121, 1613 (1974).
27. Kubaschewski, O., Hopkins, B. E., "Oxidation of Metals and Alloys", Butterworths, 2nd Edition, London (1962).
28. Schoeck, G., Tiller, W. A., Phil. Mag., 5, 43 (1960).
29. Bolling, G. F., Fainstein, D., Phil. Mag., 25, 45 (1972).
30. Patridge, P. G., Metall. Reviews, 12, 169 (1967).
31. Chou, Y. T., Eshelby, J. D., J. Mech. Phys. Solids, 10, 27 (1962).
32. Alers, G. A., Neighbours, J. R., Phys. Chem. Solids, 7, 58 (1958).
33. Lang, A. R., Polcarova, M., Proc. Roy. Soc. (A), 285, 297 (1965).



Figure 1. Berg-Barrett topograph of a zinc crystal showing an area with a high density of loop and spiral dislocations.

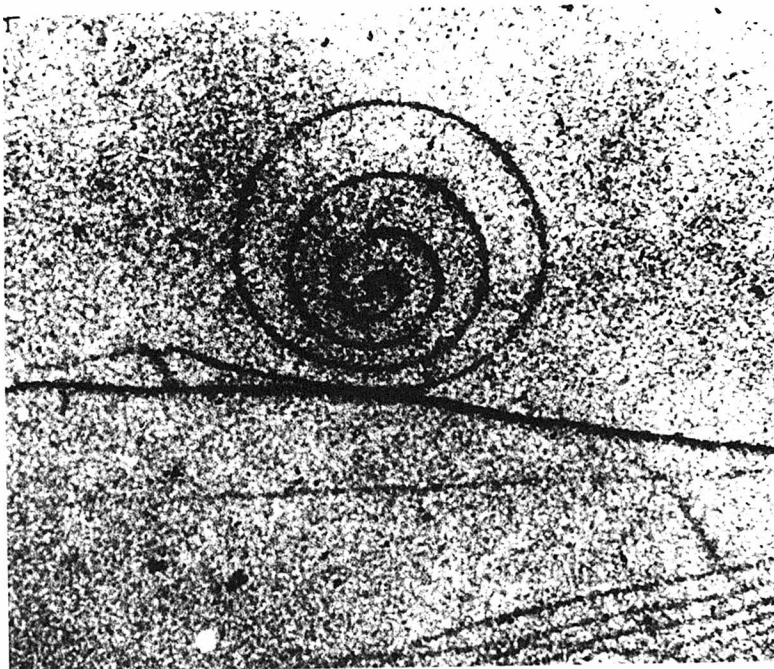


(a)

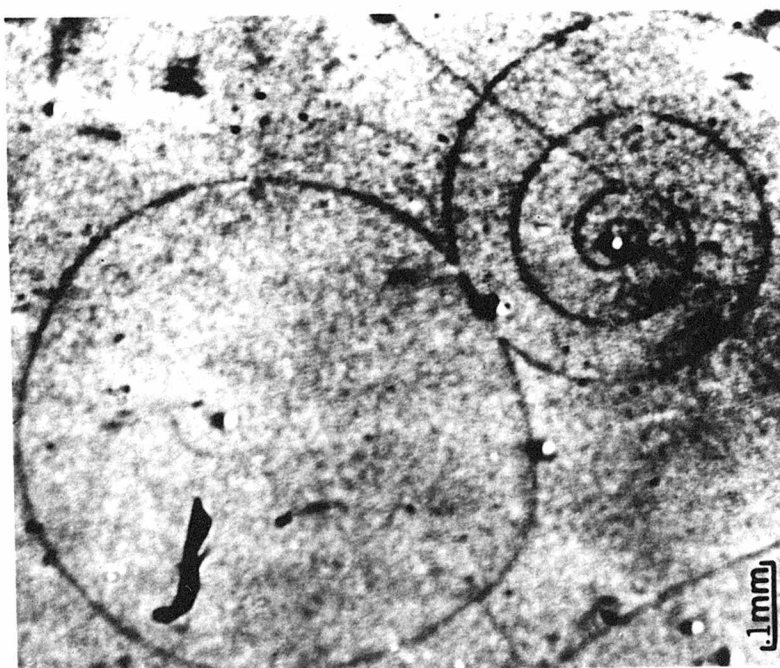
(b)

(c)

Figure 2. Three Berg-Barrett topographs of the same area which were taken by rotating the crystal in 120° intervals with respect to the incident beam.

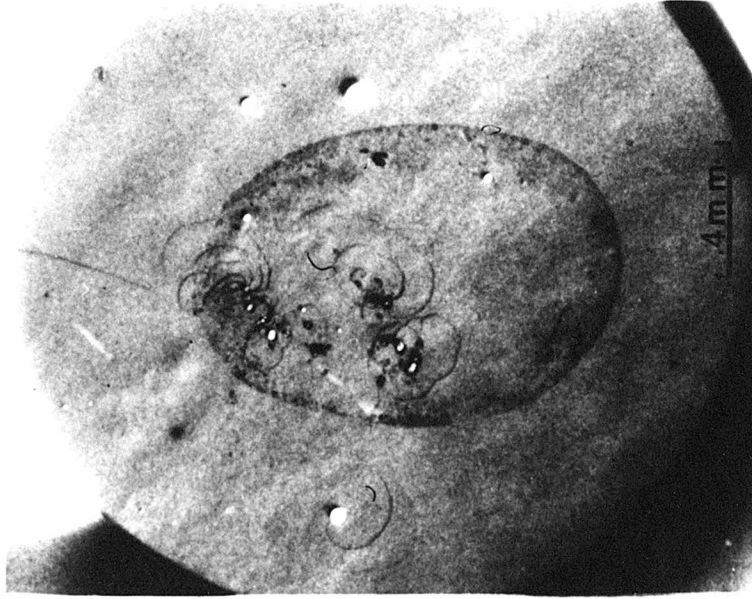


(b)

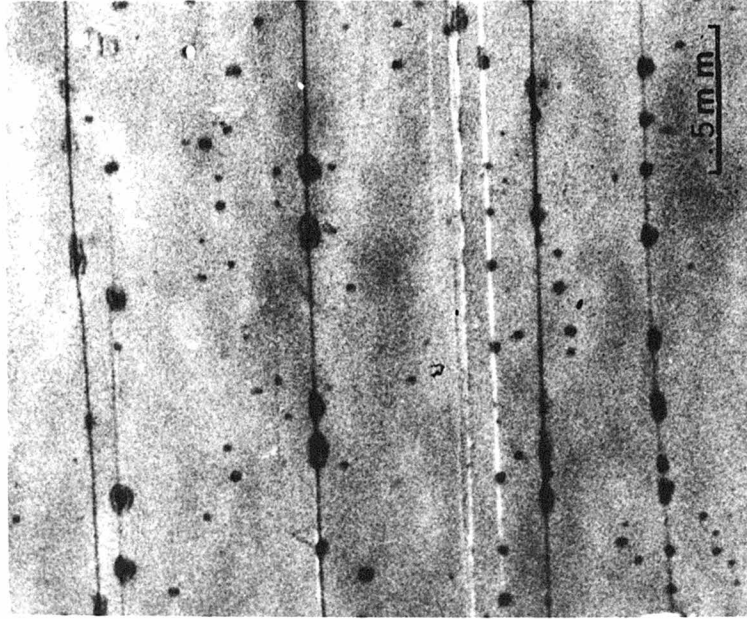


(a)

Figure 3. Berg-Barrett topograph with a spiral dislocation near a large loop (a) and a grain boundary (b).

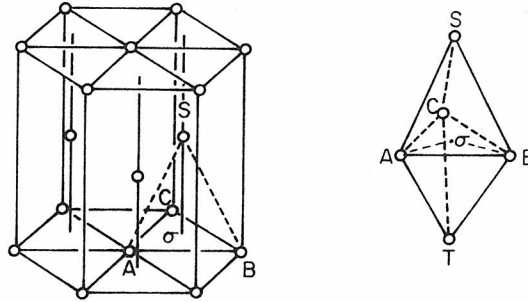


(b)

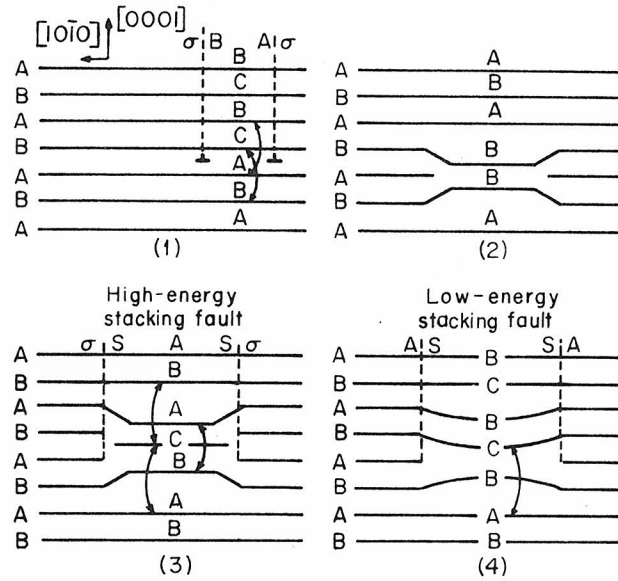


(a)

Figure 4. Berg-Barrett topographs showing loop dislocations near a cleavage step (a) and the outline of a water droplet which was placed on the crystal before the second anneal (b).



(a) Burgers vectors in zinc



(b) Stacking faults in zinc

Type of dislocation	Vector	Miller-Bravais indices of vector
Perfect dislocations		
1. AB	a_1	$\frac{1}{3}\langle 11\bar{2}0 \rangle$
2. ST	c	$\langle 0001 \rangle$
3. ST + AB	$c + a$	$\frac{1}{3}\langle 11\bar{2}3 \rangle$
Imperfect dislocations		
4. $A\sigma$	$\frac{2}{3}a_1 + \frac{1}{3}a_2$	$\frac{1}{3}\langle 10\bar{1}0 \rangle$
5. σS	$\frac{c}{2}$	$\frac{1}{2}\langle 0001 \rangle$
6. AS	$\frac{c}{2} + \frac{a}{\sqrt{3}}$	$\frac{1}{6}\langle 20\bar{2}3 \rangle$

(c) Burgers vectors of dislocations in zinc.

Figure 5. Dislocations in Zinc

APPENDIX A

OBSERVATION OF DISLOCATIONS IN ZINC BY CHEMICAL ETCHING

Chemical etching to reveal dislocation intersections with crystal surfaces is a valuable tool for dislocation studies. Etches for various crystals and surfaces are available (1) but the understanding of the complex chemical mechanism on the crystal surface is, at best, only qualitative. Numerous articles have been published on etching zinc crystals (2-6) but the etches for (0001) surfaces were found not to be very reliable in this study. The etches of references 4-6 require the segregation of solute impurities to dislocations and will not be further discussed, since an etch that reveals undecorated dislocations is of interest here.

Rosenbaum (2) made the most comprehensive study for the etching of the (0001) basal plane. We found that his recommended etching solution of 25 ml ethanol and 1.5 ml of 48% hydrobromic acid worked well for freshly cleaved surfaces but it did not work reliably on crystals which were chemically or electrolytically polished. We also found that the short etching time of about one second made the etching process hard to control. It is often desirable to polish and re-etch specimens several times and an etching technique which works well on polished as well as on cleaved surfaces is then needed.

In this report a chemical etch technique is given for etching surfaces of zinc crystals near the (0001) basal plane. The etch does not depend on impurities and is less sensitive to orientation than are those previously reported for the (0001) plane.

Experimental Procedures

Monocrystals of 99.999% zinc, grown by the Bridgman method in Pyrex molds coated with graphite, were used in this work. Specimens were machined into right circular cylinders and rectangular prisms by chemical methods previously described (7). A final electro-polishing step was used just prior to etching to flatten the surface and remove surface films. The crystal was electro-polished in a solution containing three parts ethanol and one part concentrated nitric acid by volume at 1.5 volts for twenty seconds with mild agitation. Various etching procedures were then carried out and the specimen surfaces were examined optically at magnifications between 40 and 500X. Water, ethanol and methanol were used as solvents in the etching solutions. The reactive etchants tested were hydrofluoric acid, hydrobromic acid, hydrochloric acid, acetic acid, formic acid, bromine and iodine.

Results

Attempts to use previously described solutions did not give reliable etching patterns and there was often a question as to whether the etch figures corresponded with dislocation intersections. A solution of 30 ml ethanol, 1 ml of 48% hydrobromic acid, and 1 ml of bromine was found to be the most reliable etchant. This solution has a useful shelf life of several days if the container is kept closed.

The etching time is a function of the temperature of the crystal and solution. It was found convenient first to cool the crystal and then to immerse it in the etching solution which was initially at 25°C. The etching times for a specimen at various initial temperatures and a solution initially at 25°C are: 1 second at 25°C, 5 seconds at 0°C and

10-12 seconds at -70°C . Best results were obtained at the lower temperature because the longer time gave a more controllable etch.

The procedure for cooling the specimen down to the dry ice temperature is to mildly agitate the crystal in an ethanol bath at -70°C for five minutes. The crystal is quickly dried with a stream of air before etching. The crystal is etched for 10-12 seconds depending on the dislocation density (shorter times for high densities) and brought up to room temperature under running water. A distilled water rinse follows and finally the crystal is dried in a stream of air. This procedure leaves a film-free surface.

Attempts to use a cooled solution and crystal, both at -70°C , did not offer much improvement as the solution became viscous and the crystal did not etch in thirty seconds. If the solution is cooled to -70°C and the crystal is at room temperature, the etching time is three seconds. Increased dilution of the solution gave slightly increased etching times but the pits became shallower and the results were not satisfactory.

The cooling and heating procedures were checked to see if any basal dislocations were produced by thermal stresses. Basal dislocations are visible within a few microns of the basal plane surface with the Berg-Barrett X-ray diffraction method (8). A newly cleaved and annealed crystal was cooled for five minutes in ethanol at -70°C and warmed to room temperature under running water as described. A Berg-Barrett X-ray diffraction topograph was taken of the crystal and the results indicated that no basal dislocations appeared.

The etch pits on the basal plane are hexagonal in shape and have a star-like appearance when viewed under an optical microscope. A few hexagonal pits with flat bottoms as seen in Fig. 1 occur because of general surface etching. These pits are not included in dislocation density counts. Oblique lighting is useful in determining which pits have flat bottoms. The radial arms of the dislocation etch figure are parallel to the $\langle 11\bar{2}0 \rangle$ directions.

As the surface orientation deviates from the basal plane, the starlike shape becomes less symmetrical. Figure 1 shows a segment of a curved surface which was etched. The angle between the surface and the basal plane is indicated in the figure. These measurements were made with a modified Unitron microgoniometer. The angle where one-half of each etch pit has disappeared is $0.5^\circ \pm 0.05^\circ$. This angle is close to the angle which the wall of the etch pit makes with the basal plane, and beyond this limit dislocations are not revealed.

Crystals were deformed by various means to check the correspondence of etch pits to dislocations. Crystals were twinned as described by Blish and Vreeland (9) and etched after twinning. The dislocation density measured in the vicinity of the twin was 10^7 cm^{-2} . Crystals were compressed uniaxially and perpendicular to the $\langle \bar{1}2\bar{1}0 \rangle$ basal slip directions. The correspondence of etch pits to dislocations was as expected and is discussed later.

Discussion

The evidence which suggests that there is a one-to-one correspondence of etch pits and dislocation intersections on basal surfaces is:

1. Fresh dislocations produced by twinning a crystal at room temperature cause the expected distribution of etch pits around the twins: accommodation kinks, etch pits aligned with and ahead of twin traces, and the appearance of etch pits in bands on second-order pyramidal plane is indicated. Etch pit densities are also similar to those observed by Blish and Vreeland (9).

2. Fresh dislocations were introduced by compression in the $[1\bar{2}10]$ (basal slip direction). The etch pit densities increased with increasing strain, and the pits were observed to align along traces of the most highly stressed second-order pyramidal slip planes.

3. Our observations indicated that sub-boundaries observed in Berg-Barrett topographs are also revealed by this etch pit technique. Etch pits which appear between sub-boundaries of as-grown crystals are presumably grown-in dislocations.

Summary

The etch meets the criteria for which it was developed:

1. Controllable etching times.
2. Ability to reliably etch surfaces oriented with 0.5° of the (0001) basal plane of zinc.
3. Strong evidence for a one-to-one correspondence of etch pits and dislocations.

REFERENCES

- A-1. Robinson, W. H., "Techniques of Metals Research," Vol. II, R. F. Bunshak, ed., Interscience, New York, 1968; pp. 291-340.
- A-2. Rosenbaum, H. S. and Saffren, M. M., J. Appl. Phys., 32, 1886 (1961).
- A-3. Brandt, R. C., Adams, K. H., and Vreeland, T. Jr., J. Appl. Phys., 32, 591 (1961).
- A-4. Kosevich, V. M. and Soldatov, V. P., Kristallografiya, 6, 439 (1961).
- A-5. Gilman, J. J., Trans. AIME, 206, 998 (1956).
- A-6. Gassi, G. and Hugo, J. P., J. Inst. Metals, 87, 376 (1958).
- A-7. Pope, D. P. and Vreeland, T. Jr., Trans. AIME, 245, 2447 (1969).
- A-8. Turner, A.P.L., Vreeland, T. Jr., and Pope, D. P., Acta Cryst., A24, 452 (1968).
- A-9. Blish, R. C. and Vreeland, T. Jr., J. Appl. Phys., 39, 2290 (1968).

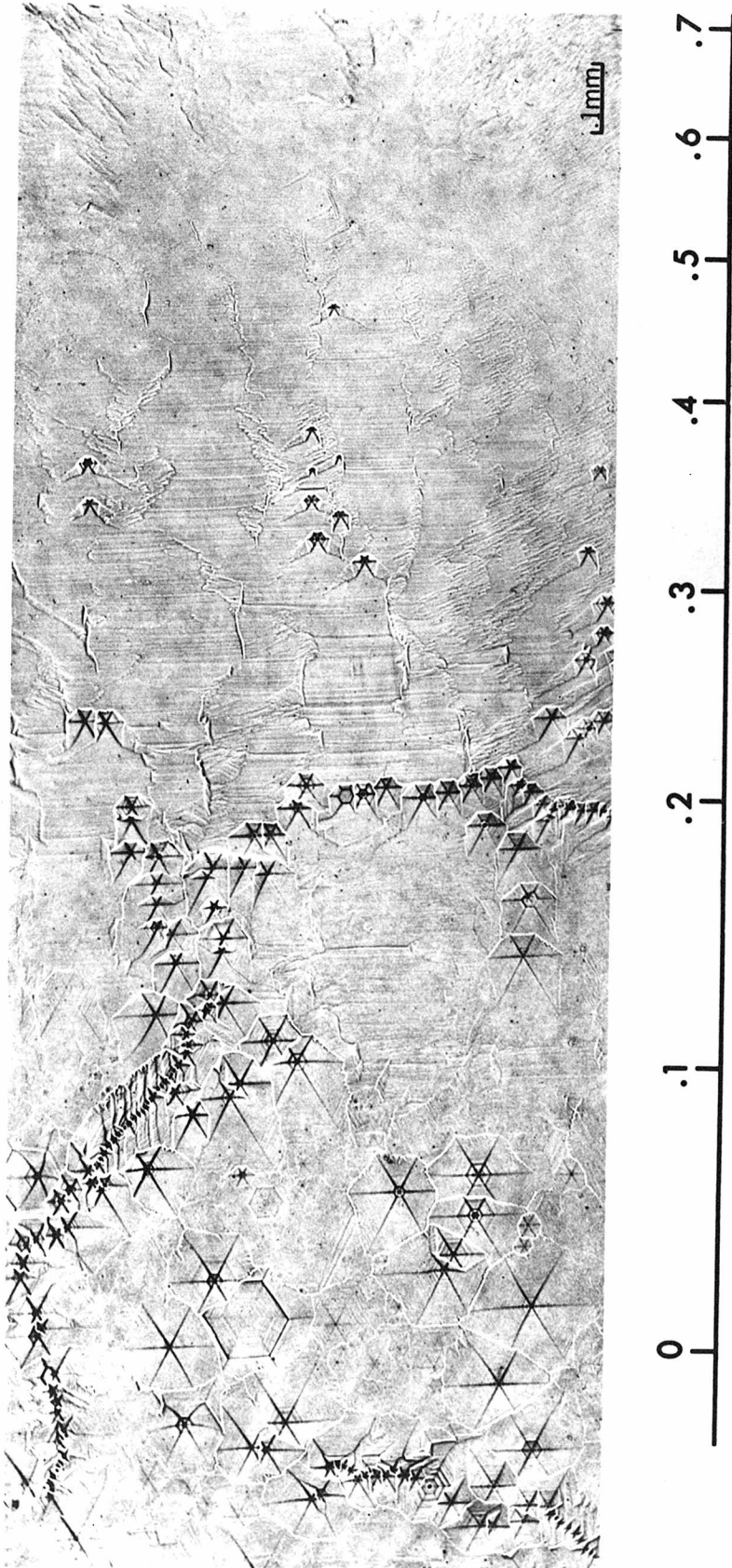


Figure 1. Etched surface of zinc showing dislocation etch pits and the dependence of the surface orientation. The scale indicates the angle between the surface and the (0001) basal plane (in degrees). (X100)